의학박사 학위논문

Synaptic mechanisms underlying trace fear conditioning and contextual fear discrimination

흔적 공포 조건화와 맥락 공포 분별의 시냅스 기전

2023년 2월

서울대학교 대학원

의과학과 생리학 전공

이 형 로

A thesis of the Degree of Doctor of Philosophy

흔적 공포 조건화와 맥락 공포 분별의 시냅스 기전

Synaptic mechanisms underlying trace fear conditioning and contextual fear discrimination

February 2023

The Department of Biomedical Sciences

Seoul National University College of Medicine

Hyoung-Ro Lee

흔적 공포 조건화와 맥락 공포 분별의 시냅스 기전

지도 교수 이 석 호

이 논문을 의학박사 학위논문으로 제출함
2022년 10월

서울대학교 대학원
의과학과 생리학전공
이 형 로

이형로의 의학박사 학위논문을 인준함
2023년 1월

위 원 장 호 원 경 (인)

부위원장 이 석 호 (인)

위 원 김 상 정 (인)

위 원 이 인 아 (인)

위 원 정 민 환 (인)

Synaptic mechanisms underlying trace fear conditioning and contextual fear discrimination

By Hyoung-Ro Lee

A thesis submitted to the Department of Biomedical Sciences in
partial fulfillment of the requirements
for the Degree of Doctor of Philosophy
at the Seoul National University College of Medicine

January 2023
Approved by Thesis Committee:

Chair Won-Kyung Ho (Seal)
Vice Chair Lee Suk-Ho (Seal)
Examiner Sang Jeong Kim (Seal)
Examiner Inah Lee (Seal)
Examiner Min Whan Jung (Seal)

Abstract

Learning the association between aversive events and environmental stimuli is essential for survival. Fear conditioning, a basic form of associative learning, is one of the widely studied paradigms in behavioral psychology. Fear conditioning is divided into cued and contextual fear conditioning (CFC). Depending on the absence or presence of a time interval between conditioned stimulus (CS) and unconditioned stimulus (US), cued fear conditioning is further subdivided into delayed fear conditioning (DFC) and traced fear conditioning (TFC), respectively. Amygdala is a center for associative memory formation and expression of fear response in all forms of fear conditioning. Whereas the amygdala is sufficient for DFC, CFC and TFC requires contributions of other cortical regions such as the hippocampus, prefrontal cortex (PFC) and retrosplenial cortex. Thus, CFC and TFC provide invaluable opportunities for studying cortical functions. Most previous studies have focused on the neuronal correlates of fear conditioning, but it has not previously been investigated whether synapse specific dysfunction of plasticity has any effects on the behavior. In this thesis, I challenged this issue by investigating the behavioral consequences of dysfunction of plasticity at layer 2/3 (L2/3) to

layer 5 (L5) pyramidal cell synapses in the prelimbic (PL) area of the medial prefrontal cortex (mPFC) and perforant pathway (PP) synapses in the hippocampal CA3 and in rodents.

Sustained increased activity in PFC during trace interval in TFC is essential for acquisition of trace fear memory. However, the neurophysiological mechanisms underlying increased activity are poorly understood. Post-tetanic potentiation (PTP) was proposed as short-term plasticity that might mediate the generation of sustained increased activity during working memory. I examined the neurobiological mechanism of PTP in the PL, and tested whether PTP plays a role in sustained increased activity and TFC. Using optogenetic stimulation, I stimulated afferent fibers to L5 pyramidal neurons (PNs) in cell-type and layer-specific manner. I found that PTP was induced in the L5 corticopontine (Cpn) PNs at the synapses made by L2/3 PNs and L5 commissural (COM) PNs, but not in the L5 COM PNs. While PTP at both synapse types onto Cpn cells was inhibited by protein kinase C inhibitor, tetraphenylphosphonium (TPP), a mitochondrial Na/Ca exchanger blocker, suppressed PTP only at L2/3-to-Cpn synapses. Studying the effect of TPP infusion into the PL area on TFC, I found that TPP did not affect the trace memory formation, but reduced the maintenance of the fear memory during fear memory extinction test.

In vivo recordings revealed that c.a. 20% of PL−PNs exhibited sustained increased activity after the cessation of CS. The TPP infusion abolished such post−CS sustained increased activity during both conditioning and extinction training. In vivo calcium imaging of COM and CPn neurons during the tone test revealed that L5 CPn and COM neurons showed different proportions of activity patterns. The largest proportion of CPn cells, but not COM cells, belonged to a delay cell type that exhibited sustained increased activity from CS onset to the expected US timing. These results imply that PTP at L2/3−Cpn synapses is required for post−CS sustained increased activity during trace fear conditioning, and plays a role in maintenance of trace fear memory.

The hippocampus is important for consolidation and retrieval of contextual fear. The network process that underlies formation of distinct ensembles representing two similar contexts is called pattern separation and is one of the important functions of the hippocampus. However, the network mechanisms underlying pattern separation of neuronal ensembles in CA3 is largely unknown. Kv1.2 expression in rodent CA3 pyramidal cells (CA3−PCs) is polarized to distal apical dendrites, and its downregulation specifically enhances dendritic responses to PP synaptic inputs. It has been previously shown that haploinsufficiency of Kv1.2 (*Kcna2*+/−) in

CA3-PCs, but not Kv1.1 (*Kcna1*+/-), lowers the threshold for long-term potentiation (LTP) at PP-CA3 synapses, and that the *Kcna2*+/- mice are normal in discrimination of distinct contexts but impaired in discrimination of similar but slightly distinct contexts. I examined pattern separation of neuronal ensembles in CA3 and dentate gyrus (DG) that represent two similar contexts using in situ hybridization of immediate early genes: Homer1a and Arc. The size and overlap of CA3 ensembles activated by the first visit to the similar contexts were not different between wildtype and *Kcna2*+/- mice, but these ensemble parameters diverged over training days between genotypes, suggesting that abnormal plastic changes at PP-CA3 synapses of *Kcna2*+/- mice is responsible for the impaired pattern separation. Unlike CA3, DG ensembles were not different between two genotype mice. The DG ensembles were already separated on the first day, and their overlap did not further evolve. Eventually, the *Kcna2*+/- mice exhibited larger CA3 ensemble size and overlap upon retrieval of two contexts, compared to wildtype or *Kcna1*+/- mice. These results suggest that sparse LTP at PP-CA3 synapse probably supervised by mossy fiber inputs is essential for gradual pattern separation in CA3.

Keywords

Trace fear conditioning, Prefrontal cortex, sustained increased activity, post tetanic potentiation, Hippocampus, CA3, Perforant pathway, Pattern separation, Kv1.2.

Student number: 2015-23245

Contents

List of Figures

Chapter 1. Role of post-tetanic potentiation in persistent activity of medial prefrontal neuron during trace fear conditioning and retrieval.

Chapter 2. Gradual pattern separation in CA3 associated with contextual discrimination learning is impaired by Kv1.2 insufficiency.

CHAPTER 1

Role of post-tetanic potentiation in persistent activity of medial prefrontal neuron during trace fear conditioning and retrieval

Introduction

post-tetanic potentiation and its mechanisms in various brain regions

A form of short-term plasticity, post-tetanic potentiation (PTP), enhances the presynaptic efficacy by increasing the release probability and the readily releasable pool of the presynapse (Zucker and Regehr 2002, Lee, Kim et al. 2008, Vandael, Borges-Merjane et al. 2020). Activation of protein kinase C (PKC) has been suggested as one of the mechanisms that mediate PTP. It has been shown that calcium-dependent activation of PKC following tetanic stimulation increases vesicle calcium sensitivity by phosphorylation of Munc18 in calyx of Held and hippocampal culture (Korogod, Lou et al. 2007, Wierda, Toonen et al. 2007, Genc, Kochubey et al. 2014). However, the PKC hypothesis does not account for PTP at all synapse types, because PTP at CA3-CA1 synapses was not altered in the hippocampus of PKC triple knockout mice in which all calcium-dependent PKC isoforms were eliminated (Wang, Weyrer et al. 2016). Moreover, a variety of PKC inhibitors had no consistent effect on PTP at the calyx of Held synapses (Lee, Kim et al. 2008). These results make it controversial that calcium-

dependent PKC is the main mechanism underlying PTP in most synapse types. Another hypothesis of the PTP mechanism is mitochondrial-mediated residual calcium. It has been suggested that PTP is induced by residual calcium generated by post-tetanic mitochondrial calcium release at the presynaptic terminal (Tang and Zucker 1997, Lee, Kim et al. 2008). Mitochondria plays as calcium buffers by uptake of calcium through the mitochondrial calcium uniporter (MCU) during tetanic stimulation (TS) and subsequent post-tetanic calcium release through the mitochondrial Na/Ca exchanger (mNCX) (Giorgi, Marchi et al. 2018). As a result of the calcium-buffering action, residual calcium was generated after TS. When mitochondrial mNCX was inhibited by tetraphenylphosphonium (TPP), the magnitude of residual calcium was reduced, and PTP was impaired (Lee, Lee et al. 2007, Lee, Kim et al. 2008). In the hippocampus, mossy fiber (MF) exhibits distinct calcium dynamics depending on postsynaptic targets. MF innervates via distinct bouton morphology onto two different postsynaptic targets. One is hilar mossy cell (MF-MC), the other is hilar interneurons (MF-HI). MF innervates MC via large mossy fiber boutons (MFBs), but HI via small MFBs. Post-tetanic residual calcium correlates with the size of boutons. Therefore, mitochondrial-mediated residual calcium has a large contribution to

the MF−MC synapse while it is small to the MF−HI synapse (Lee, Lee et al. 2007). PTP was observed in cerebellum too. However, the magnitude of PTP that occurs in the cerebellum varied depending on the postsynaptic target (Beierlein, Fioravante et al. 2007). PTP has been observed at layer 2/3 (L2/3) to layer 5 (L5) and L5 to L5 synapses of the prefrontal cortex (PFC), and it was suggested that PTP may contribute to persistent activity (PA) of the PFC (Hempel, Hartman et al. 2000). However, since the PFC receives information from several areas such as the amygdala, hippocampus, and thalamus, it is difficult to know exactly where this signal comes from (what is a presynapse neuron) (Parent, Wang et al. 2010, Anastasiades and Carter 2021). In addition, two types of pyramidal neurons exist in the PFC L5. One type of neuron axon projects to the contralateral PFC (COM) and another type of neuron projects to the pons (CPn) (Dembrow, Chitwood et al. 2010). In contrast, in the PFC, the mechanism and magnitude of PTP depending on the presynaptic cell and postsynaptic−target are still unknown.

Persistent activity in prefrontal cortex

The prefrontal cortex has been studied for a long time as a crucial

cortical area responsible for working memory. In monkeys, the activity of the prefrontal cortex was maintained with an increased spiking rate after cessation of cue in the oculomotor delayed response working memory task (Goldman-Rakic 1996). The working memory performance was impaired in the study of PFC lesion (Fuster and Alexander 1971, Funahashi and Takeda 2002). In rodents, PFC is also important for working memory. When performing alternation in a T-maze, lesions of PFC group showed performance impairment (Brito, Thomas et al. 1982). In delayed alternation T or Y maze tasks, PFC cells showed increased activity during a delay period (Yang, Shi et al. 2014). In addition, an increase in cell activity during the delay period in rodents was shown in several other behavioral tasks in which a delay period is intervened, such as the reward anticipation task and trace fear conditioning (Gilmartin and McEchron 2005, Kim, Bari et al. 2021). However, cell type-specific activity during a delay period has only recently begun to be understood for different working memory tasks (Bae, Jeong et al. 2021, Kim, Bari et al. 2021), but it has not yet been resolved for trace fear conditioning. Previously, four patterns of PFC neuronal activities were observed in response to CS during TFC or subsequent extinction test: 1) transient CS onset response; 2) CS onset response with sustained activity; 3)

gradually increasing activity; 4) decreased activity (Baeg, Kim et al. 2001, Gilmartin and McEchron 2005). The post-CS activity was preferentially mediated by the 2nd and 3rd category cells. It is controversial whether cells with increased and decreased activity are distributed equally in all layers of the cortex. Kim et al (2021) showed that cell displaying increased delay activity were preferentially located in the upper part of L5 and those with decreased activity were located in the lower part of L5 from animals performing a task in which probability and reward time should be predicted depending on a type of cue (Kim, Bari et al. 2021). While this study showed that L2/3 cells did not exhibit PA during delay periods and responded only to CS, other studies, in which animals were subject to a DMS working memory task, reported any no preferential localization of delay-tuned pyramidal cells, which were found throughout L2/3 and L5 without (Fujisawa, Amarasingham et al. 2008, Ozdemir, Lagler et al. 2020), implying that the cell type-specific delay activities might be distinct depending on the attributes of a task to which an animal is subject.

Previously my lab has reported that two types of L5 pyramidal cells, CPn and COM cells, display distinct short-term plasticity, and proposed that persistent activity can be driven by the difference in STP between PC-to-PC and PC-to-IN synapses, which have

excitatory and inhibitory influences to the network activity (Yoon, Lee et al. 2020). For both post-synaptic targets that are other pyramidal cells (PCs) and fast-spiking interneurons (FS), COM cells showed higher short-term depression (STD) than CPn cells, suggesting that COM cells have higher release probability (Pr) and/or lower refilling rate of synaptic vesicle pool. While both cells exhibited higher STD at synapses onto FS than at those onto other PCs, the extent of STD was much stronger at COM-FS synapses than at CPn-FS. Because COM cells have higher Pr and larger difference in STD between synapses onto PCs and FS, COM is expected to activate an E/I balanced recurrent network more strongly than CPn. Despite the vigorosity of COM cell outputs, it should be transient because synaptic vesicles in readily releasable pool (RRP) was easily depleted at high frequency due to high Pr and low refilling rate for RRP. In contrast, CPn cells displayed milder difference in the extents of STD between synapses onto PCs and FS, and thus induced milder excitatory bias to the network, which is more favorable for sustained activity. The view was supported by the results from the computational model in which these STP patterns and balanced recurrent network were implemented (Yoon, Lee et al. 2020). Given that the connections between CPn and COM are not bi-directional but biased toward

COM-to-CPn, COM may preferentially contribute to initial activation of network upon arrival of external excitatory inputs to the network, while CPn may contribute to subsequent maintenance of network activity after cessation of the external inputs. These hypotheses, however, have not tested in vivo.

Fear conditioning and prefrontal cortex

Classically, Pavlovian fear conditioning has been widely used to elucidate the mechanism of fear memory acquisition and extinction. Auditory fear conditioning experiments are divided into two types according to the time interval between termination of the CS and US. One is delayed fear conditioning (DFC), in which the US is delivered immediately after termination of the CS without a time interval. The other is trace fear conditioning (TFC), in which the US is delivered after a time interval of tens of seconds after CS termination (Curzon, Rustay et al. 2009). Previous studies have shown that the PFC has different roles in these two types of fear conditioning.

In a previous study, to inactivate PFC in DFC, sodium channel blocker tetrodotoxin (TTX) was injected into the PFC 45 minutes prior to DFC. The freezing behavior during fear conditioning was

significantly lower in the TTX group than in the ACSF group. However, the two groups showed similar freezing behavior in response to a tone next day. These results suggest that the absence of PFC activity during DFC has no effect on the CS-US association. Additionally, the day after DFC, TTX was injected into the PFC 45 minutes before the tone test to test the role of the PFC on fear expression. In the tone test, the freezing behavior of the TTX group was significantly lower than that of the ACSF group (Sierra-Mercado, Corcoran et al. 2006, Corcoran and Quirk 2007). In another study, after DFC, $GABA_A$ agonist muscimol (MUC) was injected into PFC for inactivation and then freezing behavior was observed. When MUC was injected into the PFC infralimbic (IL) area, the freezing behavior was higher than in the saline group during the extinction test. Conversely, when MUC was injected into the PFC prelimbic (PL) area, the freezing behavior was lower than that of the saline group (Sierra-Mercado, Padilla-Coreano et al. 2011). Taken together, these results suggest that in DFC, PFC plays an important role in fear expression but is not involved in fear learning. In DFC, PFC neurons showed no response to a tone during habituation, but increased activity to conditioned tone. In addition, the increase in the PFC neuron activity during CS appeared only in the early extinction with high freezing behavior, but not in the late

extinction without freezing behavior (Burgos-Robles, Vidal-Gonzalez et al. 2009). In DFC, PFC neuron activity and freezing behavior were correlated, and as a result, PFC is an important brain area for fear expression in DFC.

Unlike DFC, in TFC, PFC is involved in fear memory formation. In a previous study, to test the role of PFC on fear memory formation in TFC, MUC or NMDA receptor antagonist (APV) was injected into the PFC 15 minutes before TFC. In the tone test performed on the next day, the MUC and APV groups showed lower freezing behavior than the saline group (Gilmartin and Helmstetter 2010). In a study using chemogenetic tools to inhibit PL or IL activity, the group that silenced the PL before TFC showed lower freezing behavior in the tone test compared to the control group. In contrast, the IL silencing group showed similar freezing behavior to the control group in the tone test. To test the role of PFC in trace fear extinction, PL or IL was silenced after TFC. In the PL silencing group, extinction was slightly accelerated, but in the IL silencing group, extinction learning was suppressed (Mukherjee and Caroni 2018). Previous studies have shown that PFC activity during the trace interval between CS and US is required for memory formation. To specifically inactivate PFC during TFC, archaerhodopsins (ArchT) was expressed and optical fibers were implanted into the

PFC PL region. During fear acquisition test, 532nm light was illuminated during the whole trial, CS, or trace interval. Illumination of light to the PL did not show any difference in freezing behavior during TFC in all groups. In the tone test the next day, the whole trial and trace interval inactivation groups had significantly lower freezing behavior than the control group and CS inactivation groups (Gilmartin, Miyawaki et al. 2013). These results suggest that PFC neuron activity during trace interval is important for fear memory formation. As mentioned above, in TFC, the PFC neurons showed sustained increased activity during the trace interval or Post-CS period (Gilmartin and McEchron 2005). A prevailing hypothesis suggest that sustained increase in the activity of PFC neurons bridge the time gap between CS and US by carrying the CS information during the trace interval and plays a key role in association of CS and US during TFC (Gilmartin, Miyawaki et al. 2013). However, the above study inactivated the PFC entirely during TFC. It remains to be understood whether persistent activity exists in a layer or cell type dependent manner. Moreover, the behavioral changes when a layer or cell type was specifically inactivated in the PFC has not been elucidated.

Aim of this study

To determine whether PTP is induced differently in a synapse type dependent manner in the PFC, cell type specific gene expression and optical stimulation were performed. In addition, mNCX blocker (TPP) and PKC inhibitor (Ro-31-8220) were used to determine the mechanism of PTP. Trace fear conditioning was performed to test whether the injection of TPP into the PFC induces behavioral impairment in trace fear conditioning. To test the change in the activity of PFC neurons when TPP is injected into the PFC during TFC, PFC neuron activity in the TPP and PBS infused group was recorded using in vivo recording experiments. Moreover, to determine whether the activity differs depending on the cell type, I expressed genetically encoded Ca^{2+}-indicator in L5 pyramidal cells of the PFC in cell-type specific manner, and imaged the PFC cell activity during the tone test after TFC.

In the present study, I found that PTP was induced differently depending on synapse types in the PFC. In addition, the mechanisms of PTP depended on the synapse types. Mitochondria was involved in PTP at L2/3 to L5 CPn synapses, but not at L5 to L5 CPn synapses. In TFC, when TPP was injected into the PFC, fear memory formation was not affected, but fear extinction was

accelerated. Furthermore, PFC neuron activity of the TPP group did not show sustained increase in the activity during trace interval and post-CS period compared to the PBS group. During the extinction training, the decrease in fear response to CS started at an earlier trial than the PBS group. In addition, the L2/3 neurons only showed a CS response without distinct persistent post-CS activity. L5 CPn and COM cells showed different proportions of activity patterns. Interestingly, largest proportion of CPn cells, but not COM cells, belonged to a delay cell type which exhibited sustained increased activity from CS onset to the expected US timing. The present study shows that PTP at L2/3 to CPn synapse is one of the important factors of persistent activity, and when persistent activity is abolished, fear memory formation is not affected but fear memory maintenance is impaired.

Materials and Methods

Slice preparation

Brain slices were prepared from 21- to 42-d-old Sprague Dawley rats or Tg2576 transgenic mice and their littermate wild-type control mice aged from 6 weeks old. Rats and mice were sacrificed after being anesthetized with isoflurane, and the brain was immediately removed and chilled in ice-cold low-calcium artificial CSF (aCSF) containing the following (in mM): 110 choline chloride, 10 glucose, 25 $NaHCO_3$, 2.5 KCl, 1.25 NaH_2PO_4, 2 Na-pyruvate, 3 ascorbate, 0.5 $CaCl_2$ and 7 $MgCl_2$ with pH 7.4 adjusted by saturating with carbogen (95% O_2, 5% CO_2). The coronal prefrontal cortex (300 μm thick) and visual cortex (300 μm thick) were prepared using a vibratome (VT1200S, Leica, Germany). Slices were recovered at 36° C for 30 minutes and after that maintained at room temperature with standard aCSF containing the following (in mM): 125 NaCl, 10 glucose, 25 $NaHCO_3$, 2.5 KCl, 1.25 NaH_2PO_4, 2 Na-pyruvate, 3 ascorbate, 2 $CaCl_2$ and 1 $MgCl_2$ with pH 7.4 adjusted by saturating with carbogen. For recording, slices were transferred to a recording chamber and circulated with standard aCSF using a peristaltic pump (MINIPLUS3, Gilson, USA). All

experimental procedures were approved by Seoul National University Institutional Animal Care and Use Committee (SNU-200831-3-3, SNU-090115-7-9).

Electrophysiological recordings

Whole-cell current clamp and voltage clamp recordings from pyramidal neurons (PNs) and interneurons (INs) in the PFC and visual cortex (VC) were performed at room temperature. These cells were visualized using an upright microscope mounted with differential interference contrast optics (BX61WI, Olympus, Japan). Electrophysiological recordings were made by the whole cell clamp technique with an EPC-10 amplifier (HEKA, Germany) or Integrated Patch Clamp amplifier (SUTTER instrument, USA) at a sampling rate of 10 kHz. Recording pipettes (3-5 MΩ) were filled with intracellular solution contained (in mM): 130 K-gluconate, 8 KCl, 20 HEPES, 4 MgATP, 0.3 NaGTP, 1 $MgCl_2$ and 0.1 EGTA with the pH adjusted to 7.3 with KOH. EPSCs were recorded from PFC and VC in a whole cell configuration at a holding potential of -65 mV. Series resistance (Rs) was regularly checked by applying a short hyperpolarization (20 ms, 2 mV). The data in which the Rs exceeded 20 MΩ or changed (>20%) during the experiment were

discarded. For electrical stimulation, I filled a glass pipettes (2-3 MΩ) with aCSF and delivered monophasic stimulus pulses (2-15 mV, 100 μs/pulse) using a stimulus isolator (A360, WPI, USA). For L2/3 stimulation, the stimulation pipette was placed in L2/3 within 300 μm from the somata of a postsynaptic L5 cell. For L5 stimulation, the stimulation pipette was placed within 50 μm laterally from the postsynaptic L5 cell somata. For PTP induction, stimulation was adjusted to evoke baseline current amplitudes of 100 pA. For baseline EPSC recording, EPSCs were evoked by paired pulses (Inter-spike Intervals: 50 ms) every 5 s 20 times. PTP was induced by tetanic stimulation (TS, 25 Hz, 125 Pulses). After TS, paired pulse stimulations were resumed for 50 times. For optic stimulation, a collimated digital micromirror device (DMD)-coupled LED (Polygon400; Mightex Bioscience, Canada) was used to deliver 470 nm illumination to a confined region for 5 ms. The area of tissue illuminated was approximately 3-8 μm in radius. Series resistance compensation, bridge balance, or liquid junction potential correction was not applied. The mNCX blocker, tetraphenylphosphonium chloride (TPP), was purchased from Sigma (218790, Sigma, USA). The Sarco/endoplasmic reticulum Ca^{2+} ATPase inhibitor, thapsigargin (T9033), and PKC inhibitor, Ro-31-8220 (557520), were obtained from Merck Biosciences (Merck,

USA).

In utero electroporation

The pregnant rats were individually housed and maintained under a normal 12/12 h light/dark cycle. The embryonic day 17 (E17) pregnant rats were used for L2/3 specific gene expression. All surgical instruments and PBS were autoclaved before use. Plasmid DNA (pAAV-CAG-oChIEF-tdtomato) was prepared at 1 mg/ml and injection was visualized by mixing plasmid DNA with Fast Green dye (0.1 mg/ml). The plasmid solution at a volume of 1-2 μl was injected into the lateral ventricle of individual embryos using a glass capillary with a sharp and long tip. After plasmid loading, each embryo was placed between 10 mm diameter tweezer-type plate electrodes (CUY65010; NEPAGENE, Japan). Electrode pulses (50 V, 50 ms) were applied five times at intervals of 150 ms controlled by an electroporator (ECM830; BEX, USA). Uterine horns were placed back into the abdominal cavity and the abdominal cavity was filled with warm sterile PBS. After surgery, the animals recovered in the infrared lamp. The pregnant rats were returned to their home cages.

Virus Injection and cannula implantation

For COM or CPn cell-specific stimulation in the PTP experiments, AAV2-retro-CMV-hSyn-oChIEF-tdTomato (1 x 10^{12} GC/ml) or AAV-DJ-CMV-hSyn-oChIEF-tdTomato (1 x 10^{12} GC/ml) were injected into the pontine nuclei (pons) or the contralateral PFC, respectively, of Sprague Dawley rats on postnatal day 14 (P14). Animals were anesthetized with 5% (v/v) isoflurane during surgery. The scalp was shaved and the animal was placed into the stereotaxic apparatus (Stoelting, USA). The scalp was disinfected with 70% (v/v) alcohol and Povidone-Iodine, and craniotomy was performed. The stereotaxic coordinates were as follows: For pons, AP -6, ML 1, DV -9; For PFC, AP 2.6, ML 0.6, DV -3.5. The virus was injected using an Ultra Micro Pump (UMP3, WPI, USA) connected to a microcontroller (MICRO2T, WPI, USA). The virus was loaded into a Hamilton syringe (7653-01; Hamilton, USA) and needle (7762-08; 28 G; Hamilton, USA). The virus solution of 1 μl was injected at a rate of 100 nl/min for 10 minutes. The injection syringe remained for 5 minutes to allow diffusion of the virus. Immediately after surgery, the animals were recovered under the infrared lamp.

For infusion of TPP or PBS into the PFC, a bilateral cannula, dummy,

and cap were implanted into the PFC (Infusion cannula: 26G, center to center: 1 mm; dummy needle: 33G; PlasticsOne, USA). After implantation, the cannula assemblies were fixed to the skull with dental cement (Poly-F plus, Dentsply Sirona, USA). After surgery, the animals recovered in the infrared lamp. Two weeks later, TPP was injected using a Hamilton syringe and infusion pump (volume: 1 μl/side; speed: 100 nl/min for 10 minutes). The injection cannula (33G, PlasticsOne, USA) was connected to the Hamilton syringe via polyethylene tubing (PE50; BD Intramedic, USA). The infusion cannula remained for 5 minutes to allow diffusion of the virus. TFC was performed 30 minutes after the injection was finished.

Axon bouton Calcium imaging

Axon bouton calcium was measured from fluorescence of Oregon Green 488 BAPTA-1 (OGB-1, ThermoFisher, USA) loaded into the PFC L2/3 and L5 cells through whole-cell patch clamp. After forming whole-cell mode, OGB-1 in the pipette was allowed to be loaded at least for 30 minutes, which was long enough for the dye to be equilibrated with its axon terminals. Calcium imaging was performed using a confocal laser-scanning system (FV1200; Olympus, Japan) and a 60x water immersion objective (numerical

aperture, 0.9; LUMPlanF; Olympus, Japan). TS-evoked fluorescence responses were imaged by scanning a small region of interest (ROI) including a bouton in XY scan mode at 1 Hz for 150 s. Scanning time per image was 0.1 s. The minimum intensity of laser power was used to minimize photobleaching. Emission light was passed 490/590 bandpass filters ahead of detection by photomultiplier tubes for green fluorescence. Calcium transients were calculated as $\Delta F/F = (F-F_0)/(F_0-F_b)$, where F_0 is baseline fluorescence and F_b is background fluorescence of OBG-1.

In a few cells, $[Ca^{2+}]$ was calculated from background-subtracted fluorescence (F) as follows:

$$[Ca^{2+}] = K_d \frac{F - F_{min}}{F_{max} - F} = K_d \frac{F/F_{max} - 1/R_f}{1 - F/F_{max}} \qquad (1)$$

, where dynamic range (R_f) = F_{max}/F_{min}, and F_{max} value was measured during the experiment from a maximum value in the fluorescence induced by high-frequency stimulation (50 Hz, 125 pulses). The R_f was determined *in vitro* using intracellular solution plus 10 mM Ca^{2+} or 10 mM EGTA. The R_f was estimated as 11.35. The dissociation constant (K_d) of OGB-1 is 206 nM, referring to my lab's previous report (Lee, Lee et al. 2007).

Measurement of mitochondrial membrane potential

The mitochondrial membrane potential ($\Delta\Psi_m$) was assessed by the tetramethylrhodamine (TMRE, Invitrogen, USA). The brain slices were transferred to a chamber containing aCSF in which TMRE was diluted to a final concentration of 50 nM and continuously supplied with carbogen. Brain slices were loaded with TMRE for 30 minutes in the dark at 37° C. TMRE fluorescence imaging was performed using a confocal laser-scanning system (FV1200; Olympus, Japan) and a 60x water immersion objective (numerical aperture 0.9, LUMPlanFl, Olympus). TMRE fluorescence was imaged by scanning in XY scan mode at 1 Hz for 300 s. Scanning time per image was 0.15 s. The image size was 124 μm x 124 μm. TMRE were excited by a 559 nm laser and emission light was passed 575/675 bandpass filters ahead of detection by photomultiplier tubes for red fluorescence. 1 μM carbonyl cyanide 4-(trifluoromethoxy) phenylhydrazone (FCCP, Merck, USA) was applied at 150 s of recording time to dissipate the $\Delta\Psi_m$. The FCCP-sensitive TMRE fluorescence (ΔF_{TMRE}) was calculated as $\Delta F_{TMRE} = F_{aCSF} - F_{FCCP}$, where F_{aCSF} is TMRE fluorescence in the aCSF and F_{FCCP} is TMRE fluorescence after FCCP application.

Fear conditioning

The fear conditioning was performed in Context A which is a rat conditioning cage (H10-11R-TC, Coulbourn Instruments, USA) located inside a sound-attenuating box (SCITECH, Korea) with a LED lamp. The auditory cue was presented via a speaker module (H12-01R, Coulbourn Instruments, USA) located on one side of the conditioning chamber. The floor of the conditioning cage consisted of stainless steel bars to deliver a footshock (H10-11R-TC-SF; Coulbourn Instruments, USA). Two types of Context B were used for the tone test depending on the type of experiments. One is a behavior test after TPP or PBS infusion, in which the freezing behavior was monitored (Context B). The other is an in vivo recording experiments that recorded not only the freezing behavior but also in vivo neuronal activity (Context B'). Context B used for the behavior test was hexagonal (32 x 34 x 50 cm) and consisted of a white acrylic floor and wall located in the floor of the isolated room. The auditory cue was delivered through speakers located on either side of Context B. Context B' used for in vivo recording experiments was rectangular (36 x 21x 25 cm) and consisted of a black plastic floor and glass wall with blue paper on the outside, and was located inside a sound-attenuating box. The conditioning

chamber was cleaned with a 70% ethanol solution, and the tone test chamber was cleaned with ammonia (1%). In TFC (day 1), the rats received five CS–US pairings (TPP–infusion experiments) or three habituation tones (2.5 kHz, 20 s, 75 dB) followed by eight CS–US pairings (in vivo recording experiments). The CS–US pairing consisted of tones (2.5kHz, 20 s, 75 dB) and a footshock (0.7 mW, 1 s). CS and US are separated by 20 s trace interval. In DFC, rats received five CS–US pairings (TPP–infusion experiments). CS–US pairing of DFC consisted of tone presentations (2.5kHz, 20 s, 75 dB) that coterminated with footshocks (0.7 mA, 1 s). The intertrial interval of the fear conditioning was 180 ± 20 s. The next day, in the tone test (day 2), the rats received twenty presentations of tones (20 s, 2.5 kHz, 75 dB) in context B. The intertrial intervals of tone presentations were 90 ± 20 s. The behavior was recorded with a CCD camera. For TPP–infusion experiments, TPP or PBS was delivered to the PFC PL or IL area using an infusion cannula connected to a Hamilton syringe. TPP or PBS was infused 30 minutes before the conditioning or extinction test. To quantify freezing behavior, a python–based open source code ezTrack (Pennington, Dong et al. 2019) was used. The parameters we used for this analysis were a motion cutoff of 10~25, a freezing threshold of 30, and a minimum freeze duration of 30 samples.

Drive and electrodes

An in vivo electrode drive (shuttle drive) was built according to Voigts et al (2020) with modifications (Voigts, Newman et al. 2020). The drive was constructed by combining a bundle of 16 stereotrodes, a 3D-printed body, and an electrode interface board (EIB). Stereotrodes were made by folding, twisting, and heating the Formvar-coated nichrome wire. (761000, A-M systems, Netherlands). An electrode interface board (EIB) consisted of a connector (A79026-001, Omnetics, USA) and an open-source printed circuit board (PCB, SCITECH, Korea). Individual stereotrode wires were connected to the EIB with gold pins (OPES-7013, Open Ephys, Portugal). For the TPP infusion experiment, a 26-gauge stainless tube was passed through the hole in the middle of the EIB and the center of the 3D-printed body. The EIB was attached to the 3D-printed body and then glued with epoxy. A stainless steel wire soldered with skull screws was connected to the ground and reference holes of the EIB using gold pins. Before the surgery, a bundle of stereotrodes cut with sharp scissors was gold-plated to lower the impedance to 200-300 kΩ.

Shuttle drive and GRIN lens implantation

Rats were anesthetized with 5% (v/v) isoflurane. After the hair was removed, rats were moved into a stereotaxic apparatus (Stoelting, USA). the scalp was disinfected with 70% (v/v) alcohol and Povidone-Iodine. After the scalp was incised, the skull surface was cleaned using H_2O_2 and the craniotomy site was marked (PFC AP 2.6, ML 1.6, DV -3.5, Angle 16°). Then, a circular 1-mm-diameter craniotomy was made. A stereodrodes bundle of hand-made drives was slowly lowered to a depth of 3.5 mm. A ground screw was placed in the skull at the cerebellum area and a reference screw was placed in the skull at the olfactory bulb area. The surface of the skull was covered with dental cement (Super-Bond C&B, Sun Medical, Japan). Then, the shuttle drive was fixed on the head using dental cement (Poly-F plus, Dentsply Sirona, USA). Immediately after surgery, the animals recovered under the infrared lamp.

GRIN lens implantation was performed in two alternative ways depending on the use of silk fibroin. 1) AAV2-Cre was injected into the pons or contralateral PFC, and flex-GCaMP6f was injected into the PFC; One week later, a 1 mm or 0.6 mm GRIN lens was implanted in the PFC. 2) AAV2-Cre was injected into pons or contralateral PFC; One week later, after applying the flex-GCaMP6f virus to the GRIN lens using silk fibroin, the lens was implanted in

the PFC. The virus was injected for 10 minutes using a Hamilton syringe and an Ultra Micro Pump with a Micro Controller (volume 1ul, speed 100 nl/min). A week after the virus injection, a GRIN lens was implanted. In the first method, the lens was sterilized with 70% ethanol and implanted. In the second method, the lens was sterilized with UV light. Then, the virus was applied to the lens surface that enters the brain using silk fibroin (Merck, USA). After mixing flex-GCaMP6f virus ($1x10^{13}$ GC/ml) and silk fibroin in a 1:1 ratio, 1 μl of the mixture was applied to the surface of the lens and dried at room temperature for at least 1 hour. The animals were anesthetized and fixed in the stereotaxic again and a circular 1-mm-diameter craniotomy was made. Superficial cortical tissue was gently aspirated with the tip of a 22-gauge blunt needle connected to a vacuum source. After this, a 1.0 mm or 0.6 mm-diameter GRIN lens (Inscopix, USA) was lowered slowly to a depth of 3.5 mm while constantly washing the craniotomy site with sterile PBS. The surface of the skull was covered with dental cement (Super-Bond C&B, Sun Medical, Japan). Then, the GRIN lens was fixed on the head using dental cement (Poly-F plus, Dentsply Sirona, USA). Immediately after surgery, the animals recovered under the infrared lamp. To avoid surgery-related tissue swelling, rats were injected with dexamethasone (1 mg/kg) for one week after surgery.

Unit recording and data processing

One week after drive implantation, the rats were subject to TFC. The rats were placed in the laboratory for 15 minutes before TFC for acclimation. The 32-channel RHD recording headstage (C3314, Intan, USA) was connected to the Omnetics connector of the drive. PFC activity was recorded using Open Ephys software (Open Ephys, Portugal) and an RHD interface board (RHD USB interface board, Intan, USA). The headstage and RHD interface board were connected with a thin serial peripheral interface (SPI) cable (C3213, Intan, USA). All in vivo recordings were performed at a sampling rate of 30 kHz. A bandpass filter from 500 to 5000 Hz was used to remove background noises. The recording session was 34 minutes during the fear conditioning and 42 minutes during the tone test. The behavior of rats was recorded by CCD camera. The in vivo recording and tone presentations were synchronized using Bonsai software (Bonsai Foundation). After finishing the in vivo recording, a 30 μA current was applied to each stereotrode for 8 s to locate the position of the tip of stereotrodes bundle. Brains were extracted and post-fixed for 24 h in the 4% PFA. The coronal prefrontal cortex (300 μm thick) was prepared using a vibratome and imaged with a fluorescence microscope (IX53, OLYMPUS, Japan).

For spike sorting, I modified a Matlab software package published in github (https://github.com/nghorbani/NeuralDataAnalysis). Before in vivo recording data were subject to spike sorting, I concatenated the in vivo recordings of each trial from −20 s to +60 s when the onset time of tone in each trial was zero. Spike waveforms were detected by amplitude thresholding. The standard deviation (σ) of noise was calculated as median absolute deviation (MAD) of filterd signal divided by 0.6754 (Zlokolica, Pizurica et al. 2006), and the signal larger and smaller than the 5 σ was classified as a spike. The 12 and 30 data points before and after the peak of each spike was collected into a spike wavelet matrix. I refined the list of automatically detected spike waveforms by excluding spikelet such that the valley/peak amplitude ratio was greater than 0.8 or the peak amplitude was greater than 1000 μV. Next, the spikelet waveform matrix (time x spikes) was suject to principal component analysis (PCA) to extract three principal features of spikelets. The extracted features were plotted on the coordinate of three principal components, to which a Gaussian mixture model was fitted for clustering using split−and−merge expectation−maximization (SMEM) algorithm (Ueda, Nakano et al. 2000). For further manual sorting, I used MatClust software (Mattias Karlsson, 2022). To discriminate cells with increased activity during CS, first 5 tirals

were averaged, and the z-score of the firing rate was calculated with reference to the baseline firing rate.

In vivo Calcium imaging and data processing

After a 3-week virus expression period, rats were subject to TFC. The next day after TFC, the rats were placed in the experimental room for about 15 minutes for acclimation, and then the Miniscope (V4; Open Ephys, Portugal) was docked to the baseplate to record calcium signal. Calcium signals were recorded using open-source Miniscope DAQ software (Aharoni Lab, UCLA) and Miniscope. The Miniscope and DAQ were connected with a flexible coax cable, and the calcium signal was transmitted to the data acquisition system (DAQ) through the cable and saved on a personal computer. The frame rate, LED power, gain, and focus were also controlled using the Miniscope DAQ software. The calcium activity was recorded at 25 frames per second at a resolution of 600 × 600 pixels (LED intensity 2-15; gain 2.5-3.5). The behavior of rats was recorded by CCD camera. The calcium imaging and tone presentations were synchronized by Bonsai software (Bonsai Foundation). To reduce the decrease in fluorescence intensity due to photobleaching, calcium signal was not recorded in the entire behavioral experiment,

but was recorded separately for each trial. Calcium signal recording was started 30 s before the onset of the cue and was recorded for 110 s. To confirm the expression site of GCaMP6f and the location of GRIN lens implantation, brains were extracted and post-fixed for 24 h in the 4% PFA after finishing experiments. The coronal sections of prefrontal cortex (300 μm thick) were prepared using a vibratome and imaged with a fluorescence microscope.

The calcium imaging videos were down-sampled from 600x600 pixels to 300x300 pixels using ImageJ software (NIH, USA). The 5 trials of down-sampled calcium imaging videos were concatenated using ImageJ software and saved as one TIF file. The processed calcium imaging data were motion-corrected using NoRMCorre (Pnevmatikakis and Giovannucci 2017) implemented in MATLAB. After down-sampling and motion correction, I processed the image data uisng a constrained non-negative matrix factorization algorithm optimized for microendoscopic data (CNMF-E; Zhou, Resendez et al. 2018). The data was filtered with a gaussian kernel with a width of 4 pixels (gSig), and neurons were constrained to a diameter of 15 pixels (gSiz). A ring model (bg_model) was used for the background with a radius of 18 (ring_radius). Neurons with spatial overlap greater than 0.2 (merge_thr) and centroid distance less than 10 pixels (dmin) were merged. Only ROIs with a minimum

peak-to-noise ratio of 15 (min_pnr) and minimum spike size of 5 (smin) were extracted. The foopsi deconvolution method by CNMF-E was employed in all datasets. Not all ROIs classified by CNMF-E could be considered as neurons and some might be dendrites or background fluctuations. Therefore, all neurons were visually inspected, and those that displayed non-neuronal morphology were removed. Further data analysis was performed using the inferred spiking activity (neuron.S). After converting a non-zero value to 1 in the inferred spiking activity value (binarized spike activity), 5 trials were averaged to reduce trial-to-trial variability of neuron activity pattern. To differentiate CS and PA cells, which displayed increased activity during CS and during post-CS, respectively, I adopted a test for comparing two Poisson means (Krishnamoorthy and Thomson 2004), because the distribution of most ISIs followed an exponential distribution. The z value for ISIs during CS and post-CS periods versus baseline was calculated as follows:

$$Z = \frac{\hat{\lambda}_2 - \hat{\lambda}_1}{\sqrt{\frac{\hat{\lambda}_1}{N_1} + \frac{\hat{\lambda}_2}{N_2}}} \qquad (2)$$

, where $\hat{\lambda}_1$ is the mean of ISIs during baseline; $\hat{\lambda}_2$ is the mean of ISI during CS or Post-CS; N is the sample size of each period. Cells

with the z value of the Poisson mean test greater than 1.96 ($p < 0.05$) for CS and post-CS period were classified as CS cells and PA cells, respectively.

For PA cells and CS cells selected by the Poisson mean comparison test, the z score of firing rate in each cell was calculated with reference to the baseline firing rate. The z scores of all PA cells or CS cells were averaged and binned by 10 s. The binned z scores were subject to Hilbert transformation to compute the instantaneous amplitude, which was used for comparison of activity pattern over a trial between PA and CS cell (Figure 20e).

To classify the activity patterns of PL cells with increased activity during CS and/or post-CS intervals (union of CS and PA cells), the matrix (cell x time) comprised of Gaussian-filtered time series of binarized inferred spiking activity was subject to nonnegative matrix factorization (NMF) with three components. After multiplying each weight (W) with the peak coefficient of corresponding basis function, the COM and CPn activity patterns were divided into three groups according to the phase at which the peak activity was found.

Statistics

Data were analyzed with Igor Pro 7 (Wasvemetrics, USA), SPSS (IBM, USA), Prism (GraphPad, USA) and MATLAB (Mathworks, USA). The two-tailed Wilcoxon rank-sum test (Mann-Whitney U test) was used to compare independent groups. The Wilcoxon matched-pairs signed rank test was used for two paired groups. The Kruskal-Wallis H test, was used to compare three independent groups. For freezing behavior, repeated measures two-way ANOVA followed by Fisher's least significant difference tests were used to compare samples. A chi-square test was used to compare the proportions of neuronal activity patterns (Figure 21c). The level of statistical significances was indicated as follows: n.s., not significant ($p > 0.05$), *$P < 0.05$, **$p < 0.01$, ***$p<0.001$, ****$p<0.0001$. All data in the figures are presented as the mean ± standard error of mean (SEM).

Results

The mechanisms of PTP in PFC depend on cell type and layer

PTP has been proposed as one of mechanisms underlying persistent network activity in a recurrent network or as a mechanism that holds information without persistent activity (Hempel, Hartman et al. 2000, Mongillo, Barak et al. 2008). PTP occurs at synapses on layer 5 pyramidal neurons in the PFC, but the presynaptic cell of the synapse exhibiting PTP has not been identified in the previous study (Hempel, Hartman et al. 2000). Moreover, while CPn and COM cells comprise the L5 PNs, it is unknown whether the PTP mechanisms and/or magnitude depend on the postsynaptic target cell types. I induced PTP by stimulating different layers at two post-synaptic targets: corticopontine (CPn) and commissural (COM) in PFC layer 5 (L5) (Dembrow, Chitwood et al. 2010). To distinguish CPn and COM cells, I measured the input resistance (R_{in}) and sag ratio of each neuron (Figure 1a, b). Plotting each cell on the plane of R_{in} vs Sag ratio indicated two distinct clusters (Figure 1c). According to Dembrow et al (2010), I regarded the cells that displayed relatively smaller R_{in} and a larger sag ratio as

CPn, and the other as COM ($P < 0.0001$ for CPn vs COM; Figure 1b). After identifying the type of L5 PNs in the PL area of medial prefrontal cortex (mPFC), I recorded the baseline EPSCs evoked by field stimulation of layer 2/3 (L2/3) or layer (L5) using paired pulses (interspike interval (ISI), 50 ms) every 5 s, and then induced PTP by tetanic stimulation (TS, 25Hz, 125 pulses) (Figure 1d). I found that, for stimulation of either layer (L2/3 and L5), PTP occurred only when the post-synaptic target was CPn and not when the post-synaptic target was COM ($P = 0.0003$ for L2/3-CPn vs L2/3-COM; $P = 0.0003$ for L5-CPn vs L5-COM; Figure 1e, f, i). I tested whether PTP occurs at the synapses of L2/3 to L2/3-PNs and those of L2/3 to L5 interneuron (IN) synapse in the PFC PL. PTP did not occur in any of these synapses. (Figure 1 g, h, i).

Previously PKC activation and post-tetanic mitochondrial calcium release (MCR) have been suggested as mechanisms underlying PTP. PKC, activated by increased calcium upon repetitive stimulation, may enhance the calcium sensitivity of vesicle fusion through phosphorylation of Munc18 (Korogod, Lou et al. 2007, Wierda, Toonen et al. 2007, Genc, Kochubey et al. 2014). Additionally, post-tetanic MCR induced PTP through an increase in release probability at the hippocampus and calyx of Held synapses (Lee,

Lee et al. 2007, Lee, Kim et al. 2008). To determine the mechanism underlying PTP at excitatory synapses onto CPn, I tested the effects of 2 μM Ro-31-8220 and 2 μM tetraphenylphosphonium (TPP) that are inhibitors of PKC and mitochondrial Na/Ca exchanger (mNCX), respectively. At the L2/3-CPn synapses, PTP disappeared after application of either TPP or Ro-31-8220 ($P = 0.0037$ for L2/3-CPn vs L2/3-CPn_TPP; $P = 0.0011$ for L2/3-CPn vs L2/3-CPn_Ro-31-8220; Figure 2a, b), whereas at the L5-CPn synapses, PTP was abolished by Ro-31-8220, but not by TPP (TPP, $P = 0.4174$; Ro-31-8220, $P = 0.0016$; Figure 2c, d). To test whether TPP and Ro-31-8220 affect short-term plasticity (STP) in these synapses, I measured the peak EPSC amplitudes in CPn cells during 25Hz train stimulation of L2/3 or L5 in the presence of TPP or Ro-31-8220, and found that STP was not changed in either the L2/3-CPn or L5-CPn synapse (Figure 2e, f).

To test whether PTP is unique to the PL area, I performed above experiments in the PFC infralimbic (IL) area and the primary visual cortex (VC) (Figure 3a, d). Similar to the PFC, the VC L5-PNs are divided into two cell types: CPn-like type 1 cells projecting to the superior colliculus and COM-like type 2 cells projecting to the contralateral VC (Molnar and Cheung 2006). Similar to L5 cells in

the mPFC, the type 1 cells in VC have a smaller R_{in} and a higher sag ratio than type 2 cells (Larkman and Mason 1990, Mason and Larkman 1990, Kasper, Larkman et al. 1994). The type 1 cells had a greater sag ratio than type 2 CVC, but the difference in R_{in} between the two cell types was not significant ($P < 0.0001$ for SC vs CVC sag ratio; Figure 3a–c). Therefore, SC and CVC were distinguished based on the sag ratio difference. PTP was not induced by TS of L2/3 in either of type 1 or type 2 cells (Figure 3d, e). Next, I performed the above experiments in CPn cells of the PFC IL region (Figure 3f). Whereas PTP was induced by TS of IL L2/3, unlike the PL area, PTP was not affected by TPP application (Figure 3g, h). These results suggest that mechanism of PTP differs depending on the brain area, and that mitochondria play a role in PTP specifically at the L2/3 to CPn synapses of PL area.

PTP occurring in PFC is due to local connections and not inputs to other brain regions

Above results were obtained by field stimulation using a monopolar electrode placed on L2/3 or L5. In these experiments, the presynaptic cells cannot be identified, because each layer is

innervated by many different afferent fibers especially from thalamus and from other cortical and subcortical areas (DeNardo, Berns et al. 2015). For stimulation of identified synapses, I expressed oChIEF in PNs of a specific layer and then confirmed the layer-specific connection through light stimulation. To express oChIEF specifically only in L2/3 PNs, I transfected neural progenitor cells with plasmids encoding oChIEF in E17 using in utero electroporation (Figure 4a). Concerning the possibility that the electrical properties of cells may be altered by expression of oChIEF through in utero electroporation, I compared the properties of cells in which oChiEF was expressed and not. I found no difference between the two cell groups in R_{in}, resting membrane potential, action potential threshold and sag ratio (Figure 4b). In the slice in which L2/3 PNs expressed oChIEF, I repeated above experiments using opto-stimulation (473 nm, 5 ms light pulse) instead of electrical stimulation (Figure 4c). Similar to electrical stimulation of L2/3, optical tetanic stimulation (oTS) of L2/3 PNs induced PTP in L5 CPn cells, but not in L5 COM cells. PTP at L2/3-CPn synapses was abolished by both TPP and RO-31-820. ($P = 0.0016$ L2/3-CPn vs L2/3-CPn_TPP, $P = 0.0016$ L2/3-CPn vs L2/3-CPn _Ro-31-8220; Figure 4d, e, f). In contrast, TPP and RO-31-8220 did not affect the STP at L2/3-CPn synapses

(Figure 4g).

Next, to examine PTP at identified L5-to-L5 synapses, retrograde AAV encoding oChIEF was injected into the pontine nucleus (Pons) or the contralateral mPFC, which expressed oChIEF in CPn or COM cells, respectively, two or three weeks later (Figure 5a, d). The oTS of CPn cells did not induce PTP in either of postsynaptic CPn and COM cells (Figure 5b, c). In contrast, when the COM cells were stimulated, PTP was induced only when the post-synapse target was CPn, consistent with the results from electrical stimulation. (Figure 5e, g). Moreover, PTP at COM-CPn synapses was not significantly affected by TPP application (Figure 5f, g), indicating that the presynaptic cells responsible for PTP induction at L5-L5 synapses are COM cells. Moreover, these results confirmed that mitochondria are involved specifically at L2/3-to-CPn synapses. I measured the peak EPSC amplitudes in COM-CPn synapses during 25Hz oTS in the presence of TPP, and found that STP was not changed in COM-CPn synapse (Figure 5h).

Mitochondria-mediated residual calcium exists in axon terminals of L2/3 PNs and L5 COM cells but not

in L5 CPn cells

It has been previously shown that presynaptic residual calcium resulting from post-tetanic MCR is responsible for mitochondria-mediated PTP at hippocampal and calyx of Held synapses (Lee, Lee et al. 2007, Lee, Kim et al. 2008). Our results indicate that PTP can be induced at the synapses of COM or L2/3 PNs to CPn cells, but not when presynaptic cells were CPn cells. To test the correlation between the expression of PTP and mitochondria-mediated residual calcium, I loaded L2/3 PNs, COM or CPn cells with an intracellular solution containing OGB-1 (50 μM) via a patch pipette, and then imaged TS-evoked calcium transients (CaTs) at axonal bouton of each cell type before and after TPP application (Figure 6a). The amount of post-tetanic residual calcium (Ca_{res}) was quantified as the area of a CaT above the baseline measured 5 s after TS, at which the fast decay phase ended. The amount of Ca_{res} at the bouton of L2/3 PNs was significantly larger than that of COM or CPn cells (Figure 6b-e). Moreover, Ca_{res} were reduced by TPP at boutons of L2/3 PNs, ($P = 0.0079$ for L2/3 vs L2/3_TPP; Figure 6b, e) but not at those of CPn cells (Figure 6c, e). Contrary to our expectations, TPP-sensitive Ca_{res} was observed in COM cells ($P = 0.0006$ for COM vs COM_TPP Figure 6d, e). The amount

of TPP-sensitive Ca_{res}, however, was significantly larger at L2/3 PN compared to COM cells (P = 0.0451 for L2/3 vs COM; Figure 6e). Moreover, the amounts of Ca_{res} in the presence of TPP were not different among three cell types (P = 0.7006 for three TPP group; Kruskal-Wallis test), suggesting that post-tetanic MCR is responsible for the larger amount of Ca_{res} at the bouton of L2/3 PNs.

Given that mitochondria make close contact with ER membrane (Csordas, Varnai et al. 2010), mitochondrial Ca^{2+} may be transferred into ER via Ca^{2+} microdomain near the contact sites without an increase in cytosolic global [Ca^{2+}]. To test possible involvement of ER in less TPP-sensitive Ca_{res} in axonal boutons of CPn cells, I treated thapsigargin (TG) 2 μM, which blocks ER calcium uptake, and then measured post-tetanic Ca_{res} in CPn and COM cells. However, TG did not alter the TPP-sensitive Ca_{res}, suggesting that the lack of TPP-sensitive Ca_{res} in L5 CPn cells was not due to ER calcium uptake (Figure 7).

These results show that TPP-sensitive Ca_{res} was not found in the putative presynaptic boutons of CPn cells, at which PTP did not occur, and that L2/3-PNs and COM cells exhibited larger post-tetanic Ca_{res} at the putative presynaptic terminals, at which PTP occurred. Consistent with larger effects of TPP on PTP at L2/3-

PNs, the amount of Ca_{res} in L2/3-PNs was larger than that in L5 COM cells, suggesting close correlation of TPP sensitivity of PTP and Ca_{res}.

L2/3-Cpn synapse PTP did not occur in early Alzheimer's model mouse

A previous study from our laboratory showed that mitochondrial calcium clearance was impaired in the early age of Alzheimer mouse model (Lee, Kim et al. 2012). Given that mitochondria play a key role in PTP at L2/3-to-CPn synapses, I tested whether PTP is impaired at these synapses in the young adult Tg2576 mice (6 weeks old). Frist, I estimated mitochondrial membrane potential (Ψ_m) using tetramethylrhodamine ethyl ester (TMRE) in the PL L2/3 PNs of B6/SJL (WT) and Tg2576 mice. The TMRE intensity of L2/3 PNs was significantly lower in Tg2576 than that in B6/SJL ($P = 0.0004$ for B6/SJL vs Tg2576; Figure 8a, b). Next, I tested the occurrence of PTP at L2/3-CPn synapses of B6/SJL and Tg2576. L2/3-CPn synapse PTP could be induced in B6/SJL but not in Tg2576 ($P = 0.0173$ for B6/SJL vs Tg2576; Figure 8d, f). Similar to the rats, PTP at L2/3-CPn synapses of B6/SJL was abolished by

TPP application (P = 0.003 for B6/SJL vs B6/SJL_TPP; Figure 8e, f). These findings suggest that PTP at L2/3−CPn synapse of B6/SJL mice was mediated by mitochondrial Ca_{res}. Next, I examined Ψ_m in L5−PNs. The mitochondrial TMRE signals of the PL L5 PNs were smaller in Tg2576 than in B6/SJL, suggesting less negative membrane potential in mitochondria of L5 neurons in Tg mice (P = 0.0006 for B6/SJL vs Tg2576; Figure 9a, b). I was able to induce PTP in L5−CPn synapses of both genotype mice, and PTP was not sensitive to TPP (Figure 9d, e, f), suggesting that PTP in the WT and Tg mice occurs in mitochondria−independent manner similar to rats. Therefore, the abnormal Ψ_m in PL PNs of Tg mice impaired PTP specifically at L2/3−CPn synapses, but not at L5−CPn synapses.

These results support my findings from rat experiments that mitochondria play a critical role in PTP specifically at L2/3−CPn synapses.

PTP in the PFC affected the fear extinction circuit

Previously, PTP has been proposed as a mechanism underlying network activity in a recurrent network that persists even after

cessation of excitatory external afferent inputs to the network (called as ‘persistent activity’, PA) (Hempel, Hartman et al. 2000). Whereas PTP has been observed at many different synapse types (Hempel, Hartman et al. 2000, Beierlein, Fioravante et al. 2007, Lee, Lee et al. 2007, Lee, Kim et al. 2008), the role of PTP in network information processing is not understood. Especially, it has not been studied whether PTP contribute to PA. To address this question, I examined the effects of TPP on trace fear conditioning (TFC) and network activity associated with TFC. In this task, animals should associate CS (tone) and US (shock), which are presented in 20 s interval. It has been suggested that persistent activity occurs in the PFC during TFC, which is important for fear memory acquisition by connecting CS and UCS, because suppressing the activity of the PFC during trace impaired fear memory acquisition (Gilmartin and McEchron 2005, Gilmartin, Miyawaki et al. 2013). Before examining how PTP at PFC L2/3–CPn synapses affects TFC, I tested whether TPP has any effect on the electrical properties of neurons by recording the properties of L2/3 PCs, L5 PCs, and L5 INs over time after applying 2 μM TPP. I found no difference in input resistance, AP threshold, and RMP in any cell types (Figure 10). Next, I tested whether L2/3–CPn PTP disappears in the animals subjected to injection of TPP into PFC. To

this end I installed an infusion catheter into the PL area of mPFC and injected 1 μl PBS containing 20 μM TPP (Figure 11). In the animals injected with PBS, L2/3-CPn PTP was inducible regardless of the injection site distance. In the TPP group, PTP was not induced within the area 300 μm from the injection site, while PTP was induced outside the area (Figure 12).

To examine the behavioral consequences to TPP injection into the PL area, I infused PBS or TPP 30 minutes before trace fear conditioning on day 1 (D1), and compared freezing behavior between the two groups (Figure 13a). On D1 rats were subject to five TFC trials with pseudo-random intertrial intervals between 160 and 200 s. The TPP group showed a freezing behavior similar to the PBS group during the training of TFC (Group X Period : $F_{(5,90)}$ = 0.336; P = 0.8899 ; Figure 13b). On the following day (D2), both groups were presented ten times with a tone alone to explore the time course for extinction of conditioned fear (extinction test). As shown in Figure 13c, the TPP group showed accelerated extinction of conditioned fear compared to the PBS group (Group X Period: $F_{(10,160)}$ = 3.244; P = 0.001; Figure13c). Whereas the freezing ratio did not reach 40% until the 10th trial, that of PBS group began to be lower at the 4th trial and reached this asymptote level already at 6th trial (P = 0.046 for PBS vs TPP trial 4; P = 0.009 trial 5;

Figure 13c). It should be noted, however, that the freezing behavior of the TPP group was similar to that of the PBS group for first three trials, suggesting that acquisition and retrieval of fear memory were not affected, but the extinction was accelerated by TPP infusion.

Although TPP did not affect the fear memory acquisition, it is possible that dormant effects of TPP exerted during the training might be uncovered during the extinction test. To test this possibility, I injected TPP into the PL area 30 minutes before the extinction test on D2, and then freezing behavior was measured (Figure 13d). Similar to the results of TPP was injection on D1, there was no difference in freezing ratio between PBS and TPP groups during training of TFC (Group X Period: $F_{(5,70)}$ = 0.1509; P = 0.9791; Figure13e). In the extinction test, the freezing behavior of the TPP group began to decrease earlier compared to the PBS group (P = 0.005 for PBS vs TPP trial 5; P = 0.001 for PBS vs TPP trial 6; Figure 13f), supporting my view that TPP has an effect specifically on a network process related to extinction of conditioned fear memory.

In the above ex vivo experiments, PTP also occurred in the L2/3 to CPn synapse in the IL area, similar to PL, but was not affected by TPP. To determine whether the accelerated extinction in the TPP

group was due to impaired PTP at L2/3-to-CPn synapses in the PL area or other side effects of TPP, TPP was injected into the IL area 30 minutes before the extinction test, and then freezing behavior was observed (Figure 14a). Unlike the PL-TPP group, the IL-TPP group showed the similar freezing behavior as the PBS group in both fear acquisition and extinction tests (Group X Period: $F_{(5,50)}$ = 0.1965; P = 0.1002 for PBS vs TPP in D1; $F_{(10,70)}$ = 1.526; P = 0.1487 for PBS vs TPP in D2; Figure 14b, c). In summary, TPP injection into the PL of PFC did not affect the fear memory formation through CS-UCS association, but impaired maintenance of fear memory, resulting in the acceleration of fear memory extinction.

Different from TFC, CS is temporally contiguous to US in delayed fear conditioning (DFC, Figure 14d). The PFC plays a role in TFC, but not in DFC (Gilmartin and Helmstetter 2010). To rule out a possibility that the acceleration of fear memory extinction is caused by an adverse effect of TPP on the network process not related to TFC, I tested whether TPP has any effect on DFC. To this end, TPP or PBS was injected 30 minutes before DFC on D1 into the mPFC, and then observed fear responses during DFC (Figure 14d). As shown in Figure 14e, the TPP group showed no significant difference from the PBS group in delayed fear acquisition and fear

extinction (Group X Period: $F_{(5,30)}$ = 0.6306; P = 0.6778 for PBS vs TPP in D1; Group X Period: $F_{(10,60)}$ = 0.4864; P = 0.8924 for PBS vs TPP in D2; Figure 14e, f). These results suggest that TPP suppresses fear memory maintenance, consequently accelerating fear memory extinction through altering a network process related to TFC. My results obtained from in vitro studies shown above suggest that PTP at L2/3–CPn synapses is involved in this network process.

The persistent activity of prelimbic neurons was abolished by TPP infusion into the PFC

It has been previously shown that the PL neuronal activity increased and exhibited various activity patterns during CS and trace intervals of TFC and subsequent CS alone trials (Gilmartin and McEchron 2005). In addition, the PL neuronal activity during CS was highly correlated with the conditioned freezing during CS alone trials (Burgos–Robles, Vidal–Gonzalez et al. 2009). Numerous studies support the paralleled changes of PL activity and conditioned freezing behavior (Burgos–Robles, Vidal–Gonzalez et al. 2009, Gilmartin, Miyawaki et al. 2013, Gilmartin, Balderston et al.

2014). To examine the effect of TPP on the PL activity during TFC, I implanted the tetrode or stereotrode into the PFC PL area for in vivo recording, and recorded the spike activity of the PL neurons, which were sorted off-line through principal component analysis (PCA). To use only putative pyramidal neurons in further analysis, spikes with a spike width greater than 200 μs and a firing rate less than 15 Hz were classified (Figure 15a). Before recording of PL activities on D1, TPP or PBS was injected into the PL area of rats. The animals were allowed to be habituated to the conditioning chamber and CS (denoted as CS-only trials in Figure 15), and then subject to eight TFC trials with pseudo-random intertrial intervals between 160 and 200 s. PL neuronal activities binned over 1 s were expressed as z scores of firing frequencies with reference to the pre-CS baseline frequencies. The z-scores were averaged over 5-11 trials. Time series of z scores for exemplar PL neurons are displayed in the descending order of CS activities (PBS, animal = 1, n = 40; TPP, animal = 2, n = 39; Figure 15b). To compare the differences in neuron activity between the two groups, neurons with increased activity during CS (CS-responsive cells) were selected from each group, and z scores in each trial were averaged over the CS-responsive cells (PBS, animal = 5, n = 22/112; TPP, animal = 4, n = 12/76; Figure 15c). During first two trials of TFC as well as

the habituation trials, PFC neurons did not respond to CS (Figure 15c). Afterwards, PL neuronal activities of the PBS group showed distinct responses to CS and the increased activity was sustained during the trace interval (Figure 15c). Similar to the PBS group, the PL neuron activity of the TPP group showed no activity change to CS in the habituation session and first two TFC trials, and then responded to CS during subsequent TFC trials (Figure 15d). Distinct from the PBS group, however, the PL activity during CS (CS response) was not maintained in the TPP animals. Moreover, the persistent activity during the trace interval was not observed in the TPP group (Figure 15d, e). The means of z-scores over trials 5 to 11 during first 10 s of CS presentation did not differ between the two groups, and that during second half of CS period in the TPP group became lower than PBS group and first half of CS period in TPP group ($P = 0.2721$ for PBS ($n = 22$) vs TPP ($n = 12$) first 10 s of CS; $P < 0.0001$ for PBS vs TPP second 10 s of CS; $P = 0.0042$ for TPP CS (21~30 s) vs TPP CS (31~40 s); Figure 15e). During the trace interval, the difference in z scores were significantly lower in the TPP group compared to the PBS group ($P=0.0003$, Figure 15e).

On the next day (D2), I examined the PL neuronal activities during extinction trials, in which animals were presented with CS alone 20

times with pseudo-random intervals in a different context from D1. Spike activities of both groups during the tone test were averaged over 1-5 trials, and the z-score was calculated with reference to the pre-CS baseline activity to sort and display the activity during CS in descending order (PBS, animal = 1, n = 45; TPP, animal = 1, n = 44; Figure 16a). To compare the differences in neuron activity between the two groups, neurons with increased activity during CS were selected from each group, and their z scores were averaged (PBS, n = 25/153; TPP, n = 15/101). The PL neurons in PBS-injected animals responded to CS until the 7th trial, and then the responses decreased to the baseline over next 3 trials (Figure 16b, e). The PL activities averaged over first five trials are shown on the right of Fig. 16b and Fig. 16c for the PBS and TPP groups, respectively. The responses of PL neurons in the TPP-injected animals sustained only for 10 s from the CS onset (Figure 16c). Moreover, post-CS activity was not observed in the TPP group as in trace fear extinction session (P = 0.0088 for PBS vs TPP post-CS 41~60 s; Figure 16a-d). Because of significant difference between the z scores over the first and second 10 s of CS (P = 0.0008 for TPP CS (21~30 s) vs TPP CS (31~40 s); Figure 16d), I regarded the PL activity for the first 10 s of CS as the CS response in the TPP group (Figure 16e). Comparing the time course of CS

response and post-CS activity changes over trials in two group animals, I found that the CS response started to decrease already on the 6th trial in the TPP group, whereas it did on the 8th trial in the PBS group, and the post-CS activity in the PBS group started to decrease on the 4th trial, but post-CS activity in the TPP group was not observed ($P = 0.023$ for PBS vs TPP CS response (trial 7); $P = 0.001$ for PBS vs TPP CS response (trial 8); $P = 0.015$ for PBS vs TPP post-CS activity (trial 2); $P = 0.011$ for PBS vs TPP post-CS activity (trial 3); Figure 16e). Such expediting the trial number at which the prelimbic CS response started to decline was in parallel with the acceleration of fear extinction in the TPP group (Figure 13c), demonstrating a close correlation of TPP effects on the prelimbic CS responses with that on fear responses during the extinction test.

For first a few trials of the extinction test, the TPP effects on PL activity were consistent with those in the fear acquisition test on D1. Whereas TPP did not affect early CS response, it shortened the CS response and abolished the persistent PL activities during the second half of CS as well as during the trace interval. As long as CS was associated with US on D1, such inhibition of PA did not alter the CS response. When CS alone was repeatedly presented, however, lack of PA was followed by accelerated decrease in the

CS response, implying that PA may be necessary for maintaining CS response during the CS alone trials.

PFC L2/3 neurons showed CS responses alone without post-CS activity in trace fear extinction test

Prefrontal neurons exhibit differential CS responses and post-CS activities depending on the cortical layer. While L2/3 neurons exhibited CS response alone without post-CS PA, most neurons with PA resided in the L5 upper layer (Kim, Bari et al. 2021). Given that most neurons with PA are located in L5 and that TPP affects specifically PTP at L2/3-to-L5 synapses, I hypothesized that PTP at PFC L2/3-CPn synapse may contribute to persistent activity in L5. To confirm that post-CS persistent activity does not occur in the PFC L2/3 during TFC, the steretotrode bundle was placed at the PFC L2/3 and then L2/3 activity was recorded (Figure 17a). Similar to the previous study, L2/3 showed CS responses alone without PA during the trace fear extinction test (Figure 17b, c). It was noted that the mean frequency of L2/3 neurons activity during CS was 5 Hz, not 25 Hz (Figure 17c). In the above ex vivo experiments, PTP was evoked by 25 Hz tetanic stimulation in a 2 mM Ca^{2+} at room

temperature, so these experiments do not guarantee actual occurrence of PTP in vivo conditions. Therefore, it is necessary to test whether actual L2/3 activity recorded in vivo can induce PTP at L2/3-CPn synapses. A histogram of interspike interval (ISI) was drawn by selecting one cell whose activity increased to 5 Hz during CS. In both baseline and CS, most ISIs were shorter than 200 ms (Figure 17d, e), suggesting that the firing pattern of PL L2/3 neurons is random and follows a Poisson process. The plot of instantaneous frequencies (1/ISI) during CS shows that increase in the neural activity during CS is mostly ascribed the increase in burst firings (Figure 17f). I tested whether PTP is induced by such burst-type stimulation in ex vivo, and, if so, whether PTP is suppressed by TPP. Among the neurons obtained from in vivo recording, the activity pattern of cells that were fired at 5 Hz during CS was used as a train template for stimulation of afferent fibers from L2/3 (Figure 18a). To mimic in vivo conditions, recordings were done at 32℃ with aCSF containing 1.3 Ca^{2+}. Under these conditions, PTP could be induced at L2/3-CPn synapses (Figure 18b). When TPP was applied, PTP did not completely disappear as in the above ex vivo data, but the PTP magnitude was significantly reduced ($P = 0.0078$ for PBS vs TPP; Figure 18b, c). These results suggest that PTP at L2/3-CPn synapses would occur in the in vivo

conditions, and TPP may affect the occurrence of persistent activity by reducing the magnitude of L2/3-CPn PTP.

Persistent activity occurs specifically for CPn neurons

Above results show that TPP reduced both PTP at L2/3-CPn synapses and PA in the PL area. If these two TPP effects are causally related to each other, I hypothesized that the cell-type displaying PA should belong to CPn cells. To test this hypothesis, I recorded cell type-specific activity during extinction test. To this end, I injected AAV encoding flex-GCaMP6f into the PFC and retro-AAV encoding Cre into Pons or contralateral PFC in order to express GCaMP6f specifically in CPn and COM cells, respectively (Figure 19a-c). As expected CPn cells were labeled only in L5, and COM cells were expressed throughout the layers (Figure 19b). On the next day after TFC, the activity of each cell type was recorded during the extinction test to determine which cells exhibited persistent activity. The calcium spike data were analyzed using CNMF-E (Figure 19f-e). After converting the inferred spiking activity to 0 or 1, the all-or-none type spike activities were

averaged over first 5 trials, and the z-score was calculated to sort and display the activity during CS in descending order (Figure 20a). To determine whether neuronal activity during a given period is distinct from the baseline, I adopted a test for comparing two Poisson means, because most distribution of ISIs followed an exponential distribution (Krishnamoorthy and Thomson 2004). Using this method, I calculated z values for ISIs during CS and post-CS periods (30 – 50s and 50 – 70s, respectively). Cells with the z value of the Poisson mean test greater than 1.96 ($p < 0.05$) for CS and post-CS period were classified as CS cell and PA cell, respectively. The proportions of PA cells and CS cells in COM cells were comparable to those of CPn cells. (PA cell: 169/411, CS cell: 236/411, PA+CA cell: 126/411 non-response cell: 132/441 in COM cell; PA cell: 66/165, CS cell: 86/165, PA+CS cell: 50/165, non-response cell: 63/165 in CPn cell; Figure 20b). The z-score of cell activities were averaged over each of PA and CS cells, and shown in Figure 21c-d. Moreover, the instantaneous amplitudes of the averaged traces of PA cell and CS cell activities in COM and Cpn cells were calculated using Hilbert transform and binned over 10 s to compare the activity of COM and CPn neurons during trace fear extinction (Figure 20e). Hilbert transform calculates a 90° phase shift version (imaginary part) of original trace (real part), and

combination of the two parts allows us to calculate instantaneous amplitude of the trace.

Looking into the averaged activity patterns of COM and CPn cells, I found that the CPn cell activity was more fluctuating than COM cell activity, suggesting that the CPn cell activities are more desynchronized compared to those of CPn cells (Figure 21c). Both COM-PA and CPn-PA cells largely exhibited two activity peaks during a trial (Figure 21c, e). While the first peak of PA cell activity corresponded to the CS onset in both cell types, the second peak of COM cell activity preceded that of CPn cells (Figure 21e). While COM-PA cell displayed a second increase in the activity just after the CS offset ($P = 0.041$ for COM-PA vs CPn-PA 50~60 s; Figure 20e upper). While COM-PA cell activity decreased afterwards, CPn-PA cells displayed a delayed increase in the activity and peaked at the expected time of US, resulting in significantly higher activity of CPn-PA cells compared to COM around the expected US time ($P = 0.045$ for COM_PA vs CPn_PA 80~90 s; $P = 0.027$ for COM_PA vs CPn_PA 90~100 s; Figure 20e upper). Despite the fluctuation of averaged activity, the post-CS trough activities still remained above the baseline, suggesting that both COM and CPn cells contribute to post-CS activity. It is notable, the second peak of CPn cell activity corresponded to the expected timing of US

presentation (70 s) (Figure 21e), implying CPn cells might carry temporal information for US presentation. As expected from the large conjunction between PA and CS cells, the activity pattern of CS cells during CS in each cell type was similar to that of PA cells of the corresponding cell type. The COM-CS cell activity increased transiently after the onset of CS without no further increase in the activity afterwards, whereas CPn-CS cells exhibited delayed increase in activity (Figure 20d-e). (P = 0.042, 0.037, 0.008 for COM_CS vs CPn_CS 40~50, 70~80, 80~90 s; Figure 20e lower).

According to previous studies, the neuronal activity of PFC during trace fear conditioning showed several patterns, such as cells displaying an increase at CS onset and then gradually decrease in firing, and cells with a gradual increase in activity during CS (Baeg, Kim et al. 2001, Gilmartin and McEchron 2005), implying that PA cells might be a combination of the above two cell patterns. To further classify the activity patterns of PL cells with increased activity during CS and/or post-CS intervals (union of CS and PA cells), the matrix (cell x time) comprised of Gaussian-filtered time series of binarized inferred spiking activity was subject to nonnegative matrix factorization (NMF) with three components. For both COM and CPn cells, the NMF yielded three basis functions whose peaks are located at around CS onset, CS offset and during

post-CS period. The weights on each basis function were normalized by the coefficients equalizing the peak amplitude of three basis functions. I clustered COM and CPn cells into three groups depending on the type of basis function with the highest weight: CS onset, CS offset, and delay cells (Figure 21a, b). The proportions of Cs onset, CS offset and delay cells in COM and CPn cells are shown in Figure 21c. The activity patterns of each cell types are shown by mean z score or binarized inferred spiking activity of firing rate averaged over cells of each group (Figure 21d-f). For both COM and CPn cells, the activity of CS onset cell of both peaked at CS onset, but the peak activity timing was slightly different between COM and CPn cells. Most COM cells belonged to CS onset or CS offset cells [37.3% (110/279) and 39.4% (104/279), respectively], and post-CS cells occupied a minority of COM cells (23.3%, 65/279; Figure 21c). In contrast, the largest proportion of CPn cells belonged to delay cells, which displayed sustained increased activity from CS onset and peaked at the expected US timing (43.1%, 44/102). The rest belonged to CS onset (27.5%, 28/102) and CS offset cell (29.4%, 30/102; Figure 21d-f). In summary, the sustained activity from CS offset to the expected timing of US is preferentially mediated by CPn neurons in TFC, and that the activity of COM neurons is rather transient and

concentrated around CS onset and CS offset. These results imply that COM cells behave like a differentiator responding onset and offset of sensory inputs with high interest, and CPn cells behave like an integrator encoding the temporal information, which may be necessary for predicting the timing of US.

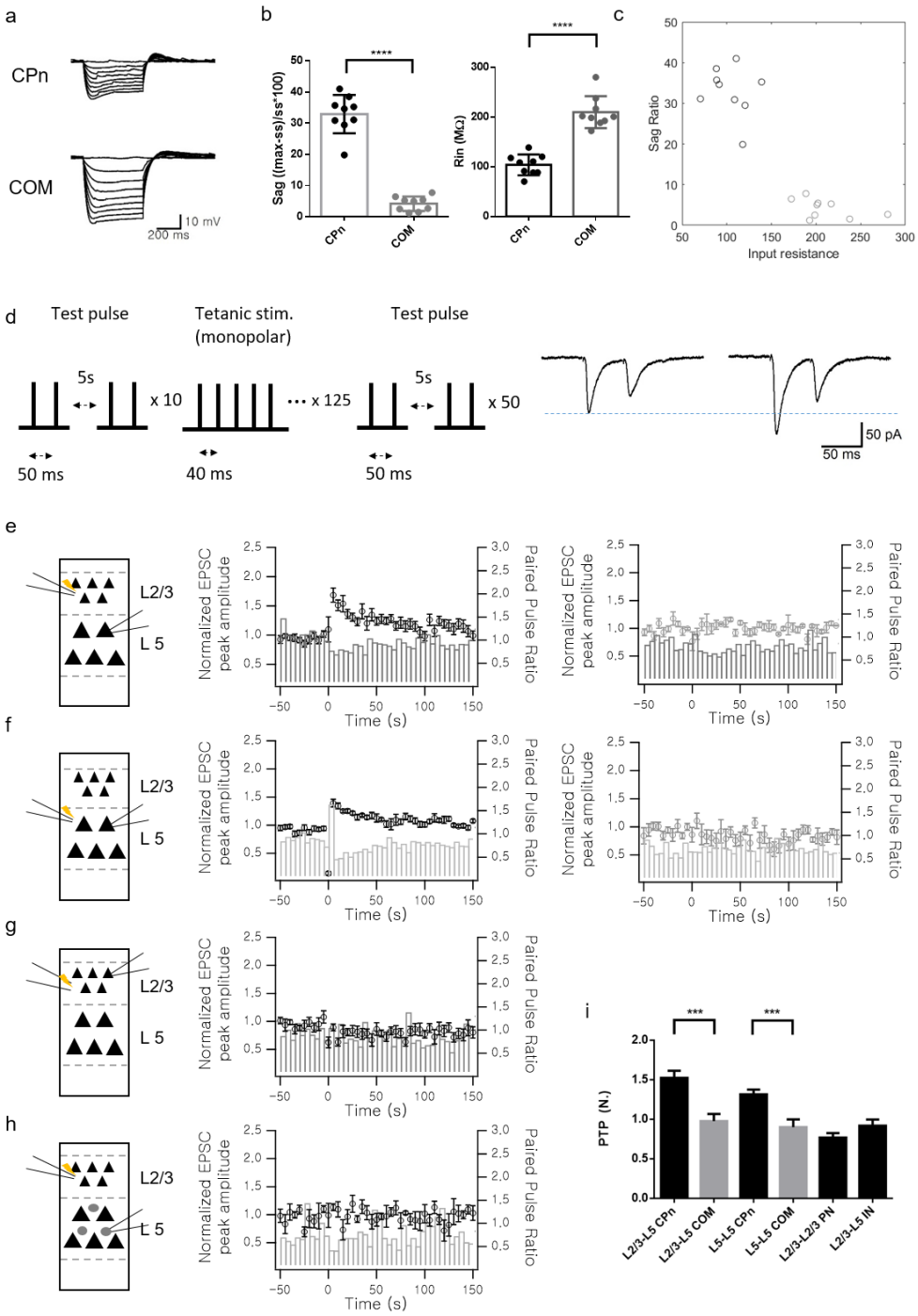
a
CPn
COM
10 mV
200 ms
b
Sag ((max-ss)/ss*100)
Rin (MΩ)
****
CPn
COM
c
Sag Ratio
Input resistance
d
Test pulse
Tetanic stim.
(monopolar)
Test pulse
5s
x 10
x 125
5s
x 50
50 ms
40 ms
50 ms
50 pA
50 ms
e
f
g
h
L2/3
L 5
Normalized EPSC peak amplitude
Paired Pulse Ratio
Time (s)
i
PTP (N.)
***
***
L2/3-L5 CPn
L2/3-L5 COM
L5-L5 CPn
L5-L5 COM
L2/3-L2/3 PN
L2/3-L5 IN

Figure 1. PTP was induced in a synapse type-specific manner. (a-c) Identification of CPn and COM cells by intrinsic properties. **(a)** Representative voltage responses of CPn and COM cells to hyperpolarizing current steps. **(b)** Mean sag ratio and input resistance (R_{in}) in the two cell types. CPn cells (n = 9) showed a larger sag ratio (*left*; $P < 0.0001$ for CPn vs COM sag ratio) and a smaller R_{in} (*right*; $P < 0.0001$ for CPn vs COM R_{in}) than COM cells (n = 9). **(c)** K-mean clustering of two cell types on the plane of Sag ratio vs R_{in} (CPn = black circles; COM = gray circles). **(d)** Scheme of tetanic stimulation (TS) protocol and representative EPSCs before and after TS. EPSCs evoked by paired pulses were recorded 10 times for the baseline EPSC amplitude (interspike interval (ISI), 50 ms) every 5 s, and then induced PTP by TS (25 Hz, 125 pulses). After TS, paired pulse stimulations were resumed for 50 times (*left*). Representative paired pulse EPSCs (*right*; dotted blue line, baseline EPSC peak amplitude). **(e-i)** Layer and postsynaptic-target specific PTP induction. *Left*, Scheme of experiments show the location of patch clamp pipette and monopolar stimulation glass electrode. *Middle* and *Right*, Time courses of baseline-normalized EPSC amplitudes before and after TS which was applied at t = 0. **(e)** Post-synaptic target-dependent PTP induction at L2/3-L5 synapses. PTP at L2/3-L5 synapses

was induced when postsynaptic-target was CPn (n = 15; normalized EPSC peak amplitude = black circle; paired pulse ratio = bar; *middle*), but not when postsynaptic target was COM (n = 5; normalized EPSC peak amplitude = gray circle; paired pulse ratio = bar; *right*). **(f)** Postsynaptic-target dependent PTP induction at L5-L5 synapse. PTP at L5-L5 synapse was induced only when the postsynaptic-target was CPn (n = 8; *middle*), but not postsynaptic target was COM (n = 7; *right*). **(g)** PTP at L2/3-L2/3 synapses was not induced (n = 9; *right*). **(h)** PTP at L2/3-L5 IN synapses was not induced (n = 8; *right*). **(i)** Summary bar graphs for normalized PTP. PTP was evoked at L2/3-CPn and L5-CPn synapses but not at L2/3-COM and L5-COM synapses (n = 15, 5, 8, 7, 8, 9); P = 0.0003 for L2/3-CPn vs L2/3-COM; P = 0.0003 for L5-CPn vs L5-COM). All data are mean ± S.E.M., ****P < 0.0001, ***P < 0.001, Mann-Whitney test.

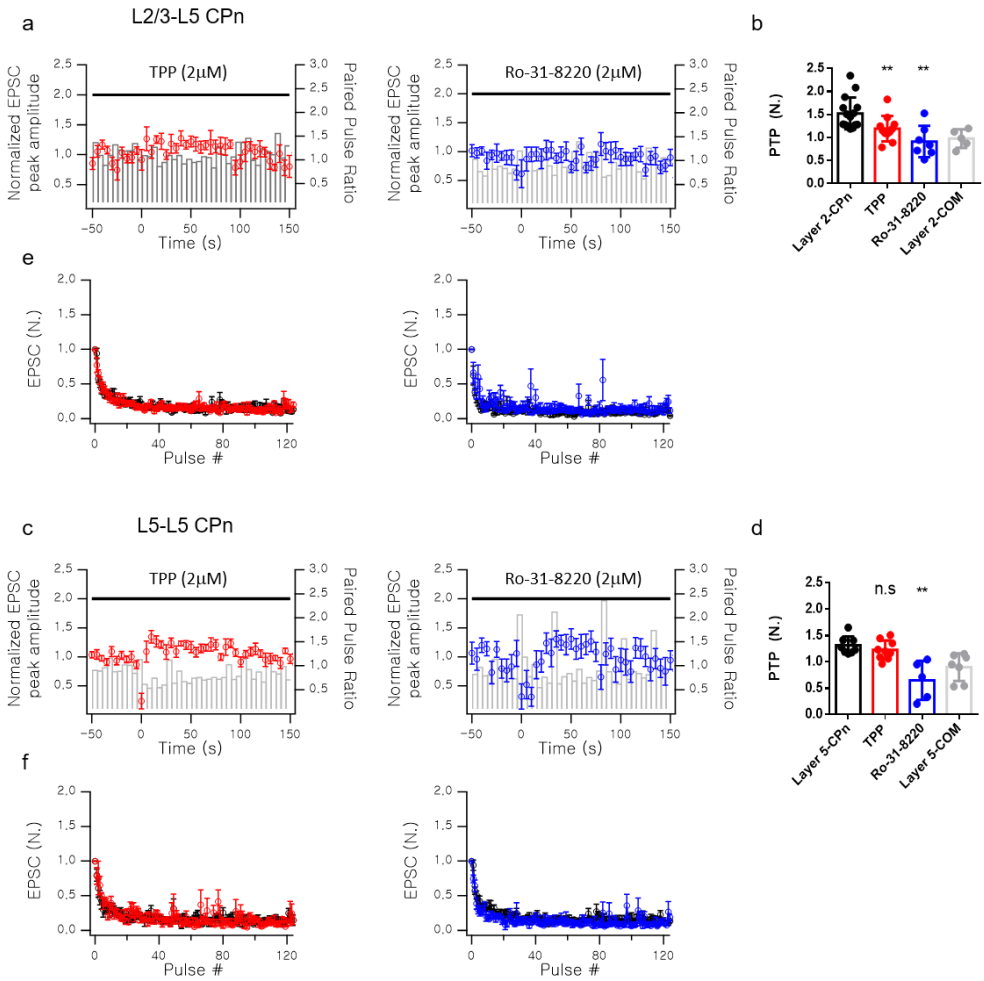

Figure 2. Mitochondria and PKC are differentially involved in PTP depending on presynaptic cell types. (a–b) Effects TPP (blocker of mitochondrial Ca2+ release) and Ro-31-8220 (PKC inhibitor) on PTP at L2/3-CPn synapses. **(a)** PTP at L2/3-CPn synapses was abolished by 2 μM TPP application (n = 11; normalized EPSC peak amplitude = red circle; paired pulse ratio = bar; *left*), and by 2 μM Ro-31-8220 application (n = 7; normalized EPSC peak amplitude = blue circle; paired pulse ratio = bar; *right*). **(b)** Summary bar

graph for the drug effects on PTP at L2/3-CPn synapses (n = 15, 11, 7, 5; P = 0.0037 for L2/3-CPn vs L2/3-CPn_TPP; P = 0.0011 for L2/3-CPn vs L2/3-CPn_Ro-31-8220). **(c-d)** Effects TPP and Ro-31-8220 on PTP at L5-CPn synapses. **(c)** PTP at L5-CPn synapses was not affected by TPP (n = 9; *left*), but was impaired by 2 μM Ro-31-8220 (n = 5; right). **(d)** Summary bar graph for the drug effects on PTP at L5-CPn synapses (n = 8, 7, 9, 5; P = 0.4174 for L5-CPn vs L5-CPn_TPP; P = 0.0016 for L5-CPn vs L5-CPn_Ro-31-8220). **(e-f)** Normalized amplitudes EPSCs evoked by TS at L2/3-CPn and L5-CPn synapse. **(e)** Neither TPP (*left*) nor Ro31-8220 (*right*) affected STP of EPSCs evoked by TS at L2/3-CPn synapse. **(f)** Both drugs dose not affect STP of TS-evoked EPSCs at L5-CPn synapse. All data are mean ± S.E.M., **P < 0.01, Mann-Whitney test. n.s = not significant.

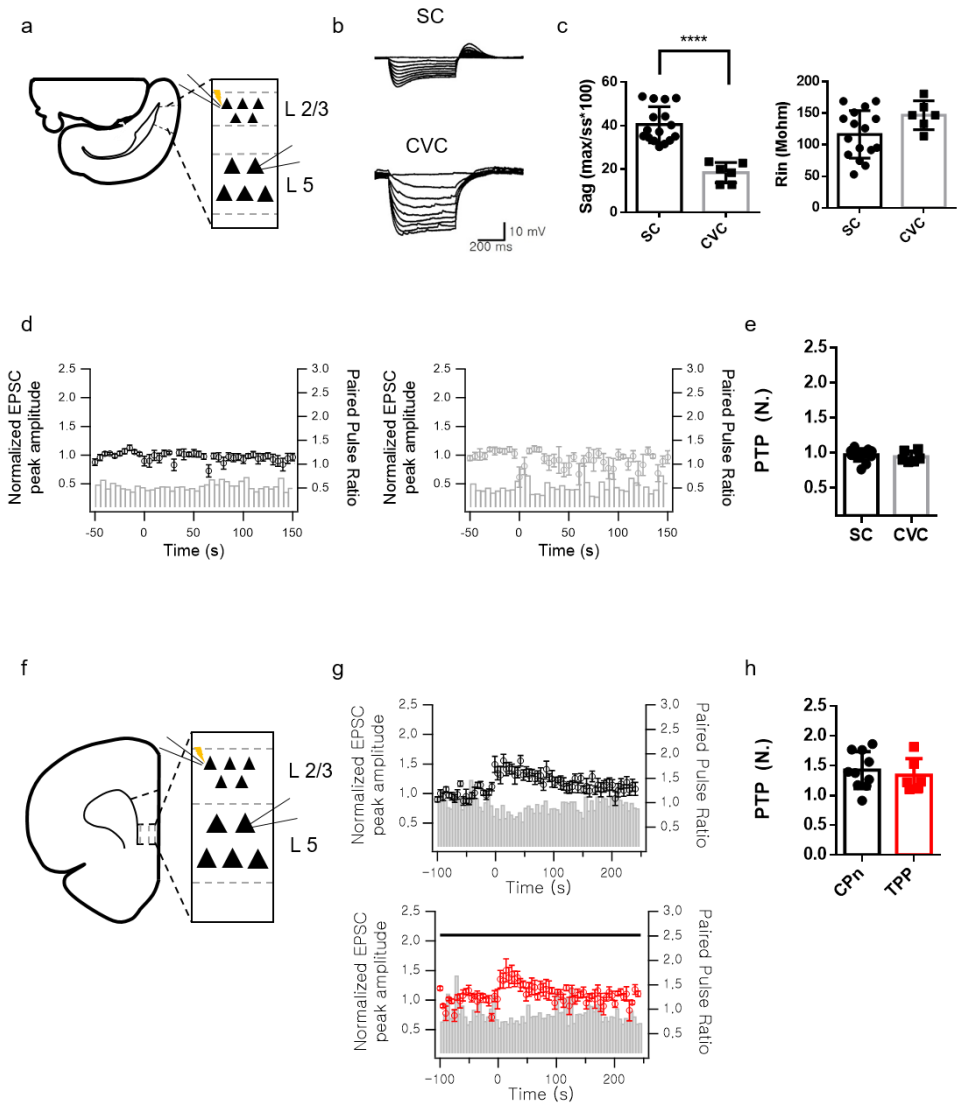

Figure 3. PTP was not induced by TS of L2/3 in L5 neurons in the visual cortex. whereas PTP was induced by TS of IL L2/3, PTP was not affected by TPP. (a-e) PTP induction at L2/3-L5 synapses in VS. (a) Scheme of experiments shows the location of patch clamp pipette and monopolar stimulation glass electrode in VC. (b) Representative voltage responses of SC and CVC cells to hyperpolarizing current steps. (c) Mean sag ratio and input

resistance (R_{in}) in the two cell types. SC cells (n = 16) showed a larger sag ratio (*left*; P < 0.0001 for SC vs CVC sag ratio) than CVC cells (n = 6). The mean of R_{in} of SC cells (n = 16) was slightly smaller than CVC cells (n = 6) but it was not significant (*left*; P < 0.1113 for SC vs CVC R_{in}). **(d)** Time courses of baseline-normalized EPSC amplitudes before and after TS which was applied at t = 0. PTP was not induced by TS of L2/3 in L5 neurons in the VC. PTP at L2/3-L5 synapses in VC was not induced when postsynaptic-targets were SC (n = 16; normalized EPSC peak amplitude = black circle; paired pulse ratio = bar; *letf*) and CVC (n = 6; normalized EPSC peak amplitude = gray circle; paired pulse ratio = bar; *right*). **(e)** Summary bar graphs for normalized PTP in VS (n = 16, 6; P = 0.494 for SC vs CVC). **(f-h)** Induction of PTP by TS of L2/3 in L5 of PFC IL. **(f)** Scheme of experiments show the location of patch clamp pipette and monopolar stimulation glass electrode in IL. **(g)** Time courses of baseline-normalized EPSC amplitudes before and after TS which was applied at t = 0. PTP at L2/3-CPn synapses in IL was induced by TS (n = 10; normalized EPSC peak amplitude = black circle; paired pulse ratio = bar; *upper*). PTP at L2/3-CPn synapses in IL was abolished by 2 μM TPP application (n = 6; normalized EPSC peak amplitude = red circle; paired pulse ratio = bar; *lower*). **(h)** Summary bar graphs for normalized PTP in IL. (n = 10, 6; P = 0.4683 for PTP vs TPP). All data are mean ± S.E.M., ****P < 0.0001, Mann-Whitney test.

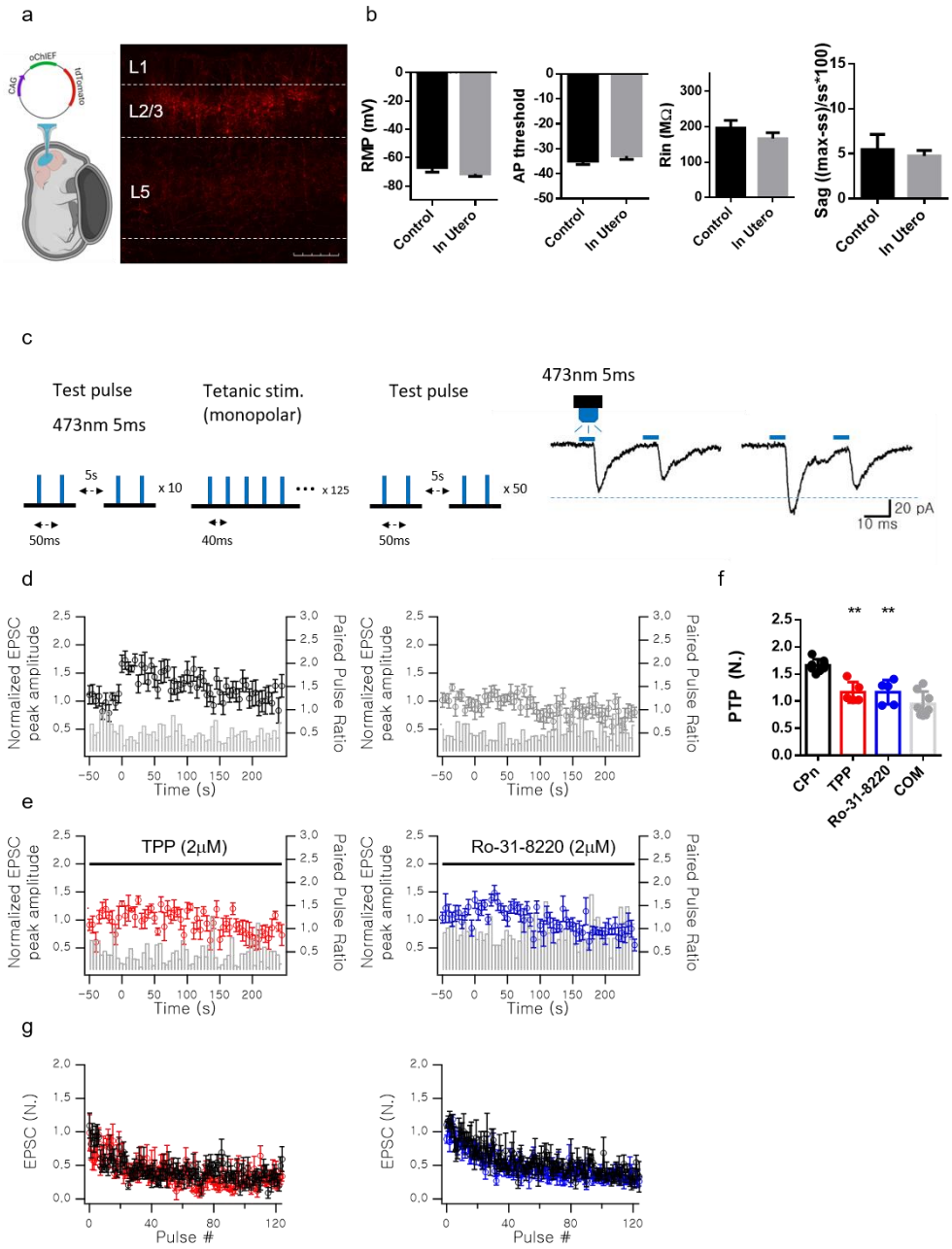

Figure 4. The optical tetanic stimulation (oTS) of L2/3 PNs induced PTP in L5 CPn cells, but not in L5 COM cells. (a) Scheme of experiments shows the injection of the plasmid (CAG-oChIEF_tdTomato) into the ventricle of an embryo for in utero

electroporation (*left*). *Right*, Representative image of oChIEF_tdTomato expression specifically only in L2/3 PNs using in utero electroporation. Scale bar, 200 μm. **(b)** Mean resting membrane potential (RMP), action potential threshold (AP threshold), input resistance (R_{in}) and sag ratio in the two cell types in which oChiEF was expressed and not. All cell properties were not different between the two groups (n = 6, 6; P = 0.3052 for control vs DNA expressing cell RMP; P = 0.2381 for control vs DNA expressing cell AP threshold; P = 0.1638 for control vs DNA expressing cell R_{in}; P = 0.5221 for control vs DNA expressing cell Sag ratio). **(c)** Scheme of optical tetanic stimulation (oTS) protocol and representative EPSCs before and after oTS. EPSCs evoked by LED optical stimulator (wavelength: 473 nm; pulse width: 5 ms) were recorded 10 times for the baseline EPSC amplitude (interspike interval (ISI), 50 ms) every 5 s, and then induced PTP by oTS (wavelength: 473 nm; pulse width: 5 ms, 25 Hz, 125 pulses). After TS, paired pulse stimulations were resumed for 50 times (*left*). Representative paired pulse EPSCs (*right*; dotted blue line, baseline EPSC peak amplitude). **(d)** Time courses of baseline-normalized EPSC amplitudes before and after oTS which was applied at t = 0. PTP at L2/3-L5 synapses was induced by oTS when postsynaptic-target was CPn (n = 8; normalized EPSC peak

amplitude = black circle; paired pulse ratio = bar; *middle*), but not when postsynaptic target was COM (n = 8; normalized EPSC peak amplitude = gray circle; paired pulse ratio = bar; *right*). **(e)** PTP at L2/3−CPn synapses was abolished by 2 μM TPP application (n = 5; normalized EPSC peak amplitude = red circle; paired pulse ratio = bar; *left*), and by 2 μM Ro−31−8220 application (n = 5; normalized EPSC peak amplitude = blue circle; paired pulse ratio = bar; *right*). **(f)** Summary bar graph for the drug effects on oTS−evoked PTP at L2/3−CPn synapses (n = 8, 5, 5, 8; P = 0.0016 for L5−CPn vs L5−CPn_TPP; P = 0.0016 for L5−CPn vs L5−CPn_Ro−31−8220). **(g)** Normalized amplitudes EPSCs evoked by oTS at L2/3−CPn synapse. **(e)** Neither TPP (*left*) nor Ro31−8220 (*right*) affected STP of EPSCs evoked by oTS at L2/3−L2/3 synapse. All data are mean ± S.E.M., **P < 0.01, Mann−Whitney test.

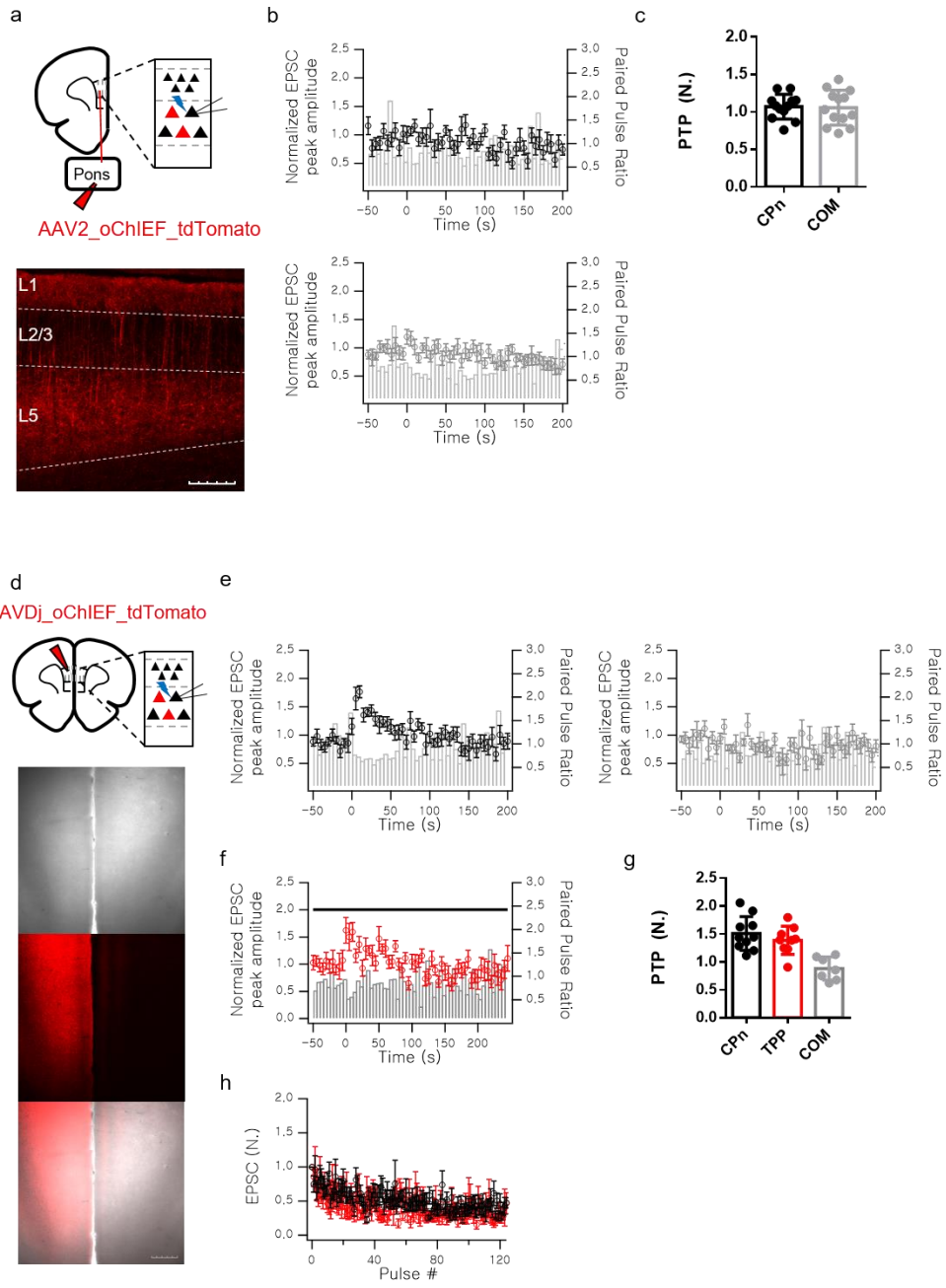
a
Pons
AAV2_oChIEF_tdTomato
L1
L2/3
L5
b
Normalized EPSC peak amplitude
Paired Pulse Ratio
Time (s)
c
PTP (N.)
CPn
COM
d
AAVDj_oChIEF_tdTomato
e
f
g
PTP (N.)
CPn
TPP
COM
h
EPSC (N.)
Pulse #

Figure 5. The oTS of CPn cells did not induce PTP in either of post-synaptic CPn and COM cells. In contrast, oTS of COM cells induced PTP in postsynaptic CPn cells, but not in post-synaptic COM cells. **(a-c)** Induction of PTP by oTS of CPn cells. **(a)** Scheme of experiments shows the injection of retrograde AAV virus (AAV2_oChIEF_tdTomato) into pontine nucleus (*upper*). *Lower*, Representative image of oChIEF_tdTomato expression specifically only in L5 CPn cells. Scale bar, 200 μm. **(b)** Time courses of baseline-normalized EPSC amplitudes before and after oTS which was applied at t = 0. The oTS of CPn cells did not induce PTP in either of postsynaptic CPn (n = 12; *upper*) and COM cells (n = 13; *lower*). **(c)** Summary bar graphs for normalized PTP induced by oTS of CPn cells (n = 12, 13). **(d-h)** Induction of PTP by oTS of COM cells. **(d)** Scheme of experiments shows the injection of anterograde AAV virus (AAVDj_oChIEF_tdTomato) into contralateral PFC (*upper*). *Lower*, Representative image of oChIEF_tdTomato expression. Scale bar, 400 μm. **(e)** Time courses of baseline-normalized EPSC amplitudes before and after oTS which was applied at t = 0. The oTS of COM cells induced PTP only when the post-synapse target was CPn (n = 10; *left*) but not in post-synapse target was COM (n = 7; *right*). **(f)** PTP at COM-CPn synapses was not affected by TPP (n = 9). **(g)** Summary bar

graphs for normalized PTP induced by oTS of COM cells (n = 10, 9, 7; P = 0.4856 for COM-CPn vs COM-CPn_TPP). **(h)** Normalized amplitudes EPSCs evoked by oTS at COM-CPn synapse. TPP did not affect STP of oTS-evoked EPSCs at COM-CPn synapse. All data are mean ± S.E.M.

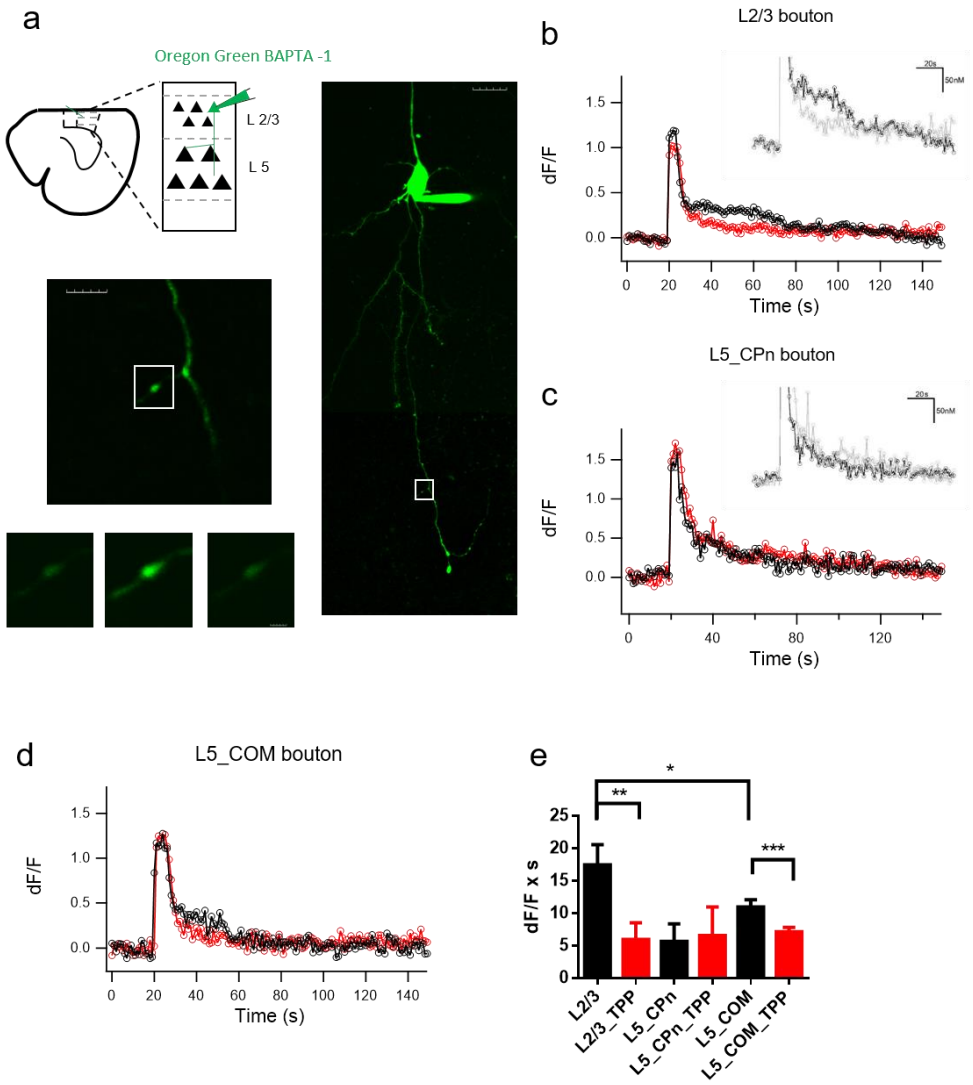

Figure 6. Post-tetanic residual calcium at axon terminals of PFC neurons. **(a)** Scheme and representative images of axonal bouton calcium. *Left upper*, Scheme of loading L2/3 neuron with OGB-1. *Right*, Representative image of an L2/3 neuron loaded with OGB-1. Scale bar, 20 μm. *Left middle*, Image of axonal boutons of an L2/3 neuron. Scale bar, 5 μm. *Left lower*, Axon bouton calcium images before, during and after TS. Scale bar, 1 μm. **(b)** Transients of

OGB-1 fluorescence evoked by TS at axon bouton of L2/3 before and after TPP application (L2/3_control = black dot; L2/3_TPP = red dot). *Insert*, Representative data of TS-evoked calcium transients in L2/3 (L2/3 = black, L2/3_TPP = gray). **(c)** Transients of OGB-1 fluorescence evoked by TS at axon bouton of L5 CPn before and after TPP application (CPn_control = black dot; CPn_TPP = red dot). *Insert*, Representative data of TS-evoked calcium transients in CPn (L2/3 = black, L2/3_TPP = gray). **(d)** Transients of OGB-1 fluorescence evoked by TS at axon bouton of L5 COM before and after TPP application (COM = black dot; COM_TPP = red dot). **(e)** Summary bar graph of TS-evoked residual calcium measured by the area under the dF/F transients 5 s after TS (n = 5, 5, 18, 5, 8, 8; P = 0.0079 for L2/3 vs L2/3_TPP; P = 0.0006 for COM vs COM_TPP; P = 0.0451 for L2/3 vs COM; P = 0.7006 for three TPP group). All data are mean ± S.E.M., *P < 0.05, **P < 0.01, ***P < 0.001, Mann-Whitney test, Kruskal-Wallis test.

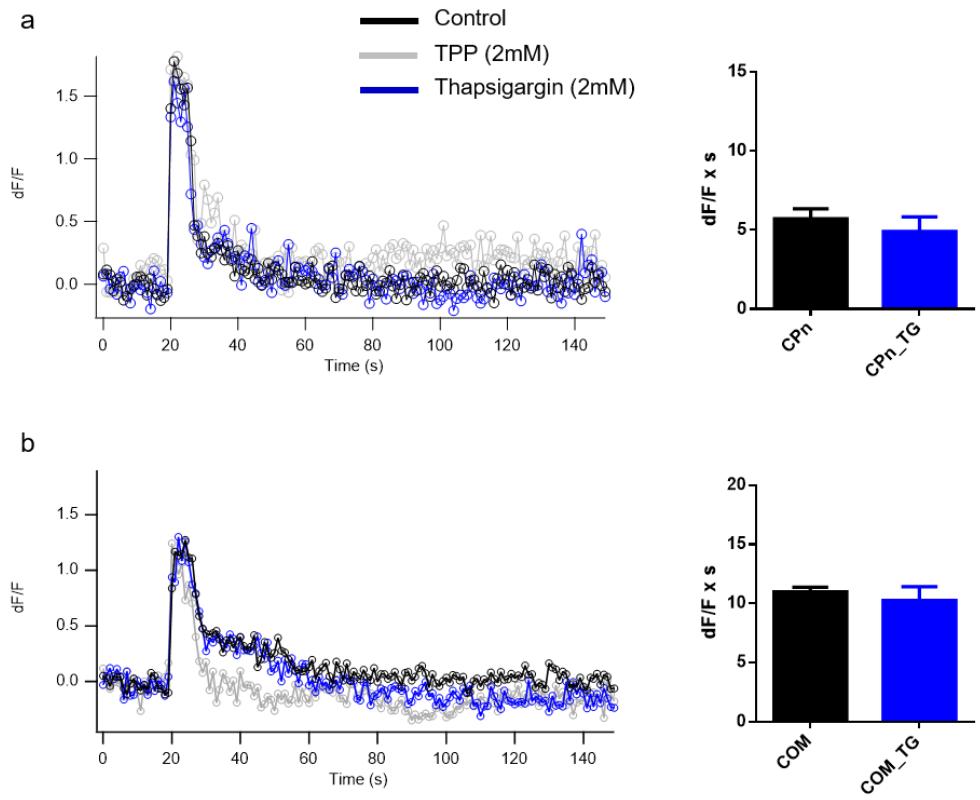

Figure 7. Thapsigargin (TG) did not alter the TPP-sensitive residual calcium. **(a)** Transients of OGB-1 fluorescence evoked by TS at axon bouton of L5 CPn after TG application (CPn_control = black dot, CPn_TPP = gray dot, CPn_TG = blue dot; *left*). *Right,* Summary bar graph of TS-evoked residual calcium measured by the area under the dF/F transients 5 s after TS (CPn, n = 18; CPn_TG, n = 8). **(b)** Transients of OGB-1 fluorescence evoked by TS at axon bouton of L5 COM after TG application (COM_control = black dot, COM_TPP = gray dot, COM_TG = blue dot; *left*). *Right,* Summary bar graph of TS-evoked residual calcium measured by the area under the dF/F transients 5 s after TS (COM, n = 8; COM_TG, n = 13). All data are mean ± S.E.M.

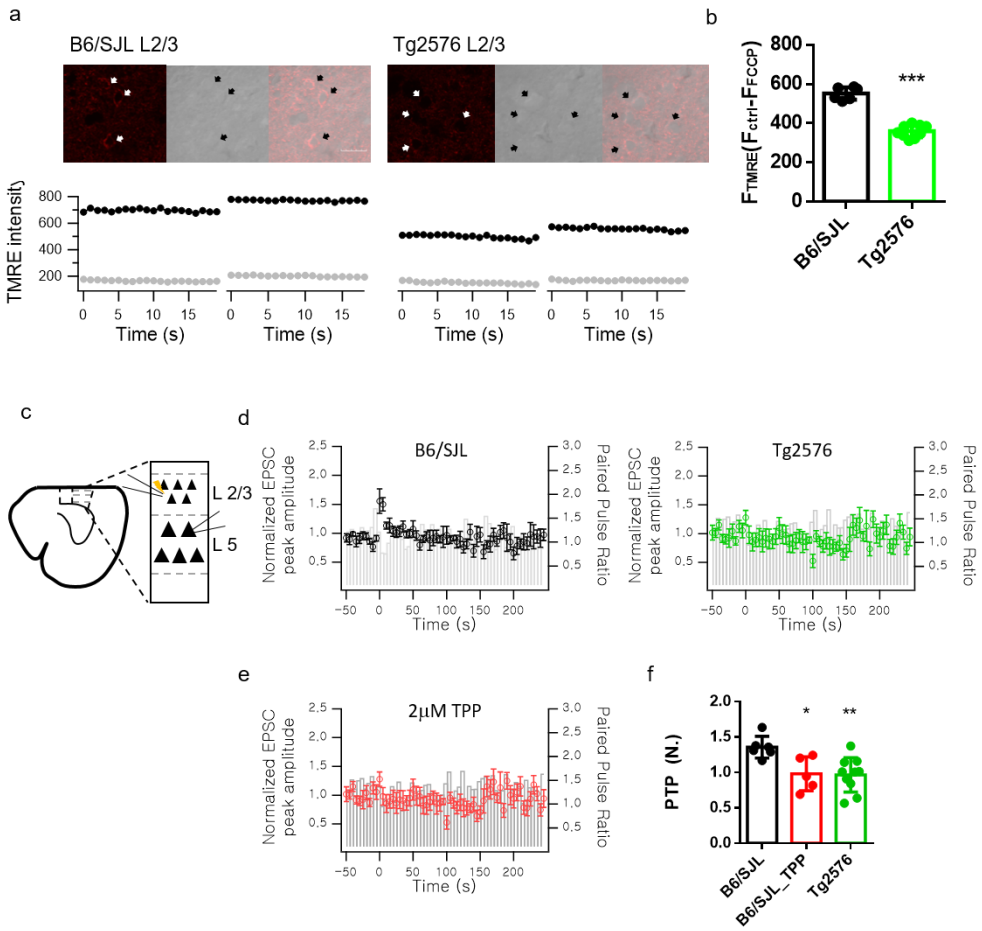

Figure 8. PTP at L2/3−CPn synapse in B6/SJL mice was mediated by mitochondrial residual calcium. **(a−b)** Estimation of L2/3 mitochondrial membrane potential (Ψ_m) using tetramethylrhodamine ethyl ester (TMRE). **(a)** *Left top*, Representative L2/3 mitochondrial TMRE fluorescence images in B6/SJL. Scale bar: 20 μm. (Arrows indicate each neuron). *Left bottom*, measurement of TMRE intensity (filled black circle) and TMRE intensity after FCCP application (filled gray circle) in B6/SJL L2/3 neuron. *Right top*, Representative L2/3 mitochondrial TMRE fluorescence images in

Tg2576. (Arrows indicate each neuron). *Right bottom*, measurement of TMRE intensity (filled black circle) and TMRE intensity after FCCP application (filled gray circle) in Tg2576 L2/3 neuron. **(b)** Summary bar graph of FCCP sensitive TMRE fluorescence of L2/3 cells in B6/SJL (animals = 2, n = 6) and Tg2576 (animals = 2, n = 9). The TMRE intensity of L2/3 PNs was significantly lower in Tg2576 than that in B6/SJL (n = 6, 9; P = 0.0004 for B6/SJL vs Tg2576). **(c–f)** Induction of PTP at L2/3–CPn synapses in B6/SJL and Tg2576. **(c)** Scheme of experiments show the location of patch clamp pipette and monopolar stimulation glass electrode. **(d)** Time courses of baseline–normalized EPSC amplitudes before and after TS which was applied at t = 0. PTP at L2/3–CPn synapses in B6/SJL was induced (animals = 4, n = 6; *left*), but PTP at L2/3–CPn synapses in Tg2576 was not induced (animals = 3, n = 10; *right*). **(e)** PTP at L2/3–CPn synapses in B6/SJL was abolished by 2 μM TPP application (animals = 4, n = 5). **(f)** Summary bar graphs for normalized PTP and TPP effects on PTP at L2/3–CPn synapses in B6/SJL and Tg2576 (n = 6, 5, 10; P = 0.003 for B6/SJL vs B6/SJL_TPP; P = 0.0173 for B6/SJL vs Tg2576). All data are mean ± S.E.M., *P < 0.05, **P < 0.01, Mann–Whitney test.

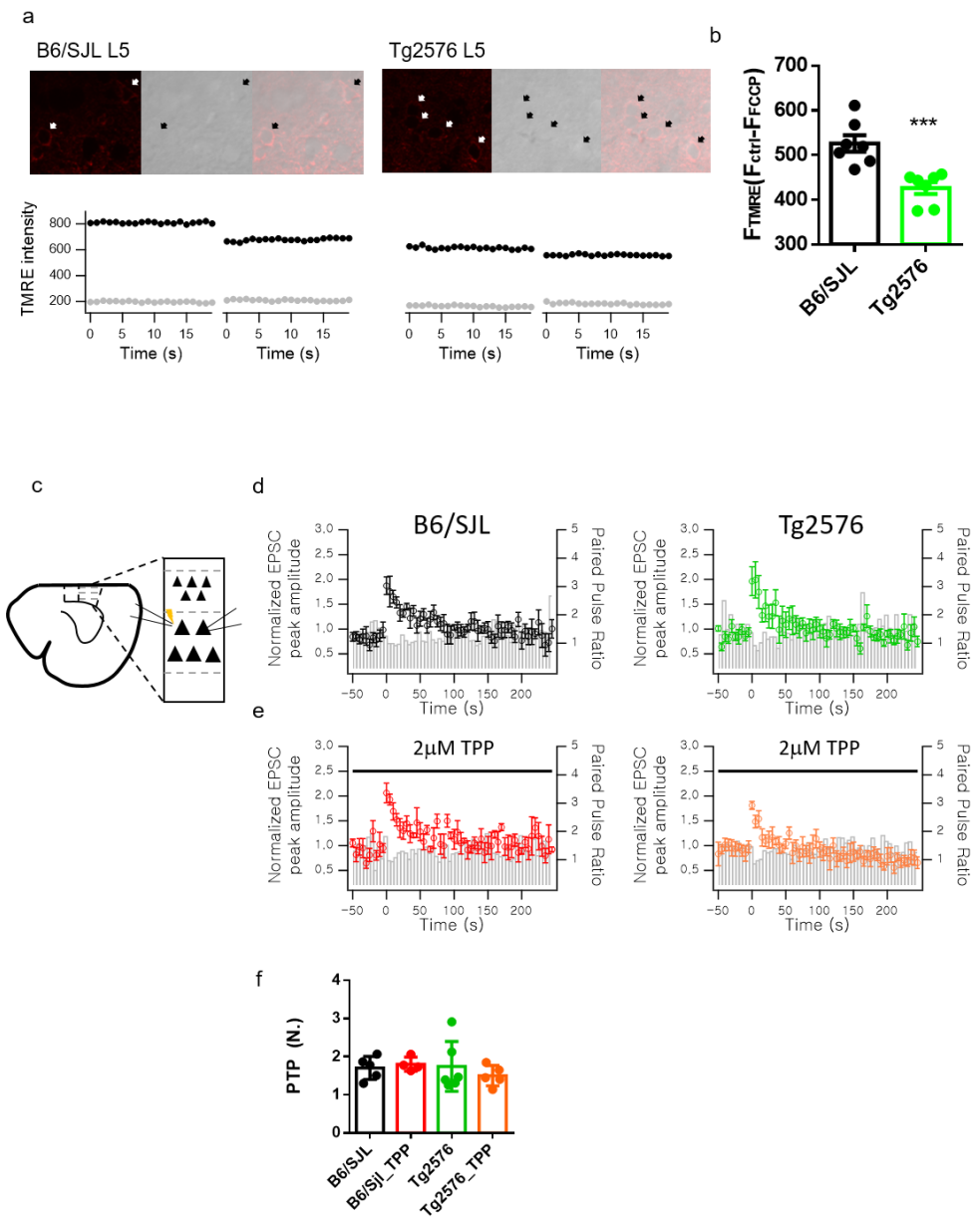

Figure 9. PTP at L5-CPn synapse in the B6/SJL and Tg2576 mice occurs in mitochondria-independent manner. (a-b) Estimation of L5 mitochondrial membrane potential (Ψ_m) using TMRE. (a) *Left top*, Representative L5 mitochondrial TMRE fluorescence images in B6/SJL. (Arrows indicate each neuron). *Left bottom*, measurement

of TMRE intensity (filled black circle) and TMRE intensity after FCCP application (filled gray circle) in B6/SJL L5 neuron. *Right top*, Representative L5 mitochondrial TMRE fluorescence images in Tg2576. (Arrows indicate each neuron). *Right bottom*, measurement of TMRE intensity (filled black circle) and TMRE intensity after FCCP application (filled gray circle) in Tg2576 L5 neuron. **(b)** Summary bar graph of FCCP sensitive TMRE fluorescence of L5 cells in B6/SJL (animals = 2, n = 7) and Tg2576 (animals = 2, n = 7). The TMRE intensity of L5 PNs was significantly lower in Tg2576 than that in B6/SJL (n = 7, 7; P = 0.0006 for B6/SJL vs Tg2576). **(c–f)** PTP Induction at L5–CPn synapses in B6/SJL and Tg2576. **(c)** Scheme of experiments show the location of patch clamp pipette and monopolar stimulation glass electrode. **(d)** Time courses of baseline-normalized EPSC amplitudes before and after TS which was applied at t = 0. PTP was induced by TS of L5 in B6/SJL (animals = 1, n = 5; *left*) and Tg2576 (animals = 2, n = 6; *right*). **(e)** PTP at L5–CPn synapses in B6/SJL (animals = 1, n = 4; *left*) and Tg2576 (animals = 2, n = 5; *right*) were not significantly affected by TPP application. **(f)** Summary bar graphs for normalized PTP and TPP effects on PTP at L5–CPn synapses in B6/SJL and Tg2576 (n = 5, 4, 6, 5). All data are mean ± S.E.M., ***P < 0.001, Mann–Whitney test.

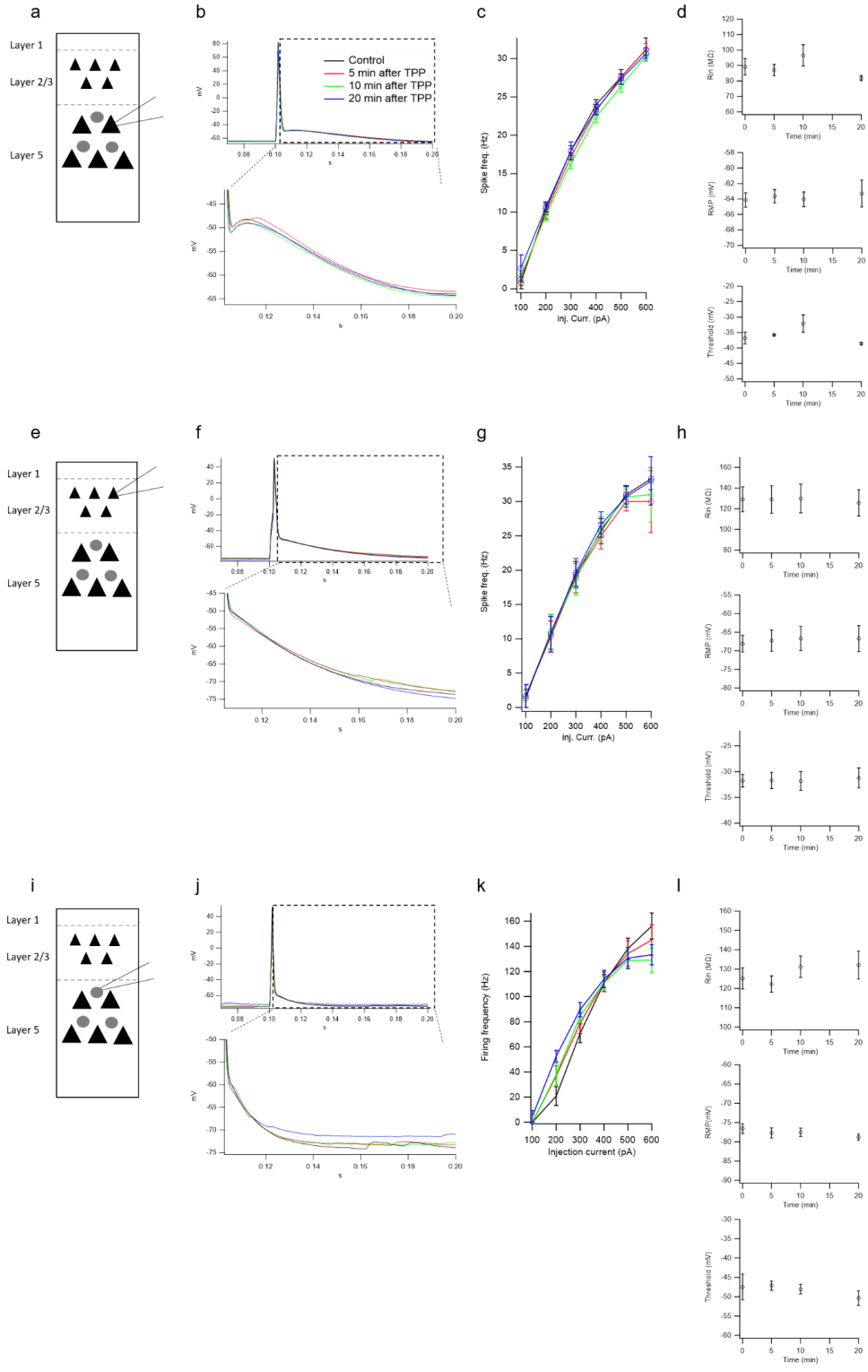
a
Layer 1
Layer 2/3
Layer 5
b
Control
5 min after TPP
10 min after TPP
20 min after TPP
mV
s
c
Spike freq. (Hz)
inj. Curr. (pA)
d
Rin (MΩ)
RMP (mV)
Threshold (mV)
Time (min)
e
Layer 1
Layer 2/3
Layer 5
f
mV
s
g
Spike freq. (Hz)
inj. Curr. (pA)
h
Rin (MΩ)
RMP (mV)
Threshold (mV)
Time (min)
i
Layer 1
Layer 2/3
Layer 5
j
mV
s
k
Firing frequency (Hz)
Injection current (pA)
l
Rin (MΩ)
RMP(mV)
Threshold (mV)
Time (min)

Figure 10. Electrical properties of neurons were not affected by TPP application. (a–d) After depolarization (ADP), firing frequency–current injection relationship (F–I curve), Input resistance (R_{in}), Resting membrane potential (RMP) and action potential threshold (AP threshold) in L5 PNs over time after TPP application. **(a)** Scheme of experiments show the location of patch clamp pipette. **(b)** Representative data of AP (*upper*) and ADP (*lower*) of L5 PNs over time after TPP application (Control = black, red = 5 minutes after TPP, green = 10 minutes after TPP, blue = 20 minutes after TPP; *top*). **(c)** Averaged plot of F–I curve of L5 PNs. F–I relationship of L5 PNs was not affected by TPP application (n = 5). **(d)** R_{in}, RMP and AP threshold were not affected by TPP application (n = 5, 5, 5). **(e–h)** ADP, F–I curve, R_{in}, RMP and AP threshold in L2/3 PNs over time after TPP application. **(e)** Scheme of experiments show the location of patch clamp pipette. **(f)** Representative data of AP (*upper*) and ADP (*lower*) of L2/3 PNs over time after TPP application (Control = black, red = 5 minutes after TPP, green = 10 minutes after TPP, blue = 20 minutes after TPP). **(g)** F–I relationship of L2/3 PNs was not affected by TPP application (n = 6). **(h)** R_{in}, RMP and AP threshold were not affected by TPP application (n = 6, 6, 6). **(i–l)** ADP, F–I curve, R_{in}, RMP and AP threshold in L5 INs over time after TPP application. **(i)**

Scheme of experiments show the location of patch clamp pipette. (j) Representative data of AP (*upper*) and ADP (*lower*) of L5 INs over time after TPP application (Control = black, red = 5 minutes after TPP, green = 10 minutes after TPP, blue = 20 minutes after TPP). (k) F-I relationship of L5 INs was not affected by TPP application (n = 13). (l) R_{in}, RMP, AP threshold were not affected by TPP application (n = 13, 13, 13). All data are mean ± S.E.M.

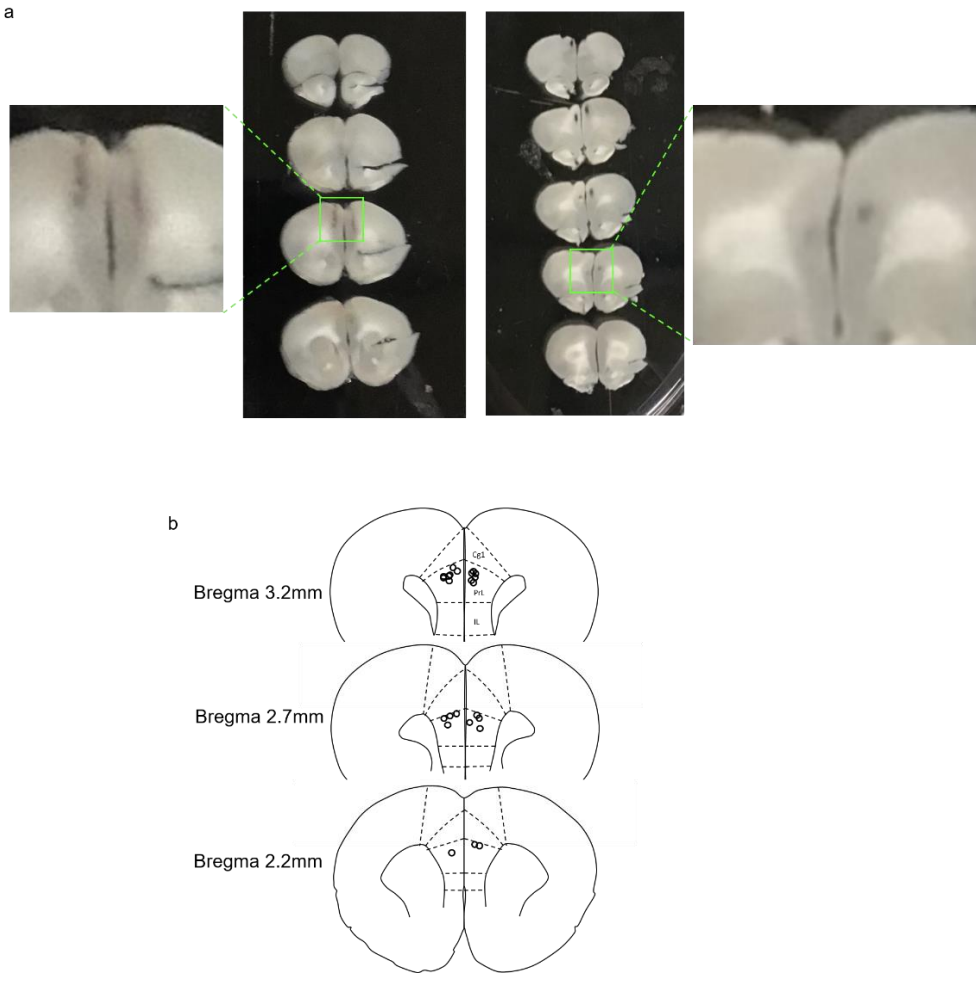

Figure 11. Bilateral infusion cannula implantation into the PFC PL area. (a) Representative image of bilateral cannula implantation. **(b)** location of bilateral infusion cannula of all rats.

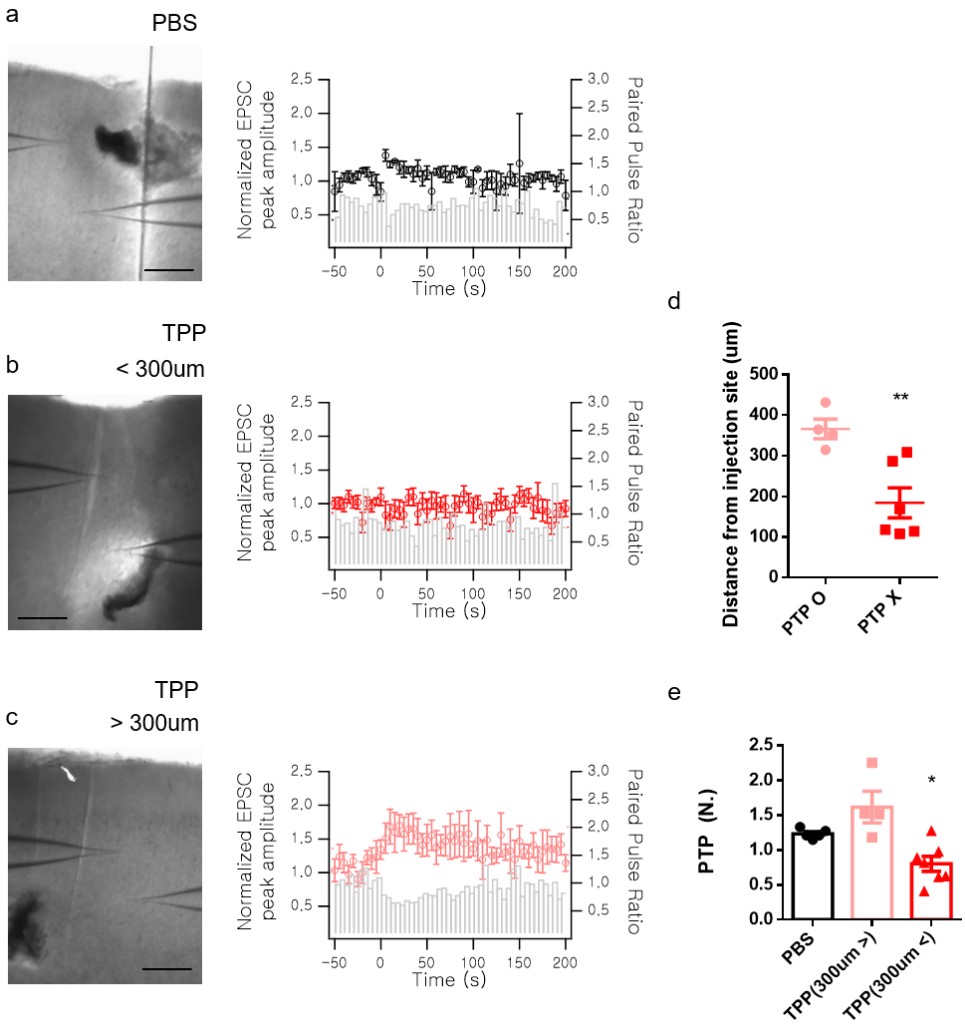

Figure 12. PTP was not induced within the area 300 μm from the injection site, while PTP was induced outside the area. (a) PTP induction at L2/3-CPn synapses in PBS injection groups. Representative image of PTP induction experiment in PBS group shows the location of patch clamp pipette, monopolar stimulation glass electrode and PBS injection site (*left*). Scale bar: 200 μm. *Right*, Time courses of baseline-normalized EPSC amplitudes before and after TS which was applied at t = 0. In PBS injected

groups, PTP at L2/3−CPn synapses was inducible regardless of the injection site distance (n = 5). **(b)** PTP induction at L2/3−CPn synapses within the area 300 μm from the TPP injection site. Representative image of PTP induction experiment within the area 300 μm from the TPP injection site in TPP group shows the location of patch clamp pipette, monopolar stimulation glass electrode and PBS injection site (*left*). Scale bar: 200 μm. *Right*, Time courses of baseline−normalized EPSC amplitudes before and after TS which was applied at t = 0. PTP was not induced within the area 300 μm from the injection site (n = 7). **(c)** PTP induction at L2/3−CPn synapses at outside the area. Representative image of PTP induction experiment at outside area in TPP group shows the location of patch clamp pipette, monopolar stimulation glass electrode and PBS injection site (*left*). Scale bar: 200 μm. *Right*, Time courses of baseline−normalized EPSC amplitudes before and after TS which was applied at t = 0. PTP was induced outside the area (n = 4). **(d)** Summary scattered plot of distance from injection site vs occurrence of PTP (P = 0.0095 for PTP o vs PTP x). **(e)** Summary bar graphs for normalized PTP. PTP was not induced within the area 300 μm from the TPP injection site, while PTP was induced outside the area (n = 7, 4; P = 0.0121 for TPP (300 μm <) vs TPP (300 μm >)). All data are mean ± S.E.M., *P < 0.05, **P < 0.01, Mann−Whitney test.

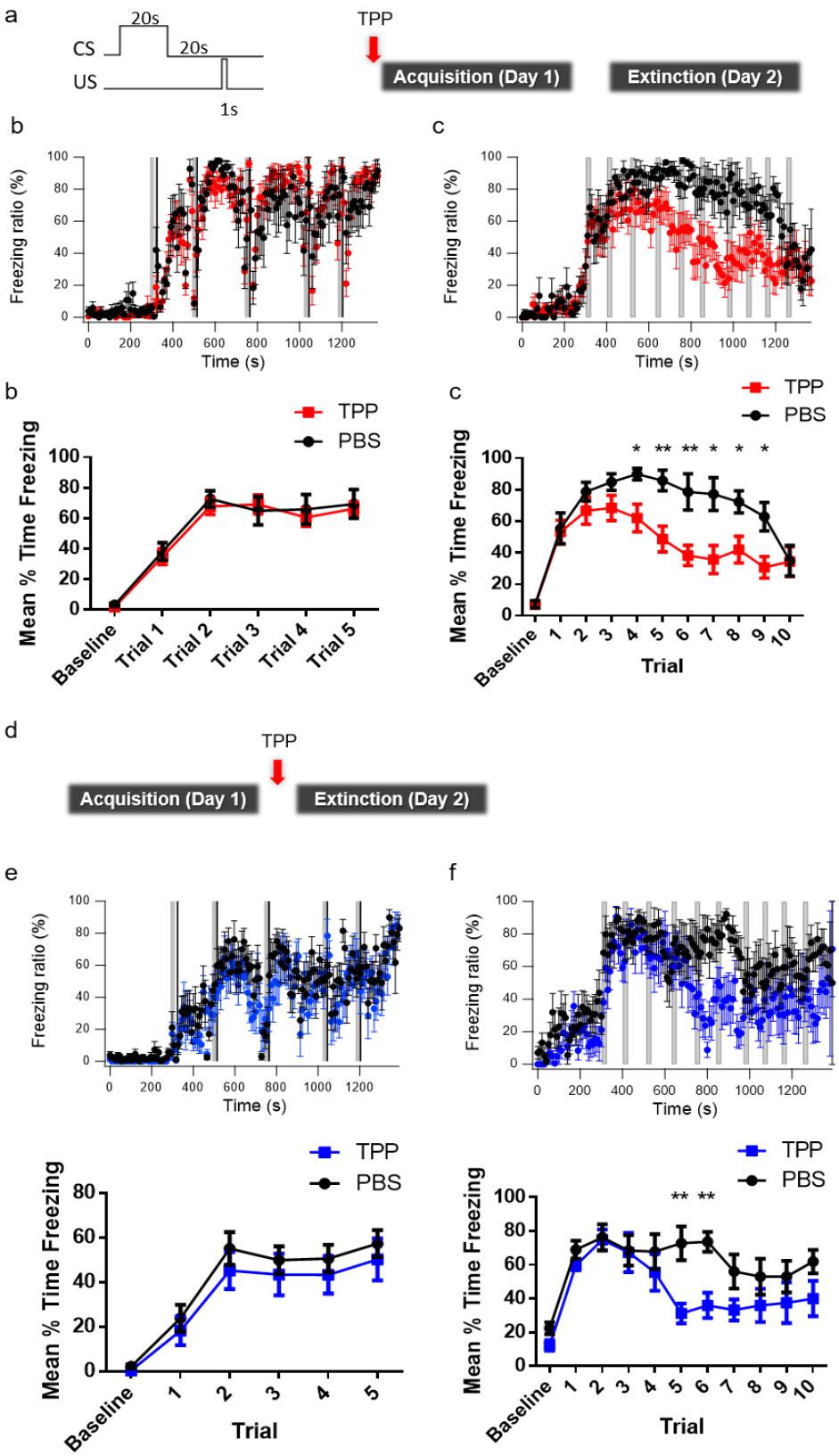
a
20s
CS
20s
US
1s
TPP
Acquisition (Day 1)
Extinction (Day 2)
b
c
Freezing ratio (%)
Time (s)
b
c
TPP
PBS
Mean % Time Freezing
Baseline
Trial 1
Trial 2
Trial 3
Trial 4
Trial 5
Trial
d
TPP
Acquisition (Day 1)
Extinction (Day 2)
e
f
Freezing ratio (%)
Time (s)
TPP
PBS
Mean % Time Freezing
Baseline
Trial

Figure 13. The TPP injection into PFC did not impair the fear memory acquisition, but accelerated the fear extinction. (a–c) Time course of freezing behavior after PBS or TPP injection into PFC 30 minutes before the trace fear conditioning (TFC; Day 1). **(a)** Scheme of TFC. Rats received five pairings of a tones (2.5kHz, 20 s; CS) and a 1 s footshock (0.7 mW, 1 s; US). CS and US separated by 20 s trace interval. Intertrial interval was 180 ± 20 s (*left*). *Right,* Timeline of TPP infusion into PFC. TPP was infused into PFC 30 minutes before the TFC. **(b)** Time course of freezing ratio during TFC. Each point represents the freezing ratio binned 10 s (*upper*) or mean freezing of each trial (20 s CS and 20 s trace interval; *lower*). During TFC, PBS (n = 6) and TPP group (n = 12) showed similar freezing behaviors (Group X Period : $F_{(5,90)}$ = 0.336; P = 0.8899). **(c)** Freezing ratio during trace fear extinction test. In trace fear extinction test, rats received CS (tone) alone for ten times. Intertrial interval was 90 ± 20 s. Each point represents the freezing ratio binned 10 s (*upper*) or mean freezing of each trial (20 s CS and 20 s trace interval; *lower*). In fear extinction test, TPP group (n = 12) showed an accelerated fear extinction than PBS group (n = 6; Group X Period: $F_{(10,160)}$ = 3.244; P = 0.001; P = 0.046 for PBS vs TPP trial 4; P = 0.009 trial 5; *P < 0.05, **P < 0.01). **(d–f)** Time course of freezing behavior after PBS or TPP

injection into PFC 30 minutes before the trace fear extinction test (Day 2). **(d)** Timeline of TPP infusion into PFC. TPP was infused into PFC 30 minutes before the TFC. **(e)** Time course of freezing ratio during TFC. Each point represents the freezing ratio binned 10 s (*upper*) or mean freezing of each trial (20 s CS and 20 s trace interval; *lower*). During TFC, PBS (n = 9) and TPP group (n = 7) showed similar freezing behaviors (Group X Period: $F_{(5,70)}$ = 0.1509; P = 0.9791). **(f)** Freezing ratio during trace fear extinction test. Each point represents the freezing ratio binned 10 s (*upper*) or mean freezing of each trial (20 s CS and 20 s trace interval; *lower*). In fear extinction test, TPP group (n = 7) showed an accelerated fear extinction than PBS group (n = 9; P = 0.005 for PBS vs TPP trial 5; P = 0.001 for PBS vs TPP trial 6). All data are mean ± S.E.M., *P < 0.05, **P <0.01, Repeated measures ANOVA, Post-hoc test Fisher's LSD pairwise comparisons.

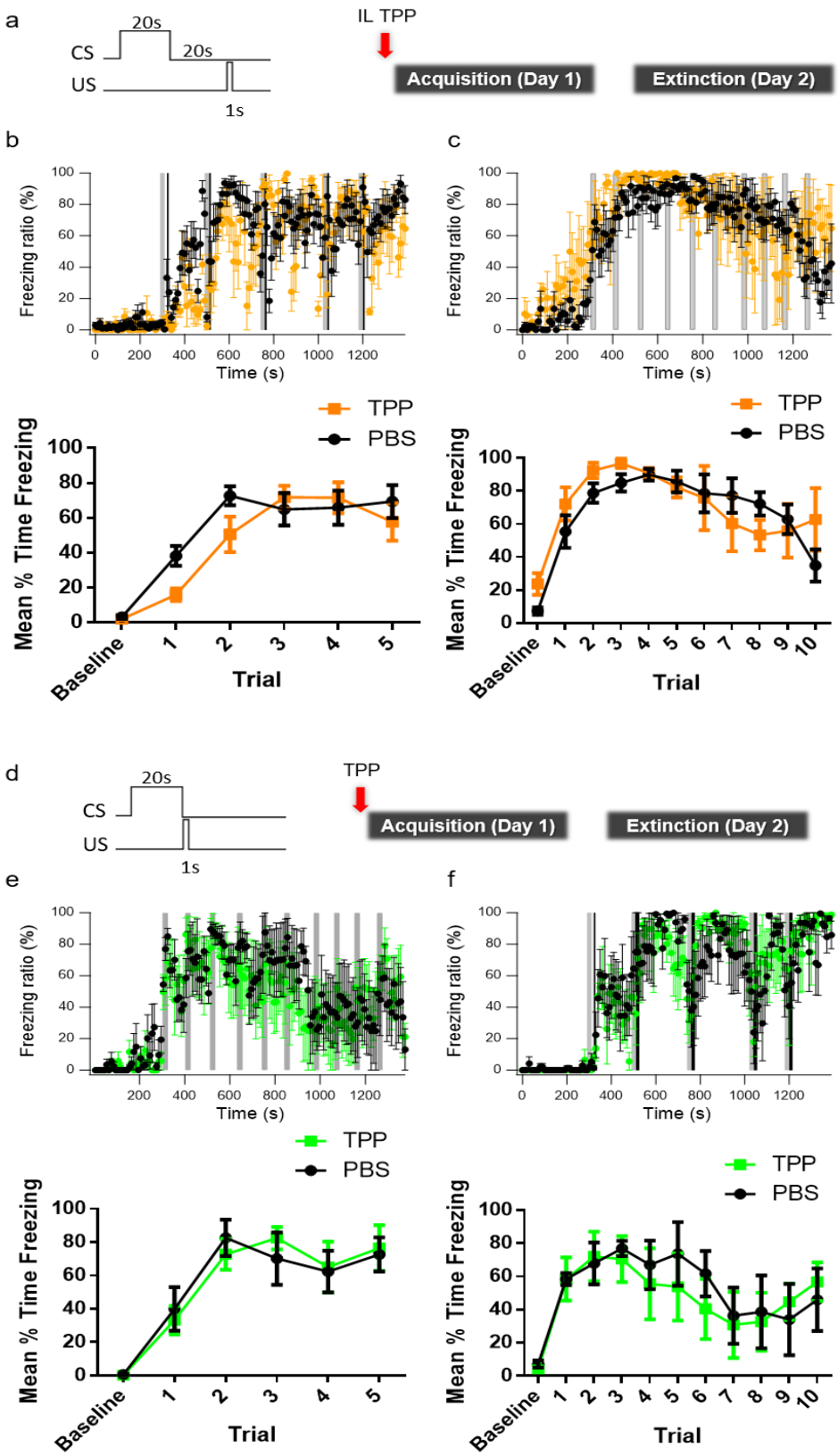
a
20s
CS
20s
US
1s
IL TPP
Acquisition (Day 1)
Extinction (Day 2)
b
c
Freezing ratio (%)
Time (s)
TPP
PBS
Mean % Time Freezing
Baseline
Trial
d
20s
CS
US
1s
TPP
Acquisition (Day 1)
Extinction (Day 2)
e
f

Figure 14. IL-TPP group showed the similar freezing behavior as the PBS group in TFC and fear extinction, and PL-TPP group showed no significant difference from the PBS group in DFC and fear extinction. (a-c) Time course of freezing behavior after PBS or TPP injection into PFC IL area 30 minutes before the TFC (Day 1). **(a)** Scheme of TFC. Rats received five pairings of a tones (2.5kHz, 20 s) and a 1 s footshock (0.7 mW, 1 s). CS and US separated by 20 s trace interval. Intertrial interval was 180 ± 20 s (*left*). *Right,* Timeline of TPP infusion into PFC IL area. TPP was infused into PFC IL area 30 minutes before TFC (*right*). **(b)** Time course of freezing ratio during TFC. Each point represents the freezing ratio binned 10 s (*upper*) or mean freezing of each trial (20 s CS and 20 s trace interval; *lower*). During TFC, PBS (n = 6) and TPP group (n = 4) showed similar freezing behaviors (Group X Period: $F_{(5,50)}$ = 0.1965; P = 0.1002). **(c)** Freezing ratio during trace fear extinction test. In trace fear extinction test, rats received CS (tone) alone for ten times. Intertrial interval was 90 ± 20 s. Each point represents the freezing ratio binned 10 s (*upper*) or mean freezing of each trial (20 s CS and 20 s trace interval; *lower*). In trace fear extinction test, IL-TPP group showed the similar freezing behavior as the PBS group (Group X Period: $F_{(10,70)}$ = 1.526; P = 0.1487). **(d-f)** Time course of freezing behavior after PBS or TPP injection into

PFC 30 minutes before the delayed fear conditioning (DFC; Day 1) **(d)** Scheme of DFC. Rats received five pairings of a tones (2.5kHz, 20 s) that coterminated with a footshock (0.7 mW, 1 s). Intertrial interval was 180 ± 20 s (*left*). *Right,* Time line of TPP infusion into PFC. TPP was infused into PFC 30 minutes before the DFC. **(e)** Time course of freezing ratio during DFC. Each point represents the freezing ratio binned 10 s (*upper*) or mean freezing of each trial (20 s CS and 20 s trace interval; *lower*). During DFC, PBS (n = 4) and TPP group (n = 4) showed similar freezing behaviors (Group X Period: $F_{(5,30)}$ = 0.6306; P = 0.6778). **(f)** Freezing ratio during delayed fear extinction test. Each point represents the freezing ratio binned 10 s (*upper*) or mean freezing of each trial (20 s CS and 20 s trace interval; *lower*). In delayed fear extinction test, PBS (n = 4) and TPP group (n = 4) showed similar freezing behaviors (Group X Period: $F_{(10,60)}$ = 0.4864; P = 0.8924). All data are mean ± S.E.M.

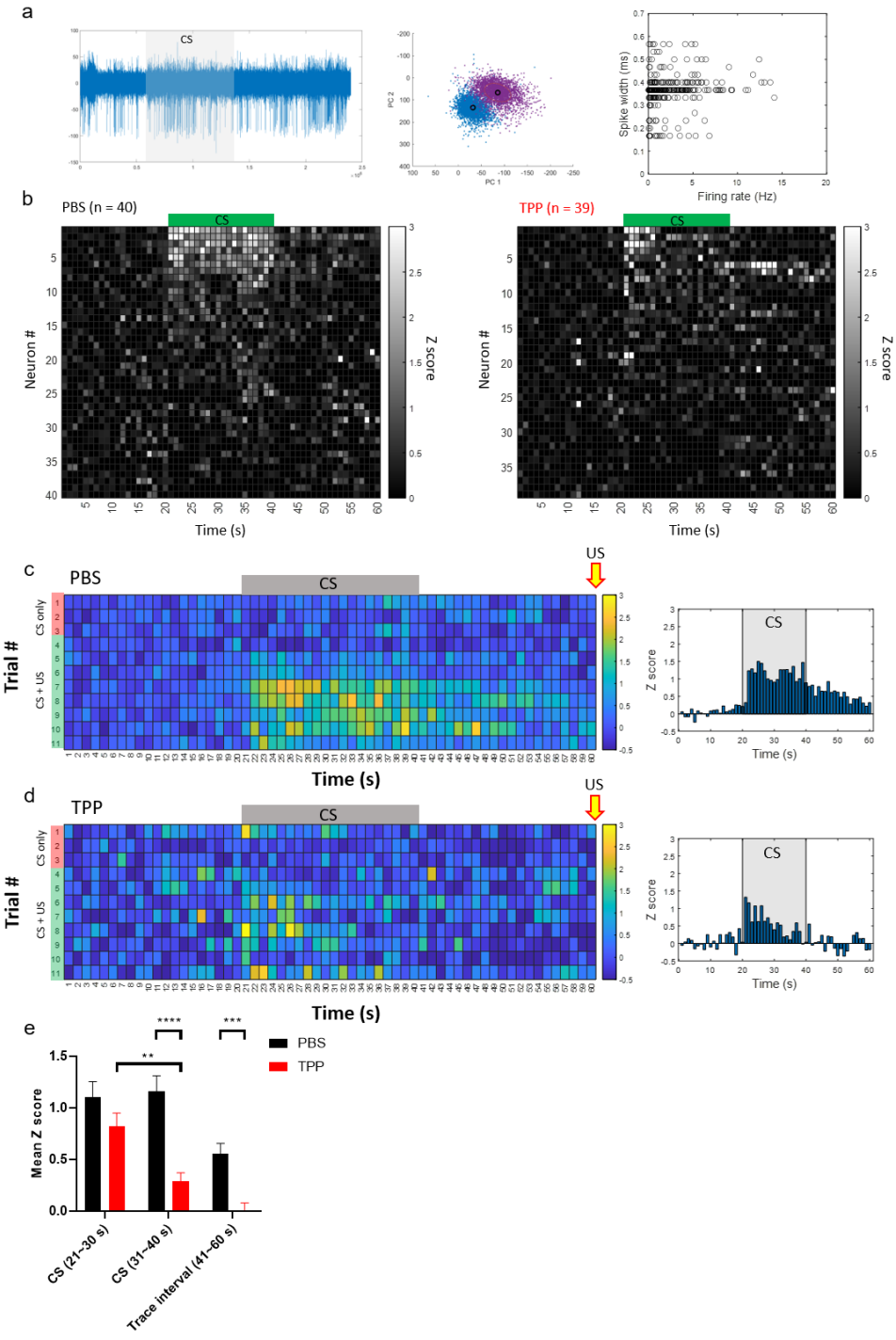
a
CS
PC 2
PC 1
Spike width (ms)
Firing rate (Hz)
b
PBS (n = 40)
TPP (n = 39)
CS
Neuron #
Time (s)
Z score
c
PBS
US
CS only
CS + US
Trial #
Time (s)
Z score
d
TPP
e
PBS
TPP
Mean Z score
****
***
**
CS (21–30 s)
CS (31–40 s)
Trace interval (41–60 s)

Figure 15. During TFC, the PBS group showed sustained increased activity in trace interval, whereas TPP group did not show sustained increased activity. **(a)** *Left,* Representative data of PFC PL neurons spikelet during TFC. *Middle,* Representative plot of spike sorting through principal component analysis (PCA). *Right,* Scatter plot showing firing rate and spike width for all recorded units. **(b)** Heat map of PL neuronal activities binned over 1 s were expressed as z scores of firing frequencies with reference to the pre-CS baseline frequencies. Z-score of PBS (animals = 1, n = 40; *left*) and TPP (animals = 2, n = 39; *right*) group PL activity averaged over 5-11 trials in the TFC. The cell activities during CS were sorted in the descending order. **(c)** PFC cell activity (z-score) averaged over PFC cells with significant CS responses in the PFC group during the TFC. *Left,* Heat map of z-score of PBS group cells activity averaged over CS responses cells (animals = 5, n = 22/112). The z-score was calculated with reference to the pre-CS baseline activity. The rats received three CS alone trials (red box) and 8 pairings of a tones (green box; 2.5kHz, 20 s) and a footshock (0.7 mW, 1s). CS and US separated by 20 s trace interval. Intertrial interval was 180 ± 20 s (CS = gray box; US = arrow). *Right,* mean Z-score of CS responses cells activity in PBS group averaged over 5-11 trials. PBS group showed increased CS response and

sustained increased activity during trace interval. (d) the same as *a* but in the TPP group. *Left,* Heat map of z−score of TPP group cells activity averaged over CS responses cells (animals = 4, n = 12/76). *Right,* mean Z−score of CS responses neurons activity in TPP group averaged over 5−11 trials. TPP group showed increased response during first half of CS period but did not show sustained increased activity during trace interval. (e) Summary bar graph of mean Z−scores from 5−11 trials in PBS and TPP animals during TFC. In the TPP group, activity decreased in the second half of CS compared to the PBS group and first half of CS in TPP group ($P < 0.0001$ for TPP vs PBS CS 31~40s; $P = 0.0042$ for TPP (CS 21~30 s) vs TPP (CS 31~40 s), and trace interval activity was significantly decreased compared to PBS group ($P = 0.0003$ for TPP vs PBS trace interval 41~60 s). All data are mean ± S.E.M., **$P < 0.01$, ***$P < 0.001$, ****$P < 0.0001$, Mann−Whitney test.

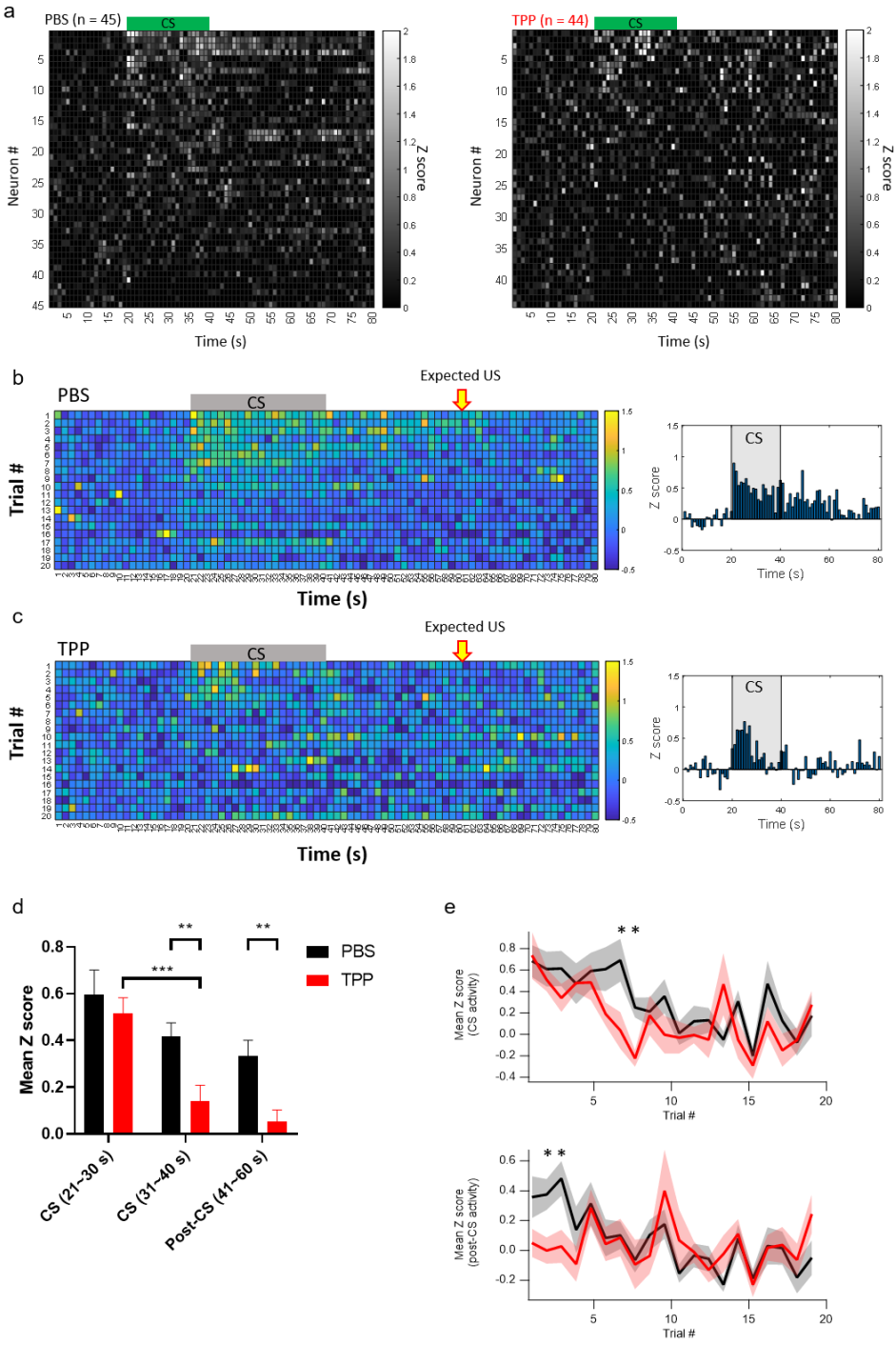
a
PBS (n = 45)
CS
Neuron #
Time (s)
Z score
TPP (n = 44)
CS
Neuron #
Time (s)
Z score
b
PBS
CS
Expected US
Trial #
Time (s)
CS
Z score
Time (s)
c
TPP
CS
Expected US
Trial #
Time (s)
CS
Z score
Time (s)
d
Mean Z score
PBS
TPP
**
**
***
CS (21–30 s)
CS (31–40 s)
Post-CS (41–60 s)
e
Mean Z score (CS activity)
Trial #
Mean Z score (post-CS activity)
Trial #

Figure 16. The PBS group showed persistent activity during post-CS in trace fear extinction, but TPP group did not show persistent activity during post-CS. **(a)** Heat map of PL neuronal activities binned over 1 s were expressed as z scores of firing frequencies with reference to the pre-CS baseline frequencies. Z-score of PBS (animals = 1, n = 45; *left*) and TPP (animals = 1, n = 44; *right*) group PL activity averaged over five trials in the tone test. The cell activities during CS were sorted in the descending order. **(b)** PFC cell activity (z-score) averaged over PFC cells with significant CS responses in the PBS group during the fear extinction test. *Left*, Heat map of z-score of PBS group cells activity averaged over CS responses neurons (animals = 5, n = 25/153). The z-score was calculated with reference to the pre-CS baseline activity. The rats received 20 trials for presentation of CS alone (CS = gray box). *Right*, mean Z-score of CS responses neurons activity in PBS group averaged over 1-5 trials. PBS group showed increased CS response and persistent activity during post-CS interval. **(c)** the same as *a* but in the TPP group. *Left*, Heat map of z-score of TPP group cells activity averaged over CS responses cells (animals = 4, n = 15/101). The z-score was calculated with reference to the pre-CS baseline activity. *Right*, mean Z-score of CS responses neurons activity in TPP group averaged over 1-5 trials. TPP group

showed increased CS response but did not show sustained increased activity during post-CS. (d) Summary bar graph of mean Z-scores from 1-5 trials in PBS and TPP animals during fear extinction. In the TPP group, activity decreased in the second half of CS compared to the PBS group and first half of CS in TPP group (P = 0.0008 for TPP (CS 21~30 s) vs TPP (CS 31~40 s); P = 0.0043 for PBS vs TPP CS 31~40 s) and post-CS activity was significantly decreased compared to the PBS group (P = 0.0088 for PBS vs TPP Post-CS 41~60 s). (e) *Upper,* Time course of PFC cell activity during first half of CS as a function of trial numbers. In the PBS group (n = 25; black), CS response was maintained up to 7 trials, whereas in the TPP group (n = 15; red), CS activity was maintained up to 4 trials (P = 0.023 for PBS vs TPP trial 7; P = 0.001 for PBS vs TPP trial 8). *Lower,* Time course of PFC cell activity during post-CS as a function of trial numbers. In the PBS group (n = 25; black), post-CS activity was maintained up to 3 trials, whereas sustained increased activity was not observed in TPP group (n = 15; red) during post-CS period. (P = 0.015 for PBS vs TPP trial 2; P = 0.011 for PBS vs TPP trial 3). All data are mean ± S.E.M., *P < 0.05, **P < 0.01, ***P < 0.001, Mann-Whitney test, Repeated measures ANOVA, Post-hoc test Fisher's LSD pairwise comparisons.

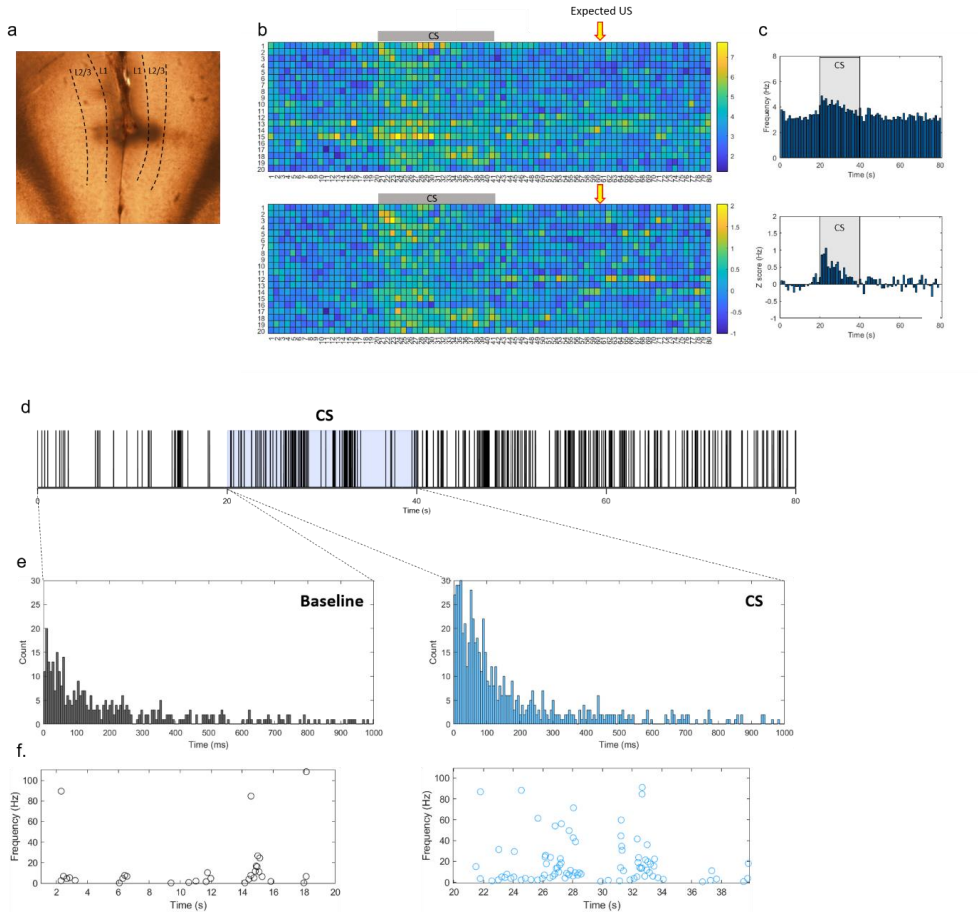

Figure 17. PFC L2/3 neurons showed CS responses alone without post-CS activity in trace fear extinction test. (a-c) PFC L2/3 cell activity (z-score) averaged over PFC cells with significant CS responses in the PBS group during fear extinction test. **(a)** Representative image of streotrodes bundle location to record specifically PFC L2/3 neuron activity. **(b)** *Upper,* Heat map of spike activity frequency of L2/3 cells which showed increased activity during CS (n = 15/89). *Lower,* Heat map of z-score of L2/3 cells activity averaged over CS response L2/3 cells in trace fear

extinction test (n = 15/89). The rats received 20 trials of CS only (CS = gray box; expected US = yellow arrow). (c) Summary bar graph of spike frequency *(upper)* and mean Z-score (*lower*) from 1-5 trials of L2/3 neurons during fear extinction. L2/3 neurons showed CS responses alone without Post-CS activity in trace fear extinction test. (d) Representative spike activity of one L2/3 cell whose activity increased to 5 Hz during CS. (e) Histogram of interspike interval (ISI) baseline (*left*) and CS (*right*). In both periods, most ISIs were shorter than 200 ms. (f) The plot of instantaneous frequencies (1/ISI) during baseline (*left*) and CS (*right*). In the L2/3 neural activity during CS is mainly ascribed to the increase in burst firing.

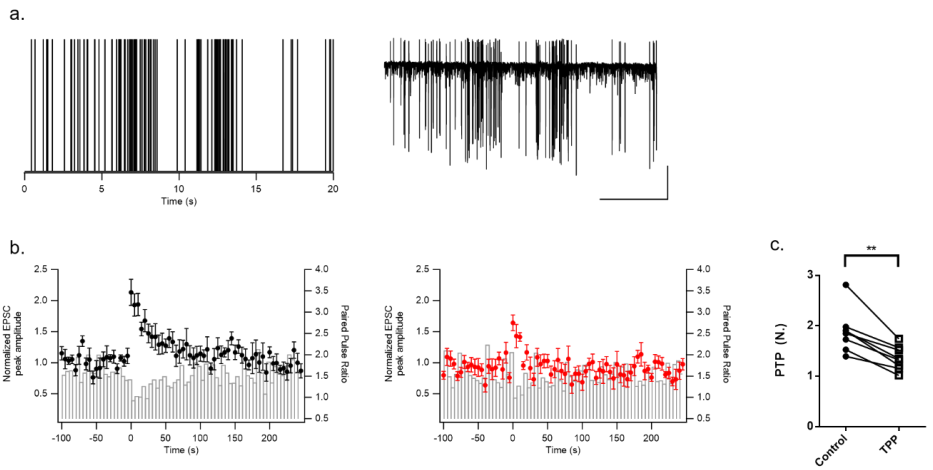

Figure 18. PTP was induced by burst-type stimulation, and magnitude of PTP was reduced by TPP. (a) *Left,* Transform activity pattern of L2/3 cell which was fired at 5 Hz during CS into stimulation train templates. *Right,* Representative EPSCs trace of burst-type stimulation. (b) Time courses of baseline-normalized EPSC amplitudes before and after burst-type stimulation which was applied at t = 0. Induction of PTP at L2/3-CPn synapse by burst-type stimulation in mimic in vivo conditions (1.3 Ca^{2+}, 32 ℃; n = 8; *left*) and after TPP application (n = 8; *right*). (c) Summary bar graph for the TPP effects on PTP at L2/3-CPn synapses induced by burst-type stimulation. When TPP was applied, PTP did not completely disappear, but the magnitude was significantly reduced (P = 0.0078 for PBS vs TPP). All data are mean ± S.E.M., **P < 0.01, Wilcoxon matched pairs signed rank test.

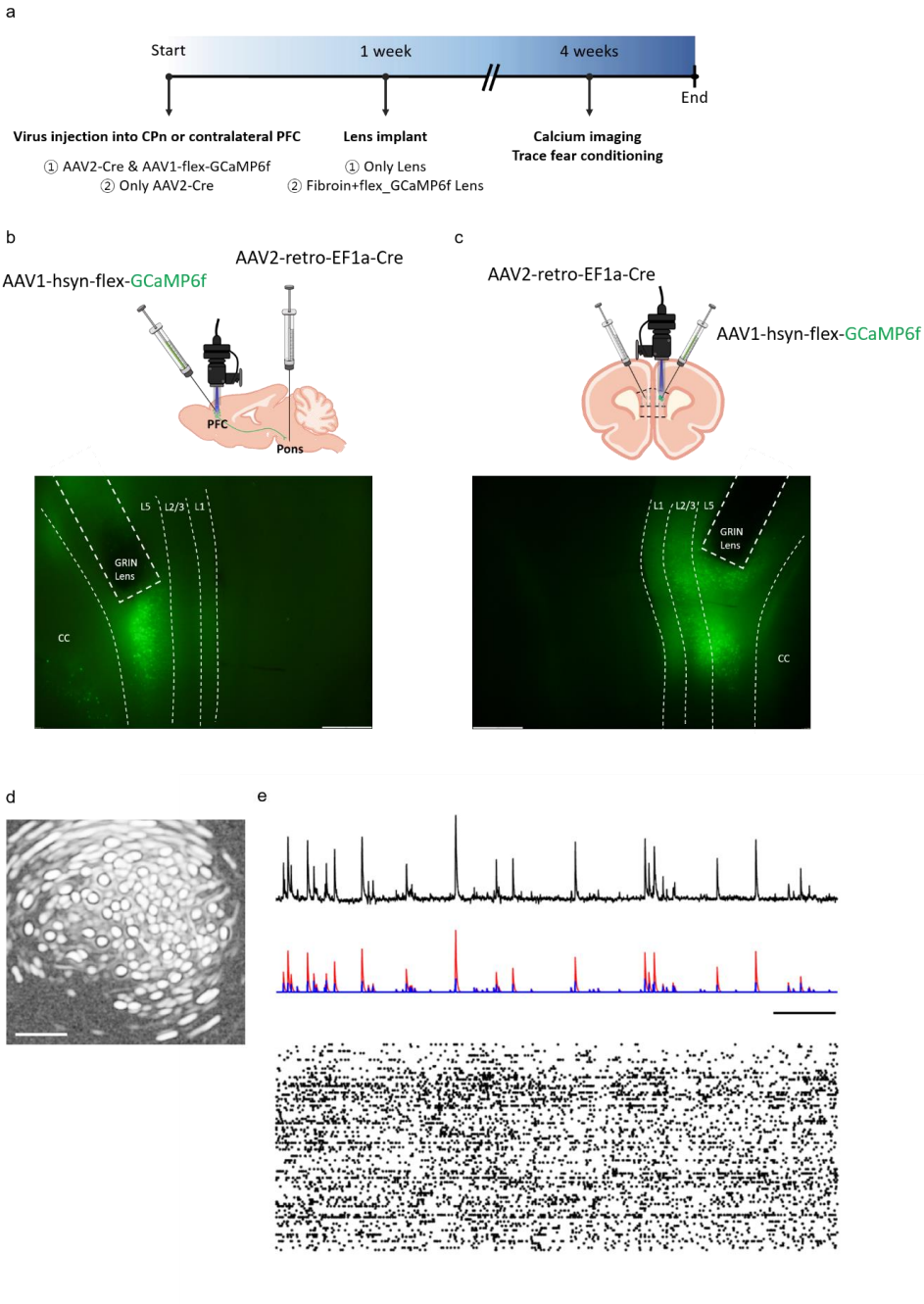
a
Start
1 week
4 weeks
End
Virus injection into CPn or contralateral PFC
① AAV2-Cre & AAV1-flex-GCaMP6f
② Only AAV2-Cre
Lens implant
① Only Lens
② Fibroin+flex_GCaMP6f Lens
Calcium imaging
Trace fear conditioning
b
AAV2-retro-EF1a-Cre
AAV1-hsyn-flex-GCaMP6f
PFC
Pons
L5
L2/3
L1
GRIN Lens
CC
c
AAV2-retro-EF1a-Cre
AAV1-hsyn-flex-GCaMP6f
L1
L2/3
L5
GRIN Lens
CC
d
e

Figure 19. Scheme of experimental procedures for cell type specific calcium activity recoding. **(a)** Experimental design. The experiments were performed in two alternative ways. 1) AAV2-Cre and flex-GCaMP6f were injected into Pons or contralateral PFC and PFC, respectively. One week later, 1 mm or 0.6 mm GRIN lens was implanted in the PFC. Calcium imaging and trace fear conditioning were performed 3 weeks later. 2) AAV2-Cre was injected into Pons or contralateral PFC. One week later, after applying the flex-GCaMP6f virus to the GRIN lens using silk fibroin, the lens was implanted in the PFC. Three weeks later, calcium imaging and trace fear conditioning were performed. **(b)** *Upper*, To record CPn activity, AAV2-retro-EF1a-Cre and AAV1-hsyn-flex-GCaMP6f were injected into the pons and PFC, respectively. GRIN lens and baseplate were implanted into PFC. *Lower*, Representative image of GCaMP6f expression. Note that GCaMP6f was expressed within L5. **(c)** *Upper*, to record COM activity, AAV2-retro-EF1a-Cre and AAV1-hsyn-flex-GCaMP6f were injected into contralateral and ipsilateral PFC, respectively. GRIN lens and baseplate were implanted into the ipsilateral PFC. *Lower*, Representative image of GCaMP6f expression. GCaMP6f was expressed over L2/3 and L5. Scale bar, 120 μm. **(d)** Representative Miniscope image of COM cells obtained using a 1 mm GRIN lens. **(e)** Representative raw and

intermediate data used for CNMF-E analyses of Miniscope images. *Upper*, Raw calcium trace from an exemplar neuron. *Middle*, Simulated calcium trace (red) calculated from convolution of inferred spike (blue; *middle*) and unitary calcium transient, which were estimated from CNMF-E. *Lower*, Rater plots of 62 cell activities during an exemplar extinction test. Each row of the raster plot represents all-or-none type spike activity, which were obtained from conversion of inferred spiking activity. Scale bar, 1 min.

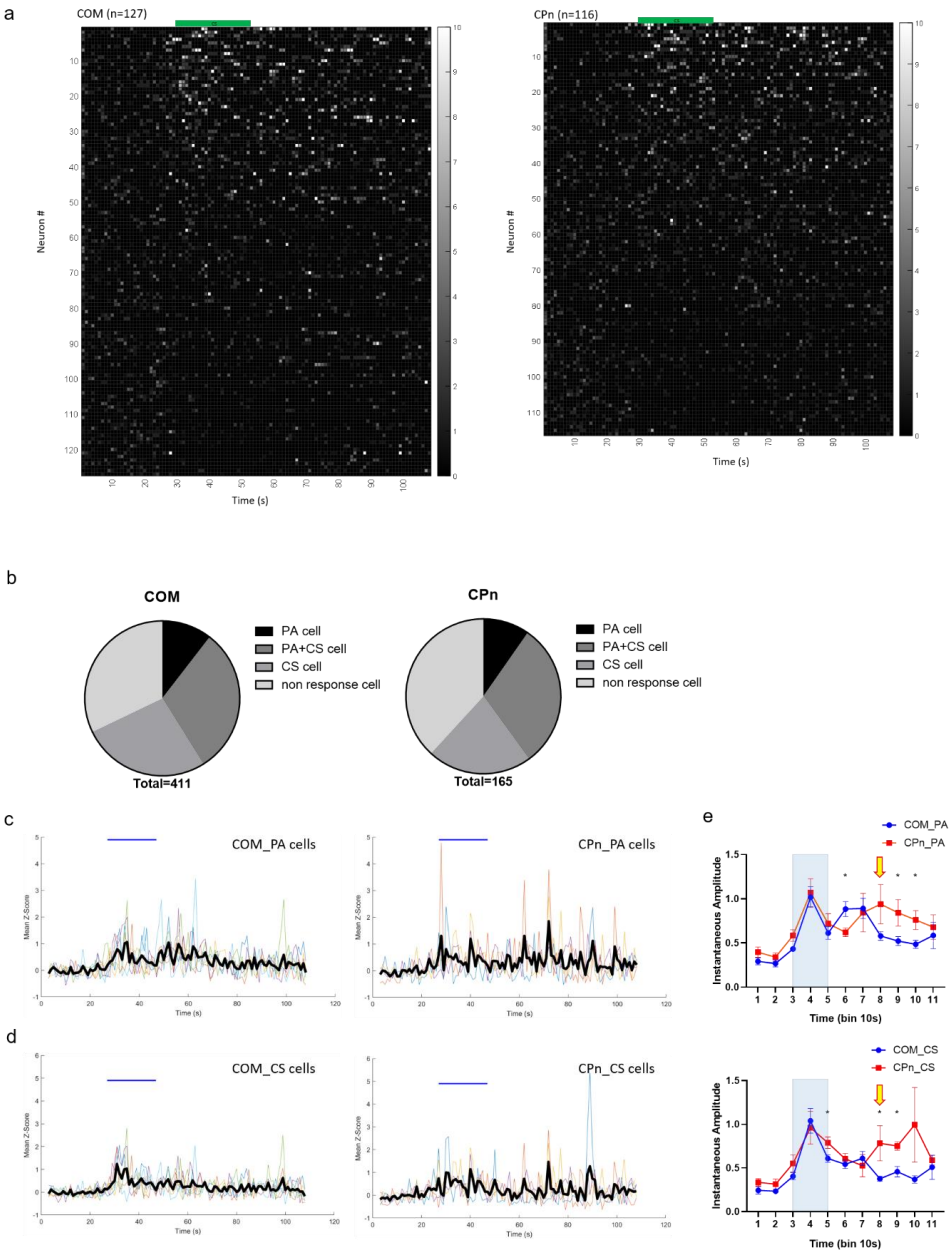
a
COM (n=127)
CPn (n=116)
Neuron #
Time (s)
b
COM
CPn
PA cell
PA+CS cell
CS cell
non response cell
Total=411
Total=165
c
COM_PA cells
CPn_PA cells
d
COM_CS cells
CPn_CS cells
Mean Z-Score
e
COM_PA
CPn_PA
COM_CS
CPn_CS
Instantaneous Amplitude
Time (bin 10s)

Figure 20. COM cell activity increased transiently at the onset and offset of CS, while the CPn cell activity increased during CS and sustained over the post-CS interval. (a) Heat map of z-score of COM (animals = 1, n = 127; *left*) and CPn (animals = 2, n = 116; *right*) activity averaged over five trials in the extinction test. After converting the inferred spike activity to 0 or 1, spike activities were averaged over first 5 trials, and the z-score was calculated with reference to the pre-CS baseline activity. The cell activities during CS were sorted in the descending order. **(b)** Pie charts of the proportions of PA cells and CS cells in COM cells (n = 411; PA cell: 169/411, CS cell: 236/411, PA+CA cell: 126/411 non-response cell: 132/411; *left*) and CPn cells (n = 165; PA cell: 66/165, CS cell: 86/165, PA+CS cell: 50/165, non-response cell: 63/165; *right*). The proportions of PA cells to CS cells was not different between COM and CPn (P = 0.478 for COM vs CPn, chi-square test). **(c)** Mean z scores of COM-PA cells (animals = 6, n = 41/97, 35/64, 45/129, 16/32, 18/48, 14/41; *left*) and CPn-PA cells (animals = 4, n = 8/27, 8/20, 21/56, 26/62; *right*) averaged over trials 1-5. The COM-PA cell activity transiently increased at the onset and offset of CS. In contrast, the CPn-PA cell activity increased during CS and showed persistent activity during Post-CS interval (*right*). Thin line, averaged z-score of individual animal;

Thick lines, z-scores averaged across tested animals. (d) the same as *c* but activities of COM-CS cells (animals = 6, n = 62/97, 37/64, 73/129, 18/32, 28/48, 18/41; *left*) and CPn-CS cells (animals = 4, n = 16/27, 11/20, 24/56, 35/62; *right*). COM-CS cell activity transiently increased at the onset of CS. In contrast, CPn-CS cells activity increased during CS and showed persistent activity during Post-CS. (e) *Upper*, 10 s-binned instantaneous amplitudes of COM-PA and CPn-PA cell activities calculated from Hilbert transform of averaged z-score displayed in *c*. Both COM and CPn activity increased at the onset of CS. The activity of COM cells, but not CPn cells, increased at the offset of CS (P = 0.041 for CPn vs COM 50~60 s). The CPn cells, but not COM cells, showed persistent activity over the post-CS interval and peaked at the expected timing of US presentation (P = 0.045 for CPn vs COM 80~90 s; P = 0.027 for CPn vs COM 90~100 s). *Lower*, the same as upper but instantaneous amplitudes of COM-CS and CPn-CS cell activities. The CPn cells, but not COM cells, showed persistent activity over the post-CS interval (P = 0.037 for CPn vs COM 70~80 s; P = 0.008 for CPn vs COM 80~90 s). All data are mean ± S.E.M., **P < 0.01, Repeated measures ANOVA, Post-hoc test Fisher's LSD pairwise comparisons.

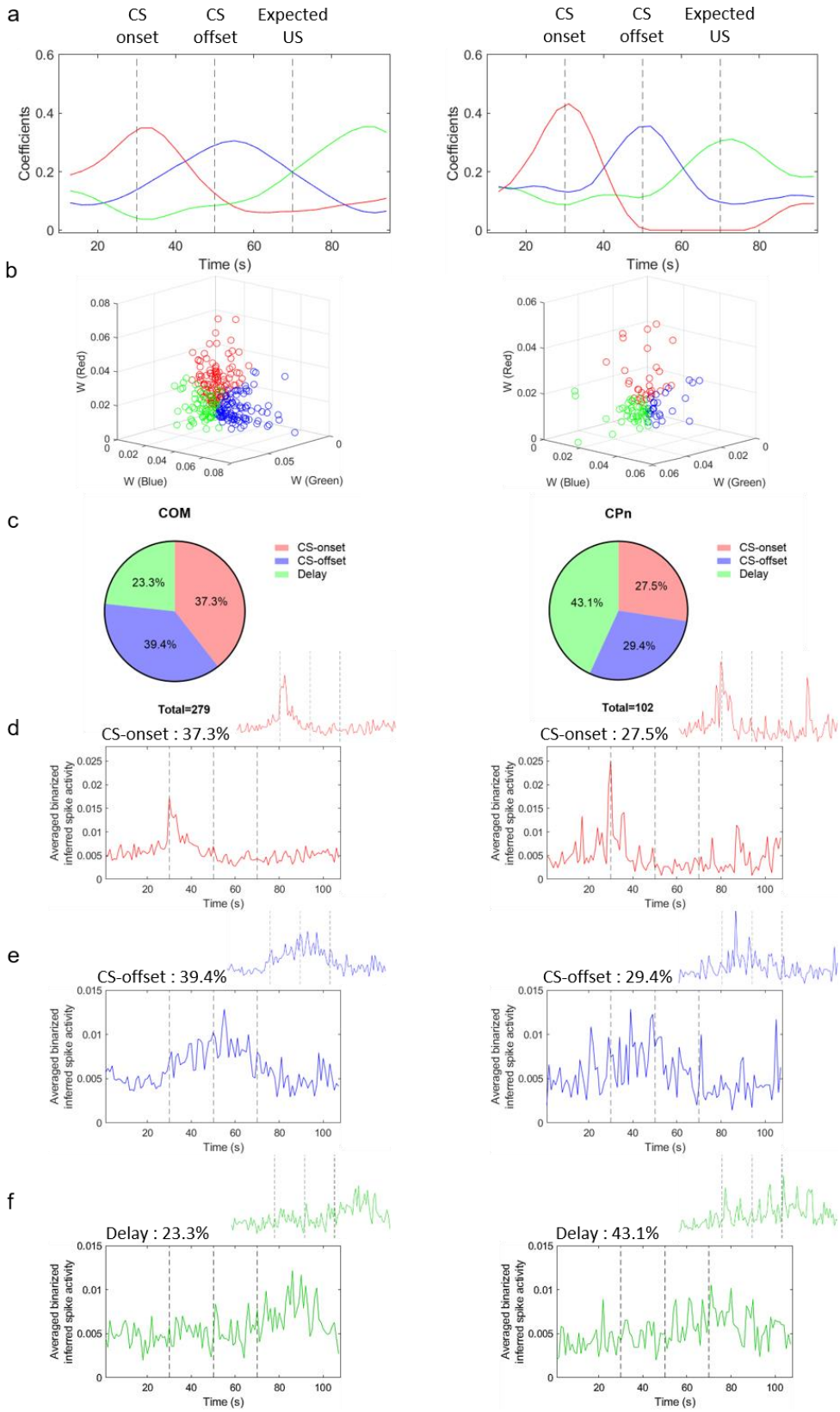
a
CS onset
CS offset
Expected US
Coefficients
Time (s)
b
W (Red)
W (Blue)
W (Green)
c
COM
CPn
CS-onset
CS-offset
Delay
23.3%
37.3%
39.4%
27.5%
43.1%
29.4%
Total=279
Total=102
d
CS-onset : 37.3%
CS-onset : 27.5%
Averaged binarized inferred spike activity
e
CS-offset : 39.4%
CS-offset : 29.4%
f
Delay : 23.3%
Delay : 43.1%

Figure 21. Larger proportion of CPn cells showed increasing post-CS activity that peaked at the expected US timing compared to COM cells. (a-b) Classification of COM and CPn cell activities using nonnegative matrix factorization (NMF). **(a)** Basis functions of COM (*left*) and CPn (*right*) cell activities. The COM and CPn neurons activity patterns were classified into 3 groups according to the basis function type to which each cell has the maximal weight. The basis functions were named CS onset (red), CS offset (blue) and delay (green). **(b)** After multiplying each weight (W) with the peak coefficient of corresponding basis function, the COM (*right*) and CPn (*left*) activity patterns were divided into three groups. **(c)** Percentages for the three activity patterns in COM (n = 279; CS-onset: 110/279, CS-offset: 104/279, Delay: 65/279; *left*) and CPn cells (n = 102; CS-onset: 28/102, CS-offest: 30/102, Delay: 44/102; *right*). In COM, CS-onset (37.3%) and CS-offset groups (39.4%) had more proportion than delay group (23.3%), whereas in CPn, Delay group (43.1%) occupied more proportion than CS-onset (27.5%) and CS-offset groups (29.4%). largest proportion of CPn cells, but not COM cells, belonged to a delay cell type (P = 0.001 for COM vs CPn, chi-square test). **(d-f)** Averaged binarized inferred spike activity of each cell group. *Left*, COM cells; *Right*, CPn cells. *e*, CS onset cell; *f*, CS offset cell; *g*, delay cell. *Insert*, Averaged normalized (z-score) activity of each cell group.

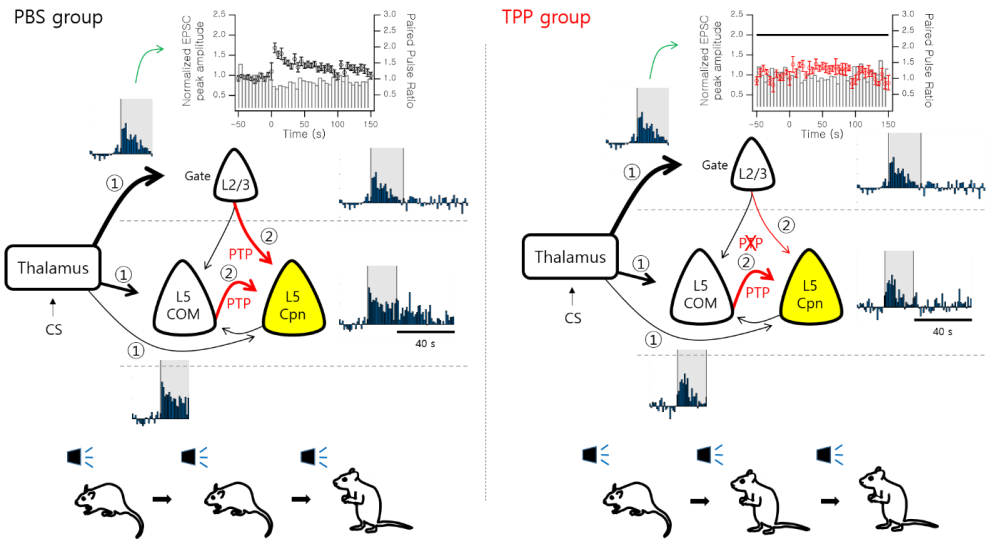

Figure 22. Schematic illustrations for the contribution of mitochondrial residual calcium-mediated PTP to mPFC persistent activity and trace fear extinction learning. During the trace fear extinction learning, CS information may be delivered to the mPFC through the thalamus. The thalamus input to PFC L2/3 was stronger than to L5, and the thalamus input to PFC L5 COM cells was stronger than to L5 CPn (①; Collins, Anastasiades et al. 2018). Some PFC L2/3 and L5 putative pyramidal neurons showed increased activities during CS period. In PBS groups, PTP at L2/3 to L5 CPn and L5 COM to L5 CPn synapses was induced by CS response (②). CPn neurons received presynaptic input with enhanced efficacy for tens of seconds following the CS. These enhanced inputs from L2/3-to-L5 PNs may contribute to persistent activity after CS period, whereas L2/3 PN did not show

persistent activity. For TPP group, however, PTP at L2/3 to L5 CPn synapse was not induced by CS response because mitochondria-mediated residual calcium was abolished by TPP (②). Therefore, L2/3 inputs to CPn PNs after CS period would not be enhanced. The lack of PTP at these synapses may prevent post-CS persistent activity in L5 PNs of TPP group. In tone test on the next day, both groups showed similar freezing behavior at first three trials, but TPP group showed accelerated extinction of conditioned fear compared to the PBS group. These results suggest that mitochondrial-residual calcium-mediated PTP at L2/3-to-CPn synapses is one of the essential factors for PA of PFC PL area during the post-CS period of trace fear extinction learning, and PA of PFC PL area may be required for hindrance of extinction learning.

Discussion

In this study, I demonstrated that 1) presynaptic mitochondria-dependent and TPP-sensitive PTP occurs specifically at L2/3-CPn synapses of the PL area; 2) TPP abolishes the persistent activity (PA) in the PL area during trace intervals of TFC and post-CS activity during subsequent retrieval of fear memory; 3) The pattern of neuronal firing during trace interval is cell type specific manner, and PA is observed preferentially in CPn cells rather than COM cells. I summarized the findings of the present study in Figure 22. Taken together, I conclude that mitochondrial-residual calcium-mediated PTP at L2/3-to-CPn synapses is one of the essential factors for PA of CPn cells of PFC PL area during the trace intervals of TFC. TPP not only abolished PA during trace intervals but also prematurely shortened the CS response even though CS continued. In contrast to the prevailing hypothesis that the information of CS is held by PA during trace intervals, I did not observe any deficit in retrieval of trace fear memory in the TPP-treated animals, even though PA was abolished during the trace interval of TFC. The lack of PA was rather correlated with acceleration of fear extinction. These results elaborated previous findings of Mukerjee & Caroni (2018). Activities and plastic

changes in the PL area are required for new memory formation of CS-US association during TFC (Runyan, Moore et al. 2004, Gilmartin and Helmstetter 2010, Gilmartin, Miyawaki et al. 2013), but not for recall of already learned rule (Mukherjee and Caroni 2018). Nevertheless, extinction of conditioned fear memory was accelerated by inhibition of the PL. More generally, PL activities promoted learning a new rule for cue-reward association (intradimensional shift), but were dispensable for recall of a learned rule (Mukherjee and Caroni 2018). Although the present study did not show direct causal relationship between the lack of prelimbic PA and acceleration of fear memory extinction, my results imply that prelimbic PA may interfere with extinction learning. It remains to be elucidated whether prelimbic PA also contributes for an animal to adhere to the previously learnt rule even if the animal is repeatedly exposed to an alternative rule.

Effect of afferent inputs from other brain areas to PFC on fear memory formation and extinction

Many different afferent fibers from other prefrontal areas especially thalamus, amygdala and hippocampal areas innervate the PFC

(DeNardo, Berns et al. 2015). Various inputs to the PFC may affect fear memory formation or extinction learning. Twining and Gilmartin (2020) showed that the ventral hippocampus (VH) input to PL of PFC did not affect the trace cued memory formation, but disrupts contextual fear memory learning (Twining, Lepak et al. 2020). To inactivate the VH input to PL during TFC, archaerhodopsin (ArchT) was expressed in VH, and 532 nm laser light was illuminated through the optic fiber which was located in the PL. Most PFC neurons showed a sustained increased firing activity during photoinhibition, and minority of PFC neuron showed sustained decreased firing activity during photoinhibition. To examine the role of VH input to PFC on trace cued or contextual fear memory formation during TFC, 532 nm laser light was illuminated on each trial for 70 s starting 20 s before CS onset and ending 20 s after US offset during TFC. TFC was performed over the 3 consecutive days with 6 minutes baseline period and two CS-US pairing trials per day. Tone test was performed 5 h before the TFC on each day. In tone test, GFP- and ArchT- expressing groups showed similar freezing behavior. However, in contextual fear learning, VH-PL silencing group showed temporally dynamic deficit in the formation of a contextual fear memory (Twining, Lepak et al. 2020). These results suggest that VH input to PL is not

necessary for auditory trace fear memory formation, but is essential factor of the formation of contextual fear memory.

Mediodorsal thalamus (MD) was also one of the major long range inputs to PFC PL area (DeNardo, Berns et al. 2015). Mediodorsal thalamic low and high frequency stimulation induced long term depression (LTD) and long term potentiation (LTP) of field response in the mPFC, respectively. Plasticity of mPFC was associated with the delay fear extinction (Herry and Garcia 2002). To investigate the correlation between LTD at MD thalmus to mPFC synapses and delay fear extinction learning, the freezing behavior and to MD stimulation-induced mPFC field potentials were recorded during tone test given after DFC. Tone test was performed over 4 consecutive days with 4 tone only trials per day. The non-stimulated group showed a decrease in the field response of the mPFC on the first tone test day, and the reduced mPFC field response was restored to the baseline on the third tone test day. The MD-stimulated group which received LFS at MD on the second and third tone test days displayed a larger reduction in mPFC response on the second and third tone test days than the non-stimulated group. The freezing behavior of both groups was similar on first and second tone test days. However, MD-stimulated groups showed larger freezing behavior on third tone test day. These

results suggested that LTD of the mPFC field response induced by LFS of MD impaired delay fear extinction learning. To investigate the correlation between LTP at MD-mPFC synapses and delay fear extinction learning, the freezing behavior and mPFC field potentials of non-stimulated and MD-stimulated groups were recorded during tone test after DFC. Fear extinction procedure comprised a single day with 16 tone only trials. Additionally, long term maintenance of extinction was examined at 1 week later using single day with four tone only trials. The MD-stimulated group received HFS at MD 32 minutes before the tone test the day after DFC and showed LTP of mPFC field response during the tone test and 1 week follow-up test. The non-stimulated group was divided in two groups. One group showed persistently decreased mPFC response during tone test and 1 week follow-up test. The other group also showed a decreased mPFC response, but the decreased mPFC response was restored to the baseline during the tone test. The freezing behavior of all groups was similar during the tone test. However, the persistently decreased mPFC response group showed larger freezing behavior than MD-stimulated group and mPFC response restored group on the 1 week follow-up test. These results suggested that LTP in the mPFC was associated with the maintenance of extinction (Herry and Garcia 2002). However, the

effect of MF input to mPFC in trace fear memory formation and extinction remains to be elucidated. The MD input to PFC L5 COM cells was stronger than to L5 CPn. In addition, the MD input to PFC L2/3 was stronger than to L5 (Collins, Anastasiades et al. 2018). In a previous study of my lab, PTP was not induced by tetanic stimulation at MD into PFC L5 PN synapses. However, I did not test whether PTP was induced at MD to PFC L2/3 PN or PFC IN synapses. The thalamus input to PFC L2/3 PN or PFC IN may contribute to trace fear memory extinction learning.

Moreover, other afferent inputs to PFC PL other than those from hippocampus and thalamus may be involved in trace fear memory formation or extinction learning. However, in this study, I did not test the effect of TPP on these inputs to the PFC. It also remains to be elucidated whether TPP affects other afferent inputs to the PFC and these afferent fibers to PFC contribute to the trace fear memory formation or extinction.

Persistent activity in PL of mPFC and attentional processes of ACC during TFC

Previous human studies implicated a role of the anterior cingulate

cortex (ACC) in various cognitive functions including attention (Cohen, Kaplan et al. 1999, Davis, Hutchison et al. 2000, Jovicich, Peters et al. 2001). In rodent study, Han and Anderson (2003) suggested that attentional process is necessary for TFC, and ACC played an essential role in trace fear memory formation (Han, O'Tuathaigh et al. 2003). To examine whether attentional process is required on the TFC or DFC, the distraction conditions consisting of a flashing white light were presented with a random interstimulus interval of 5, 10, 15, or 20 s during TFC or DFC. On the next day after TFC or DFC, both control mice that did not receive the distractor and those that received distractor stimuli did not show freezing behavior to the light stimulus. In tone test after DFC, both groups showed similar freezing behavior. However, in tone test after TFC, the freezing behavior of the distracted group significantly was lower than that of control group. Since the both groups showed similar freezing behavior during tone test after DFC and does not show freezing behavior during light test the day after TFC or DFC, the flashing light may not compete with the tone as a CS. Lower freezing after TFC in the distracted group implies that the distractor stimulus may interfere TFC by distracting the animal’s attention during TFC. Next, Han et al (2003) observed freezing behavior during tone test after bilateral neurotoxic lesions

of the ACC using N-methyl-D-aspartate before the TFC or DFC to investigate the requirement of an ACC for TFC or DFC. The sham and ACC lesion group showed similar freezing behavior during tone test the day after DFC. However, ACC lesion group showed lower freezing behavior than sham group during tone test the day after TFC. Taken together, the attentional processes were necessary for formation of trace fear memory and ACC was essential area for trace fear memory formation (Han, O'Tuathaigh et al. 2003).

During the tone test the day after TFC, the animal would have been in a high-level of attentional state during post-CS period of the first few trials, because the animal received CS-US pairing trials with a probability of 100% the day before the tone test. After the first few trials, the level of attention of animals would decrease as the trials progressed, because the US did not present consistently after the CS. I hypothesized that the ACC input to PFC may be essential factor of the occurrence of persistent activity in PL, because the ACC axon fibers were one of the major afferent inputs to the PFC (DeNardo, Berns et al. 2015). Therefore, a persistent activity in the PL area that occurred during the post-CS period of the first few trials in the tone test and disappeared as the trials progressed may be implicated in attentional processes regulated by

ACC.

COM and CPn cells encode different information during working memory and set shifting tasks

According to previous studies, the two cell types of PFC are differentially involved in working memory or set-shifting tasks depending on the ambiguity of CS-US relationship. The neocortical deep layer pyramidal neurons are generally classified as intratelencephalic (IT), pyramidal tract (PT), and corticothalamic (CT) projection neurons. CPn and COM correspond to PT and IT, respectively (Harris and Shepherd 2015, Baker, Kalmbach et al. 2018, Anastasiades and Carter 2021). In the delayed match-to-sample (DMS) task, which is a type of working memory task, inactivation of PT during the delay period did not impair the task performance, whereas inactivation of IT cells did (Bae, Jeong et al. 2021). Consistently, in the DMS task, IT encoded target-specific information during the delay period while the activity of PT neurons did not correlate with the target. The PT activity encoded more temporal information compared to IT (Bae, Jeong et al. 2021). However, in the probabilistic reversal task, in which flexible choice

behavior is required for an animal to obtain reward with contingency characteristics, the effects of ET and IT inactivation on animal behavior were different. In the probabilistic reversal task, inactivation of IT had no effect on behavior, but the inactivation of PT and CT significantly increased a bias in choice (Nakayama, Ibanez-Tallon et al. 2018). In the set-shifting task, another task that requires flexible behavior, trial outcome (correct/incorrect) was represented by PT neurons, and set shifting was impaired by inactivation of these cells (Spellman, Svei et al. 2021). These previous studies imply that COM neurons seem to play a key role in encoding target-specific information under consistent and strong CS-US relationship, whereas CPn cells come into play when the CS-US relationship is highly ambiguous. Taken together, it suggests that neurons located in the deep layer of the PFC differently contribute to animal behavior depending on the degree of ambiguity of the task.

Persistent activity during trace interval is not necessary for CS-UCS association in TFC

Bilateral injection of APV or muscimol into PFC 15 minutes before

conditioning did not affect fear memory formation in DFC but did in TFC (Gilmartin and Helmstetter 2010). Gilmartin et al (2013) reported that inactivation of PFC during the trace interval impairs fear memory formation, suggesting that PA during trace intervals in the PFC associates CS with US (Gilmartin, Miyawaki et al. 2013, Gilmartin, Balderston et al. 2014). However, in my experimental results, fear memory formation was not affected even in the absence of PA during the trace interval in TFC, and only fear memory extinction was accelerated by repeated presentation of CS alone on the next day (Figure 13). As mentioned above, recent studies revealed that prefrontal pyramidal neurons encode different kinds of information depending on the projection cell types. The present study showed that the COM cells displayed transient activation during CS onset and CS offset while CPn cells rather than COM cells exhibited PA, suggesting that COM cells would temporarily store information about CS (Figure 20). It should be noted that entire PFC was inactivated in Gilmartin et al (2013). Given that PA is primarily mediated by CPn cells, the role of PA in TFC would not correctly evaluated based on the results from the inactivation of the entire PFC. In the present study, I found that CPn cells display PA, and that, when PA was specifically abolished by TPP, fear memory formation was little affected, whereas fear

memory maintenance was impaired (Figure 13).

In TFC, the retrosplenial cortex (RSC) is also involved in fear memory formation and extinction learning (Kwapis, Jarome et al. 2014, Kwapis, Jarome et al. 2015). In a previous study, to test the role of RSC on fear memory formation in trace fear conditioning (TFC) or delay fear conditioning (DFC), the protein synthesis inhibitor (anisomycin, ANI) was injected into the RSC before the DFC or TFC and then freezing behavior was observed. In DFC, ANI and ASCF injected groups showed similar freezing behavior in response to a tone during tone test. However, in TFC, the freezing behavior during tone test was significantly lower in the ANI group than in the ACSF group. In contrast, when ANI was injected into the RSC just after TFC, ANI and ACSF groups showed similar freezing behavior during tone test, raising a doubt whether RSC is required for consolidation of trace fear memory (Kwapis, Jarome et al. 2015). In another study, NMDA receptor blocker (APV) was injected into the RSC before tone test on the day following TFC or DFC. In TFC, the freezing behavior of APV group was significantly lower than in the ASCF group. However, in the DFC, the freezing behavior of two groups was not different (Kwapis, Jarome et al. 2014). Since the APV group after DFC showed similar freezing behavior to the ACSF group, the APV-induced reduction of freezing

response to CS in TFC group may be attributed to failure of retrieval of fear memory rather than freezing expression. In the extinction retention test on the day after the tone test in the DFC group APV and ASCF groups showed similar freezing behavior. However, in the TFC group the APV injection resulted in higher freezing behavior than the ASCF group, suggesting that NMDARs in the RSC are important for both the retrieval and extinction of trace fear memory (Kwapis, Jarome et al. 2014).

The amygdala is also an important area for fear memory formation, expression and extinction learning in the TFC or DFC (Kochli, Thompson et al. 2015, Gilmartin et al. 2012, Kwapis, Jarome et al. 2014). In a previous study, to test the role of amygdala on fear memory formation in TFC or DFC, $GABA_A$ agonist muscimol (MUC) was injected into amygdala before the DFC or TFC. In both conditionings, the freezing behavior during tone test was significantly lower in the MCU group than in the saline group (Gilmartin et al. 2012). Another study observed freezing behavior during tone test after bilateral neurotoxic lesions of the amygdala before TFC or DFC. In both conditionings, the freezing behavior during tone test was significantly lower in the amygdala lesion group than in the sham group (Kochli, Thompson et al. 2015). These results demonstrate that amygdala is an important brain area

for fear memory formation in DFC and TFC. In another study, APV was injected into the amygdala before tone test on the day following TFC or DFC to test the role of the amygdala in the expression or retrieval of the fear memory in DFC or TFC (Kwapis, Jarome et al. 2014). In both conditionings, APV and ACSF injected group showed similar freezing behavior in response to a tone during tone test. However, In the extinction retention test on the next day, the APV group showed higher freezing behavior than the ASCF group in DFC group but not in TFC group. These results suggest that NMDARs in amygdala plays an important role in the extinction of delay fear memory. However, when an AMPA receptor antagonist (CNQX) was injected into the amygdala before tone test on the day following TFC or DFC, the freezing behavior during the tone test was significantly lower in the CNQX group than in the ACSF group at either DFC or TFC (Kwapis, Jarome et al. 2014). In the extinction retention test, the CNQX group showed higher freezing behavior than the ASCF group only in DFC. These results suggest that AMPA-mediated amygdala activity plays an important role in fear expression in the DFC or TFC and is required for delayed fear extinction, and that both AMPAR and NMDAR-mediated amygdala activity play little role in trace fear extinction while AMPAR-mediated activity is required for fear expression after TFC.

Collectively, other brain regions other than the PFC may contribute to trace fear memory formation and extinction, raising a possibility that the trace fear memory may be stored in other brain regions and the persistent activity of the PFC may be required for fear memory maintenance or extinction learning.

PFC-Thalamus circuit and fear conditioning

The PL activity is necessary for acquisition of fear memory in TFC, but not in DFC (Gilmartin and Helmstetter 2010). Intriguingly, however, the PL activity is required for fear expression during conditioning and recall of fear memory in DFC (Sierra-Mercado, Padilla-Coreano et al. 2011, Sotres-Bayon, Sierra-Mercado et al. 2012). It has been suggested that positive feedback loop between PL and BLA support sustained fear response to CS in animals that underwent DFC (initiated by the amygdala, but sustained by PL). In contrast, PL activity was dispensable for recall of fear memory or fear expression after TFC (Fig 4c of Mukerjee, Caroni 2018), suggesting that fear expression circuit for TFC differs from that for DFC. Therefore, it is unlikely that prelimbic PA resulting from positive feedback loop between PL and BLA plays a role in sustained fear expression during CS alone session after TFC.

Consistent with this view, silencing PL-to-amygdala input during trace interval did not affect the fear response to CS tested during and after TFC (Kirry, Twining et al. 2020).

Thalamic PLCß4-/- mice showed abnormal fear extinction behavior compared to WT (Lee, Ahmed et al. 2011). PLCß4-/- mediodorsal thalamic nucleus neurons increased T-type channel-mediated burst firing compared to WT. Furthermore, in the extinction test, the tonic firing increased over the trial in mediodorsal thalamic nucleus neurons of WT, whereas in PLCß4-/- mice, burst firing increased over the trial (Lee, Ahmed et al. 2011). The thalamus input to the PFC L2/3 is stronger than to L5 (Collins, Anastasiades et al. 2018). The present study showed an increase in burst firing of L2/3 neurons during CS compared to the baseline, and that this burst firing was sufficient to induce PTP in the L2/3-CPn synapse (Figure 17, 18). Thalamic burst inputs to L2/3 is expected to facilitate spike transfer because of short-term facilitation and depression at thalamic synapses onto pyramidal and interneurons in L2/3, respectively (Lee, Choi et al. 2020). Together, with these studies, my results imply that the increased burst firing in the thalamus of PLCß4-/- mice may provide excitatory inputs that allows L2/3 PFC neurons to fire more in bursts during CS. It is plausible that PTP at L2/3-CPn synapses of PLCß4-/- mice would

more readily induce due to the increased burst firing of L2/3 neurons, resulting in impaired fear extinction.

PFC neurons projecting to the thalamus are located in both L5 and L6, while there are more numerous cells in L6 (~80%) than in L5 (~20%) (Xiao, Zikopoulos et al. 2009, Collins, Anastasiades et al. 2018). Contrary to the number of thalamic projecting cells, thalamus-projecting L6 neurons form small boutons in the thalamus while L5 neurons form large boutons (Xiao, Zikopoulos et al. 2009). Moreover, L5-to-thalamic synapses display stronger synaptic weights with higher release probability compared to L6-to-thalamic synapses. Recently, activities of L6 were shown to be depressed during the delay period of the reward anticipation task, while PFC L5 neurons showed PA (Kim, Bari et al. 2021). Although post-CS L6 activity remains to be studied, I showed that post-CS PA is mediated by L5 CPn cells. Given that L5 CPn cells efficiently drive firing of thalamic neurons, and that burst firing of L2/3 neurons driven by thalamic inputs induces PTP at L2/3-CPn synapses, I imagine a positive feedback loop comprised of L2/3, CPn, and MD thalamus. This trisynaptic feedback loop may support PA in TFC similar to the feedback loop between PL and BLA does in DFC (Sotres-Bayon, Sierra-Mercado et al. 2012).

Persistent activity occurs in cell type dependently

The cell type which mediates PA in the PFC remains to be understood. In monkey and rodent studies, there is a model in which the activation of postsynaptic α2A adrenoceptors (α2A-ARs) inhibits cAMP production, which causes HCN channels to close and PA occurs more actively, increasing working memory performance (Wang, Ramos et al. 2007). In ex vivo experiment, treatment with clonidine, an α2A-ARs agonist, in the PFC significantly increased R_{in} for both CPn and COM neurons, but the effect on CPn neurons was significantly greater. Also, the sag ratio was significantly decreased only in CPn neurons. Acetylcholine also increases the performance in working memory tasks. Carbachol (CCh), an acetylcholine receptor agonist, did not affect R_{in} in both cell types of PFC. However, the sag ratio was significantly decreased only in CPn neurons. To test the effect of CCh on the suprathreshold responses, the amount of current sufficient to generate action potential was injected into each cell type after CCh treatment. In CPn, 8 of 11 neurons showed PA longer than 30 s, and in COM, 3 of 13 neurons showed PA (Dembrow, Chitwood et al. 2010). In addition, DHPG, a Group 1 mGluR agonist, increases the R_{in} of CPn

and reduces the sag ratio, but does not affect COM neurons. When DHPG was treated, CPn showed more PA than COM (Kalmbach, Chitwood et al. 2013). Therefore, these ex vivo experiments showed that neuromodulators which affects PA and working memory also have greater effects on CPn neurons.

A previous in vivo study showed that PA occurred in upper L5 of the PFC, but not in L2/3 (Kim, Bari et al. 2021), and that PT and IT cells were found in lower and upper L5, respectively, because lower layer neurons had a higher voltage sag ratio than upper layer ones. This study suggested that IT may mediate PA because PA was observed in the upper L5. However, other studies demonstrated that IT neurons are evenly distributed throughout the L5, and PT neurons exist in the upper L5b (Collins, Anastasiades et al. 2018, Anastasiades and Carter 2021). It may not be accurate to distinguish IT and PT according to the layers they reside. I distinguished CPn and COM cells by their definition by labeling them according to their projection targets using retro-AAV Cre and AAV flex-GCaMP6f virus. Therefore, CPn and COM neurons activities shown in the present study should be more reliable compared to previous studies. Using these methods, I clearly demonstrated that the post-CS neuronal activities are mediated by CPn neurons (Figure 19, 20).

Validity for the specific effects of TPP on PTP at L2/3-CPn synapses

The interpretation of in vivo results of the present study critically depends on the hypothesis that TPP specifically inhibits PTP at L2/3-CPn synapses with little adverse effects. TPP did not significantly affect mitochondrial respiration when used at low doses (Aiuchi, Matsunaga et al. 1985, Karadjov, Kudzina et al. 1986). However, TPP has not been used in vivo previously. Therefore, I tested whether TPP has any effects in the cell properties other than mNCX, and found that it had no effect on cell properties including after depolarization (ADP), firing frequency-current injection relationship (F-I curve), Input resistance (R_{in}), resting membrane potential (RMP) and action potential threshold (AP threshold). Nevertheless, it cannot be ruled out the possibility that TPP has some side effects in vivo on the cell and network properties other than PTP at L2/3-CPn synapses. To test the specificity of TPP, I used the early stage of Tg2576 that is an Alzheimer's mouse model, which is known to have damaged mitochondria, and found that PTP was not observed in this model (Lee, Kim et al. 2012). Consistently, it was recently shown that

PTP and early LTP also decreased in the hippocampus Schaffer collateral-CA1 synapse of mice in the early stage of 3xTg-AD, which is another Alzheimer's mouse model (Chakroborty, Hill et al. 2019). In addition to Alzheimer's disease, there have been studies on mitochondrial impairment in Parkinson's disease. In the study of the molecular causes of Parkinson's disease, the PD genes that cause Parkinson's disease have been identified. PD genes include α-synuclein, leucine-rich repeat kinase 2 (LRRK2), DJ-1, ATP13A2, parkin and PTEN-induced kinase 1 (PINK1) (Wood-Kaczmar, Deas et al. 2013). Mutations in PINK1 cause early onset parkinsonism and, in the absence of PINK1, sustained increases in mitochondrial calcium. Increased mitochondrial calcium in the absence of PINK1 is due to impaired mNCX activity (Gandhi, Wood-Kaczmar et al. 2009). In addition, impaired mNCX activity in PINK1 deficiency was rescued by PKA (Kostic, Ludtmann et al. 2015). However, studies on PTP in Parkinson's disease have not been established.

Collectively, my study revealed that mitochondrial-mediated PTP in the PFC closely correlates to PA occurrence, and that extinction of fear memory was accelerated when PA was abolished by TPP during the CS alone test. Given that TPP specifically inhibits PTP at L2/3-CPn synapses and that the post-CS PA is mediated by CPn

cells, my results suggest that cell type specific occurrence of PA is important for fear memory extinction circuit. Furthermore, this result would have a great influence on the interpretation of several behavioral experiments in which PFC is associated, and is expected to be meaningful in understanding diseases in which mitochondria are impaired.

CHAPTER 2

Gradual pattern separation in CA3 associated with contextual discrimination learning is impaired by Kv1.2 insufficiency

Introduction

Hippocampus has been proposed as a complementary-learning-system specialized for rapid formation of discrete representations of contextual memories in contrast to the neocortex, which gradually adjusts internal model in response to new information (McClelland and Goddard 1996, Norman 2010). Information from entorhinal cortex (EC) is transmitted to CA3 pyramidal cells (CA3-PCs) directly via perforant pathway (PP) and indirectly via mossy fibers (MFs) after being pre-processed by dentate gyrus (DG). Previous theoretical and lesion studies support the notion that DG performs pattern separation, a computational process that orthogonalizes overlapping inputs (O'Reilly and McClelland 1994, Rolls and Kesner 2006). Pattern separation in DG is thought to be underpinned by a large number and low excitability of dentate granule cells (GCs) and extensive inhibitory networks in DG leading to sparse activity (GoodSmith, Chen et al. 2017, Kim, Yeon Lee et al. 2020). Moreover, not only overlap of neuronal ensembles but also temporal similarity between input and output spike trains are decorrelated over synaptic transmission at PP to GC and MF to CA3-PC synapses (Madar, Ewell et al. 2019).

The CA3 network displays discrete and decorrelated representations of episodic memories (Leutgeb, Leutgeb et al. 2004, Rolls and Kesner 2006, Leutgeb, Leutgeb et al. 2007). Because MFs sparsely innervate CA3-PCs (Amaral, Ishizuka et al. 1990) and convey input patterns pre-processed by DG to CA3, computational models proposed that MF inputs contribute to pattern separation in CA3 (Treves and Rolls 1992, O'Reilly and McClelland 1994). In contrast to MFs, PP densely innervates CA3-PCs and makes weak and Hebbian synapses onto CA3-PCs (Amaral, Ishizuka et al. 1990, McMahon and Barrionuevo 2002). A formal model implies that cued memory retrieval of a pattern stored in recurrent network requires afferent inputs mediated by large number of associatively modifiable synapses, which correspond to PP-CA3 synapses (Treves and Rolls 1992). In addition, to avoid for input pattern being interfered with patterns already stored in a recurrent network, the input pattern should be represented by a small number of principal neurons driven by strong afferent input (sparse coding). The sparse coding in CA3 can be accomplished by sparse and strong MF input, which enhances the variance in distribution of excitatory inputs over the CA3-PC population and thus governs the firing pattern of CA3-PCs during a learning phase under competitive k-Winners-Take-All regime (Treves and Rolls

1992, O'Reilly and McClelland 1994). Therefore, it was postulated that memory representation driven by MF input during learning phase would be stored by Hebbian long-term potentiation (LTP) at PP and recurrent synapses to a subset of CA3-PCs, which are chosen by decorrelated DG inputs (Treves and Rolls 1992, McMahon and Barrionuevo 2002, Mishra, Kim et al. 2016). Accordingly, lesion or inactivation of DG outputs to CA3 revealed that MF inputs are required for the memory acquisition, whereas MF inputs, but not PP inputs, are dispensable for retrieval of acquired memories (Lee and Kesner 2004, Bernier, Lacagnina et al. 2017), implying that plastic changes at PP-CA3 synapses constitute the encoding of contextual memories in the CA3 network. In order for PP inputs to activate a decorrelated CA3 ensemble on retrieval, LTP at PP synapses should be induced in a small number of CA3-PCs during hippocampal learning. For sparse encoding at PP synapses, induction of LTP at PP synapses should be tightly regulated, and thus it would be of crucial importance to keep the minimal strength of synaptic inputs required for LTP induction (referred to as LTP threshold) high at PP-CA3 synapses.

The CA3 region displays the highest expression of Kv1.2 transcripts in the rodent hippocampus (http://mouse.brain-

map.org/gene/show/16263). Somatodendritic expression of Kv1.2 is polarized to distal apical dendrites, at which PP synaptic inputs arrive (Hyun, Eom et al. 2015). Consistent with the notion that D-type K^+ current ($I_{K(D)}$) is activated by low voltage depolarization near the AP threshold (Storm 1988), distal dendritic Kv1.2 subunits regulate the threshold for dendritic Na^+ channel-dependent amplification of PP-evoked EPSPs (PP-EPSPs) (Hyun, Eom et al. 2013, Hyun, Eom et al. 2015). Because PP synapses exhibit Hebbian plasticity, I hypothesized that downregulation of Kv1.2 and consequent enhancement of EPSP-to-spike (E-S) coupling would have a profound effect on the propensity of LTP induction at PP synapses. It has previously shown that insufficiency of Kv1.2 in CA3-PCs caused by heterozygous knock-out of *Kcna2* (*Kcna2*+/-) lowers the LTP threshold at PP-CA3 synapses, and impairment of behavioral pattern separation based on the performance in multi-trial contextual fear discrimination learning paradigm. To investigate the network bases of the impaired behavioral pattern separation, I investigated the hippocampal cell activities using fluorescence *in situ* hybridization (catFISH) of immediately early genes (IEGs: Homer1a and Arc) (Vazdarjanova and Guzowski 2004, Ramirez-Amaya, Angulo-Perkins et al. 2013). Here I show that genetic haploinsufficiency of *Kcna2* is closely correlated with

abnormal enlargement of CA3 ensembles during contextual fear discrimination task and impairment in gradual pattern separation of CA3 ensembles representing similar contexts.

Materials and Methods

Animals and Ethical approval.

All of studies and experimental protocols described in this article were approved by the Institutional Animal Care and Use Committee (IACUC) of Seoul National University. The animals were maintained in standard environmental conditions (Temperature: 25 ± 2 ℃, Humidity: 60 ± 5%, Dark/Light cycle: 20:00 – 8:00 of next day/8:00 – 20:00) and monitored under veterinary supervision by Institute for Experimental Animals, Seoul National University College of Medicine. All animals used in behavioural experiments were singly housed for 1 weeks before the experiments. For alleviation of compound factors by different experimenters, cohorts that were used in each experiments were handled by single experimenters. All behavioural experiments were done at 09:00–12:00, and 13:00–16:00 of each day.

Kv1.1 or Kv1.2 mutant mice

Heterozygous *Kcna1* and *Kcna2* knock-out mice (C3HeB/FeJ-*Kcna1*^{tm1tem} and C3HeB/FeJ-*Kcna2*^{tm1tem}, denoted as *Kcna1*+/− and

Kcna2+/−, respectively) were kindly donated by Dr. Bruce Tempel (University of Washington, Seattle) and purchased from The Jackson Laboratory (Bar Harbour, ME, USA; Donating Investigator: Dr. Bruce Tempel, University of Washington School of Medicine), respectively. These mice were maintained under the veterinary supervision by Institute for Experimental Animals, Seoul National University College of Medicine. By inter−crossing heterozygote mice, I bred homozygous knock−out mice, heterozygote mice and wild−type littermate (WT) for two genotypes. For genotyping, DNA was isolated from the tail of each mouse in a litter aged 6–8 days as described by (Brew, Gittelman et al. 2007). Detailed protocols are available online (*Kcna2*: https://www.jax.org/Protocol?stock Number=010744&protocolID=24908; *Kcna1*: https://www.jax.org/ Protocol?stockNumber=003532& protocolID=27668). Although *Kcna2*−/− and *Kcna1*−/− mice had a severely reduced life span (range P18–P23; P4−6 wks, respectively) (Brew, Gittelman et al. 2007), they appeared normal during the first 2 weeks of their life.

In situ hybridization

Fluorescence in situ hybridization (FISH) for RNA transcripts was performed using RNAscope probes [Advanced Cell Diagnostics

(ACD), Hayward, CA, USA] for target genes following the manufacturer's instructions and previous studies (Guzowski, McNaughton et al. 1999, Vazdarjanova and Guzowski 2004). A harvested brain was quickly frozen on liquid nitrogen and stored at −70° C until further processing. Coronal brain sections were prepared using a cryostat and thaw−mounted onto Superfrost Plus Microscope Slides (Fisher Scientific #12−550−15). The sections were fixed in 4% PFA for 10 min, dehydrated in increasing concentrations of ethanol for 5 min, and finally air−dried. Tissues were then pre−treated for protease digestion for 10 min at room temperature. For hybridization, prepared slides were incubated in HybEZ hybridization oven (ACD) for 30 min at 40° C. Unbound hybridization probes were removed by washing the sections three times with 1x wash buffer at room temperature for 2 min. For signal amplification, slides were incubated with amplification solutions (Amplifier #−FL): #1 for 30 minutes at 40° C, #2 for 15 min at 40° C, #3 for 30 minutes at 40° C, #4 for 15 min at 40° C. After the completion of each session, slides were washed twice with 1x wash buffer for 2 min at room temperature. Nuclei were counterstained with 4′ ,6−diamidino−2−phenylindole (DAPI, ACD). For detection of *Homer1a (H1a)*, *Arc*, and *Kcna2* mRNA in Figure 4 and 5, RNAscope Probes Mm−Homer1−tvS (Cat#, 433941), Mm−

Arc-C3 (Cat#, 316911-C3), Mm-Kcna2-C2 (Cat#, 462811-C2) were used, respectively. The slides were viewed, analysed, and photographed using TCS SP8 Dichroic/CS (Leica, Germany) or Olympus Fluoview FV1200 (Japan) confocal microscope equipped with 488 nm and 633 nm diode lasers. For *H1a* and *Arc*, the settings for photomultiplier and laser power were optimized for detection of intra-nuclear foci and for minimizing weaker cytoplasmic signals (Almira, McNaughton et al. 2002). The number of *Kcna2* mRNA dots and intra-nuclear foci of *H1a* and *Arc* were counted on 60 x magnified photographs (N.A. = 1.2).

Image acquisition and analysis for catFISH

Hippocampal slices obtained from *WT*, *Kcna1+/-*, and *Kcna2+/-* mice were analysed with RNAscope assay using target probes for Arc (Cat#, 540901) and Homer1a (Cat#, 433261) for catFISH described in Figure 4. Confocal z-stacks composed of 1-μm-thick optical sections were collected for the CA3 and DG areas in dorsal hippocampi of coronal brain sections (anteroposterior, about -2 mm from bregma; 20 μm thick) from 4 slides/animal and stored for offline analysis. The Z-series of confocal images were obtained for the entire length of stratum pyramidale of CA3 area and the granule

cell layer of DG upper blade. Stacks for CA3 or DG (one stack per slide) were collected with a 20× objective to collect comparable numbers of cells from each subjects. Non-neuronal cells, identified as small cells (c.a. 5 μm in diameter) with intensely bright and uniformly stained nuclei, were excluded from the analysis. Only large, diffusely stained nuclei present in the sections were regarded as neuronal cells, and included in our analysis. Neuronal nuclei from the CA3 region were classified as negative (containing no transcription foci), H1a(+) (containing only H1a transcription foci), Arc(+) (containing only Arc transcription foci), or Arc/H1a(+) (containing transcription foci for both Arc and H1a) by an experimenter blind to the mice genotype and the relationship between the image stacks and the behavioural conditions they represented. The percentage of ratio of the number of neuronal nuclei expressing IEG in context X (n_X) to the total number of neuronal nuclei (N) in the CA3 area of a slice was defined as an ensemble size activated in context X, and denoted as P(X).

Contextual fear discrimination test

I tested 30 male mice of three genotypes between 14 and 19 weeks of age [11 WT mice (16.18 ± 0.32 weeks), 10 *Kcna1*+/- mice (16.3 ± 0.36 weeks) and 9 *Kcna2*+/- mice (16.3 ± 0.47 weeks)]

for fear conditioning in a pair of similar contexts using a protocol adopted from (McHugh, Jones et al. 2007). This test assesses an animal's ability to discriminate between two similar contexts, A and B, through repeated experience of a foot shock that is associated with Context A but not with B. Context A (conditioning context) is a chamber (18 cm wide × 18 cm long × 30 cm high; H10-11M-TC; Coulbourn Instruments 5583, PA 18052, USA) consisting of a metal grid floor, aluminium side walls, and a clear Plexiglass front door and back wall. The context A chamber was lit indirectly with a 12 W light bulb. The features of Context B (safe context) were the same as Context A, except for a unique odour (1% acetic acid), dimmer light (50% of A; 6 W light bulb), and a slanted floor by 15° angle. Each chamber was cleaned with 70% ethanol before the animals were placed. On the first 3 days of the experiment, the mice were placed in Context A, where they were allowed a 3-min exploration, received a single foot shock (1 mA, for 2 s) and were returned to their home cage 60 s after the shock. Freezing levels were measured during the 3 minutes before the shock delivery. On day 4, mice of each genotype were divided into two groups; one group of genotype visited Context A and the other Context B. On day 5, I had each mouse visit the context opposite to the one visited on day 4 for 5 min, and freezing levels were

measured again. On day 4−5, neither group received a shock in Context A and B. The mice were subsequently trained to discriminate these two contexts by visiting the two contexts daily for 9 days (discrimination task day 6 to 14), always receiving a footshock 3 minutes after being placed in Context A but not B (Figure 4a3). The freezing ratio (measured during the first 3 min) in each context was used to calculate discrimination ratio for each animal over the 9 days of training (McHugh et al. 2007). I defined freezing behaviour as behavioural immobility at least for 2 s except for movement necessary for respiration. The criterion for analysis of animal's movement was based on the contour of animal's torso. All videos were recorded using a video camera fixed to the ceiling of the chamber connected with EthoVision XT (Noldus Information Technology, Wageningen, Netherlands). Freezing behaviour was assessed from the video image of the mouse using the ezTrack (Pennington, Dong et al. 2019). Freezing ratio was calculated as the total duration of freezing (in sec) divided by the total duration of observation (180 sec or 300 sec; see Results for details). Discrimination ratios were calculated according to F_A / (F_A + F_B), where F_A and F_B are freezing ratio in Contexts A and B, respectively. All experiments and analyses were performed blind to the mice genotype.

Data Analysis

Statistical data are expressed as mean ± standard error of the mean (SEM), and the number of cells/animals measured (denoted as n; details were described in results). Statistical data were evaluated for normality and variance equality with Kolmogorov–Smirnov (K–S) test and Levene's test, respectively. For data that satisfy normality and equality of variances, statistical evaluations were performed with student's t–test, analysis of variance (ANOVA) and generalized linear model (GLM). For statistical evaluation of repetitively measured data from the same cells or slices or animals, I used paired t–test or repeated–measures (RM) ANOVA or GLM. Otherwise, I used independent t–test or conventional ANOVA and GLM. Interaction between each independent variable was shown in Tables, and it was described in Results too when it is statistically significant. For data that inappropriate for parametric tests, non–parametric tests were performed for evaluation. The number of cells and statistical tests for determining statistical significance are stated in the text using following abbreviations: *n.s.*, no statistical significance; *, $P < 0.05$; **, $P < 0.01$; ***, $P < 0.005$. Statistical analyses were performed using PASW Statistics 18 (SPSS Inc, 2009, Chicago, IL, USA).

Results

Kv1.2, but not Kv1.1, is crucial for decorrelation of CA3 ensembles

Previously it has been shown that *Kcna2*+/− mice are impaired in rapid discrimination of the contexts A and B (Eom, Lee et al. 2022). I hypothesized that the impaired contextual discrimination in *Kcna2*+/− mice may be caused by larger overlap between neuronal ensembles representing the two slightly different contexts in the hippocampal CA3 region. To test this hypothesis, I examined CA3 neuronal ensembles activated upon memory retrieval of contexts A and B for the three genotype mice (WT, *Kcna1*+/−, and *Kcna2*+/−). Animals were singly housed and handled daily for a week before the experiment to suppress unnecessary expression of IEGs. An ensemble of active cells in each context was detected using catFISH of IEG transcripts, Arc and Homer1a (H1a), which are expressed after patterned neuronal activities associated with synaptic plasticity (Almira, McNaughton et al. 2002, Guzowski, Timlin et al. 2005). Designing Arc/H1a RNA probes targeting different locations from transcriptional initiation sites [22 bases for Arc and 51.6 kilobases (exon 5) for H1a] allows us to detect intra−

nuclear foci (INF) of Arc/H1a transcripts at different timing from cellular activities (Almira, McNaughton et al. 2002, Vazdarjanova and Guzowski 2004). Typically, INF of Arc and H1a transcripts are expressed at 5 and 30 min, respectively, after an animal visited a novel context (Almira, McNaughton et al. 2002). When Arc and H1a transcripts were stained at opposite timings (H1a at 5 min and Arc at 30 min), most CA3−PCs were devoid of INF of H1a and Arc transcripts, indicating little non−specific expression of H1a and Arc transcripts (Figure 1a). As a control, I estimated an overlap between CA3 ensembles activated upon acquisition and retrieval of context A. To this end, WT and *Kcna2*+/− mice were handled daily for a week before the experiment to habituate to the general handling procedure. Little expression of *c*−fos in CA3 was confirmed in three handled mice which stayed in homecage (Figure 1b1), compared to the handled mice which visited context A for 4 min and were shocked (3 mice, Figure 1b2). Other handled WT and *Kcna2*+/− mice visited the context A twice for 4 min with a 20 min interval, during which mice were kept in their home cage (Figure 2a1). In the first visit, the mice received a footshock 3 minutes after being placed and returned to homecage 1 minutes after the footshock. After the second visit, mice were sacrificed, and their hippocampi underwent the Arc/H1a catFISH procedure. In the

exemplar catFISH images of WT (Figure 2a2) and *Kcna2*+/− CA3 cells (Figure 2a3), H1a (green) and Arc (red) INF represent transcripts expressed upon 1st and 2nd visits, respectively. The fractions of H1a(+) or Arc(+) CA3 cells were not significantly different between WT and *Kcna2*+/− mice, suggesting that the increased distal dendritic excitability in *Kcna2*+/− CA3−PCs has little effect on the ensemble size activated by a novel context [For WT, H1a: 7.34 ± 0.49%, Arc: 7.21 ± 0.37%, 4 mice, 3 slices/mice, 607.98 ± 23.62 cells/slice (range, 441−732); For *Kcna2*+/−, H1a: 6.66 ± 0.83%, Arc: 6.61 ± 0.35%, 3 mice, 2 slices/mice, 549.93 ± 43.35 cells/slice (range, 430−702); genotype: $F_{(1,32)}$ = 0.419, p = 0.522; context, $F_{(1,32)}$ = 2.797, p = 0.104; two−way ANOVA; Figure 2a1]. The overlap between H1a(+) and Arc(+) ensembles [ratio of the number of double positive nuclei to the total nuclei in CA3 area of a slice, denoted as P(A∩B)] was 3.70 ± 0.32% for WT and 3.00 ± 0.34% for *Kcna2*+/− (cells indicated by yellow arrowhead in Figure 2a2−2a3; t = 1.363, p = 0.192, independent t−test). The conditional probability for re−activation of ensemble cells of the 1st visit (A_1) among ensemble cells of the 2nd visit (A_2) [$P(A_1 \mid A_2) = P(A_1 \cap A_2)/P(A_2)$] was not different between the two genotypes either (WT, 51.21 ± 3.47%; *Kcna2*+/−, 45.9 ± 3.11%).

Next, I estimated the proportion of ensemble cells re-activated upon retrieval of contexts A and B in the same mice using catFISH techniques (Vazdarjanova & Guzowski, 2004). After habituation for a week in homecage, mice were subject to a modified contextual fear discrimination (CFD) protocol as shown in Figure 2b1. Mice of the three genotypes daily visited a pair of two contexts (context A and B, 20 min interval) twice a day, and received a footshock only in context A [WT: 4 mice, 4 slices/mice, 522.50 ± 22.02 cells/slice (range, 272-652); *Kcna1*+/-: 4 mice, 4 slices/mice, 394.63 ± 15.93 neurons/slice (range, 278-518); *Kcna2*+/-: 4 mice were used and 4 slices/mice, 344.30 ± 21.59 neurons/slice (range, 225-526)]. On day 3, WT and *Kcna1*+/- mice began to distinguish the two contexts, whereas *Kcna2*+/- mice did not, as shown by the difference in the freezing ratio between two contexts (Figure 2b2-2b3). On day 4, each genotype mice were divided into two subgroups. One subgroup was exposed to context A for 4 min with no footshock, returned to its home cage for 20 min, and then exposed to context B for 4 min (A/B). The other subgroup was subject to the same protocol except switching the order of A and B (B/A). On day 4, *Kcna2*+/- mice still did not distinguish the two contexts, in contrast to WT and *Kcna1*+/- (Figure 2b2-2b3). After visiting the second context, the mice were killed, and their

hippocampi were examined for expression of Arc/H1a transcripts in CA3. Figure 2c1−2c3 shows exemplar Arc/H1a catFISH images of CA3 regions of the three genotype mice. The ratio of the number of nuclei expressing IEG in context X (n_X) to the total number of nuclei (N) in the CA3 area of a slice was defined as an ensemble size activated in context X, and denoted as P(X) (= n_x / N). Both of P(A) and P(B) were about 1.5 times larger in *Kcna2+/−* compared to WT, and those in *Kcna1+/−* mice were slightly larger than WT (WT vs. *Kcna2*+/−, $p < 0.001$; WT vs. *Kcna1*+/−, $p = 0.036$; 2−way ANOVA and Tukey−Kramer post−hoc test, Figure 2d1). Although P(A) and P(B) were not different in WT and *Kcna2*+/− mice, they were unexpectedly different in *Kcna1+/−* mice (WT, $p = 0.868$; *Kcna1*+/−, $p = 0.005$; *Kcna2*+/−, $p = 0.432$; 2−way ANOVA and simple effect analysis). The fraction of CA3 cells active in both of contexts A and B [denoted as P(A∩B)] was not different between WT and *Kcna1*+/− mice, but it was about three times larger in *Kcna2+/−* than other genotypes. To test whether larger ensemble size in *Kcna2*+/− is responsible for larger overlap, I calculated the conditional probability for reactivation of the A ensemble cells among the B ensemble cells [$P(A \mid B) = P(A \cap B)/P(B)$] (referred to as conditional overlap). Because conditional overlap was not different between the two subgroups

(A/B and B/A in Figure 2d2), results are presented with respect to the context in Figure 2d. The conditional overlap for *Kcna2+/−* was significantly higher than those of *Kcna1+/−* and WT (Figure 2d2), and rather similar to the value for WT and *Kcna2*+/− mice which visited context A twice [denoted as WT(AA) and *Kcna2*+/−(AA), respectively] [WT(AA) vs. *Kcna2*+/−(AB), p = 0.188; *Kcna2*+/−(AA) vs. *Kcna2*+/−(AB), p = 1.00; one−way ANOVA and Tukey−Kramer post−hoc test; Figure 2d2]. Therefore, larger overlap in *Kcna2+/−* cannot be explained by larger ensemble size alone. The cumulative distribution (line) and probability density function (histogram; the same color codes as cumulative plot) of the conditional overlap shows a significant shift to the right in *Kcna2+/−*(AA), *Kcna2*+/−(AB) and WT(AA), compared to WT(AB) and *Kcna1+/−* [WT(AA) vs. WT(AB), Z = 2.4, p < 0.001; WT(AA) vs. *Kcna1+/−*, Z = 2.4, p < 0.001; WT(AA) vs. *Kcna2+/−*(AB), Z = 1.255, p = 0.083; WT(AA) vs. *Kcna2*+/−(AA), Z = 0.667, p = 0.766, Kolmogorov−Smirnov test, Figure 2d3], indicating larger overlap between A and B ensembles in *Kcna2*+/−. These results together with the behavioral results of previous study (Eom et al., 2022) show that the averaged conditional overlap of CA3 ensembles correlates with the averaged performance of CFD task across the three genotypes, implying that

high conditional overlap of CA3 ensembles may underlie the impaired contextual discrimination in *Kcna2*+/− mice.

CA3 ensembles undergo decorrelation over training days

To further confirm the correlation between contextual discrimination and the overlap of CA3 ensembles, I examined the changes of CA3 ensemble size and their overlap over training days in WT and *Kcna2*+/− mice. To this end, mice were subject to the same protocol of Figure 2b1, but were killed for catFISH after one paired visits (session 1) on day 1 (D1) or after the session 1 on day 2 (D2) (Figure 3a). Figure 3b1−3b4 shows exemplar Arc/H1a catFISH images of CA3 regions of WT (*upper row*) and *Kcna2*+/− (*lower row*) mice on D1 and D2. For comparison, catFISH data on retrieval of contexts on day 4 (D4) were adopted from Figure 2. Because the ensemble sizes for A and B [denoted as P(A) and P(B), respectively] in the same slice were not statistically different in the CA3 of WT or *Kcna2*+/− mice for day 1, 2, and 4 (context, $F_{(1,62)}$ = 0.341, p = 0.561; genotype, $F_{(1, 62)}$ = 0.101, p = 0.758; two−way ANOVA, Figure 2), the averaged ensemble size on each day was

measured as (n_A + n_B) / 2 N. The size of CA3 ensembles for the exposure of context A and B increased over training days in both genotypes, but the expansion of CA3 ensemble size in *Kcna2*+/− (red) was more pronounced compared to WT (gray) (Figure 3c1; genotype, $F_{(1,62)}$ = 36.528, $p < 0.001$; day, $F_{(2,62)}$ = 51.758, $p < 0.001$; genotype × day, $F_{(2, 62)}$ = 12.303, $p < 0.001$; WT vs *Kcna2*+/− for day 1: p = 0.635, day 2: p = 0.008, day 4: $p < 0.001$; two−way ANOVA and simple effect analysis). Whereas in WT mice the ensemble overlap [$P(A \cap B)$] decreased over training days, it rather increased in *Kcna2*+/− mice (genotype, $F_{(1,62)}$ = 38.687, $p < 0.001$; day, $F_{(2, 62)}$ = 3.159; p = 0.024, genotype × day, $F_{(2,62)}$ = 20.287, $p < 0.001$; two−way ANOVA; Figure 3c2). The increase of P(A∩B) in *Kcna2*+/− mice can be attributed to the increase in the ensemble size, because the conditional overlap [P(A∩B)] remained static over days (Figure 3c3). In contrast, $P(A \mid B)$ in WT mice decreased over days (gene, $F_{(1,62)}$ = 40.702, $p < 0.001$; day, $F_{(2,62)}$ = 4.458, p = 0.016; gene × day, $F_{(2,62)}$ = 19.566, $p < 0.001$; two−way ANOVA; For WT: $F_{(2,62)}$ = 21.305, $p < 0.001$, D1 vs. D2, p = 0.024; D2 vs. D4 or D1 vs. D4, $p < 0.001$, 2−way ANOVA and simple effect analysis; Figure 3c3).

Figure 3d1 shows the changes in the cumulative distribution (line) and probability density function (histogram, the same color code as

the lines) of the conditional overlap in CA3 for two genotypes. The conditional overlap of *Kcna2*+/− mice was not different from that of WT on day 1 (Figure 3d1). The distributions in WT mice shifted to the left over training days, whereas the conditional overlap of *Kcna2*+/− mice remained unaltered ($F_{(2,62)}$ = 2.719, p = 0.074, 2−way ANOVA and simple effect analysis; Figure 3d1). To examine the correlation between neuronal and behavioral pattern separation, I plotted discrimination index based on freezing behavior as a function of the conditional overlap of CA3 neuronal ensembles obtained from the same animals (Figure 3d2) (Marrone, Adams et al. 2011, Yassa and Stark 2011, Allegra, Posani et al. 2020, Woods, Stefanini et al. 2020). This plot was well fitted by a sigmoid function, which has a half value at the conditional overlap of 0.3. Mixed linear model analysis revealed that the discrimination indices significantly correlated with the CA3 conditional overlap (Fixed effect of conditional overlap, $F_{(1,22)}$ = 14.72, p = 0.001).

DG ensembles remain unaltered over training days

Figure 3 demonstrates a contribution of Kv1.2 subunits to decorrelation of CA3 ensembles and behavioral contextual discrimination. DG is thought to provide CA3 with decorrelated

input patterns. To find out whether DG is involved in the impaired decorrelation of CA3 ensembles in *Kcna2*+/− mice, I examined the concomitant changes of DG ensembles representing the contexts A and B. Unlike CA1− and CA3−PCs (Guzowski, McNaughton et al. 1999), transcription of Arc in DG ensemble cells is sustained up to 8 hours after a novelty exposure (Ramirez−Amaya, Angulo−Perkins et al. 2013). Therefore, newly activated DG granule cells expressing only Arc INF (Arc−INF−only cells; Figure 4a1−4a2, red arrowhead) are observed only at 5 minutes after a novelty exposure, while at 30 min and later time points they express cytoplasmic Arc mRNA (Arc−cyto cells; Figure 4a2−4a4, white arrowhead), part of which express Arc INF too (Ramirez−Amaya, Angulo−Perkins et al. 2013). Consistently, I found that a majority of GCs expressing H1a INF [H1a(+) cells] exhibited the feature of the Arc−cyto cells, regardless of the genotype and training days [gene: $F_{(1,27)}$ = 0.039, p = 0.845, day: $F_{(2,27)}$ = 0.987, p = 0.386; General linear model (GLM)]. Thus, I regarded Arc−INF−only cells as GCs that are activated by context B, and H1a(+) cells as GCs activated by context A. In Figure 4a1−4a4, Arc−INF−only cells are marked with red arrowheads, cells expressing both H1a and Arc−INF−only with yellow arrowheads, and Arc−cyto cells with white arrowheads. Because cells in the upper blade of DG responded in an

environment-specific fashion (Chawla, Guzowski et al. 2005), I counted the number of GCs only in the upper blade of DG. The sizes of GC ensembles were neither different between WT and *Kcna2*+/- animals nor between the two contexts over training days (gene: $F_{(1,84)}$ = 0.007, p = 0.935, day: $F_{(3,84)}$ = 0.599, p = 0.617, context: $F_{(1,53)}$ = 3.916, p = 0.051, GLM; Figure 4b1). The ensemble overlap [P(A∩B)] and the conditional overlap [P(A|B)] in DG were different neither between genotypes nor between training days (For P(A∩B), gene: $F_{(1,27)}$ = 0.125, p = 0.726, day: $F_{(2,27)}$ = 0.075, p = 0.928, p = 0.612, 2-way ANOVA, Figure 6b2; For P(A|B), gene: $F_{(1,27)}$ = 0.149, p = 0.703, day: $F_{(2,27)}$ = 0.071, p < 0.932, gene × day: $F_{(2,27)}$ = 0.452, p = 0.641, 2-way ANOVA; Figure 4b3). However, both parameters, P(A∩B) and P(A|B), were significantly lower than those in CA3 [For P(A∩B), gene: $F_{(1,89)}$ = 19.03, p < 0.001, region: $F_{(1,89)}$ = 266.9, p < 0.001, day: $F_{(2,89)}$ = 1.86, p = 0.162, gene × region × day: $F_{(2,89)}$ = 8.577, p < 0.001; For P(A|B), gene: $F_{(1,89)}$ = 3.357, p = 0.07, region: $F_{(1,89)}$ = 340.68, p < 0.001, day: $F_{(2,89)}$ = 5.71, p = 0.005, gene × region × day: $F_{(2,89)}$ = 4.013, p = 0.021; GLM and simple effect analysis between DG and CA3].

Figure 4c shows the changes in the cumulative distribution (*c1*) and probability density function (*c2*) of the DG conditional overlap over

training days for two genotypes. In contrast to CA3, the strong decorrelation of DG ensembles already occurred on the very first day of training, and did not further evolve over training days in both genotypes. Moreover, the conditional overlap of DG ensembles did not correlate with improvement of behavioral discrimination index over training regardless of the genotypes as shown in the plot discrimination index *vs.* conditional overlap of DG ensembles [Figure 4d; linear regression, slope = −0.15 (p = 0.864), intercept = 0.09, (p = 0.302), R^2 = 0.037].

Fig. 4e shows paired conditional overlap values measured in DG and CA3 of the same individual mice. Both of CA3 and DG ensemble overlap values on the first visit were not different between WT and *Kcna2*+/− mice (D1, triangles in Fig. 4e). While the CA3 ensembles for the context A and B evolved into more distinct ones over training days in WT mice, the same training induced little decorrelation of CA3 ensembles in *Kcna2*+/− mice. On the other hand, the DG ensembles were already more distinct on D1 compared to CA3 ensembles, did not further evolve during the training, and little affected by Kv1.2 haploinsufficiency. Because the conditional overlap in CA3, but not in DG, was closely correlated with contextual discrimination, lack of the CA3 ensemble decorrelation in *Kcna2*+/− mice may at least in part be responsible

for the impaired contextual discrimination.

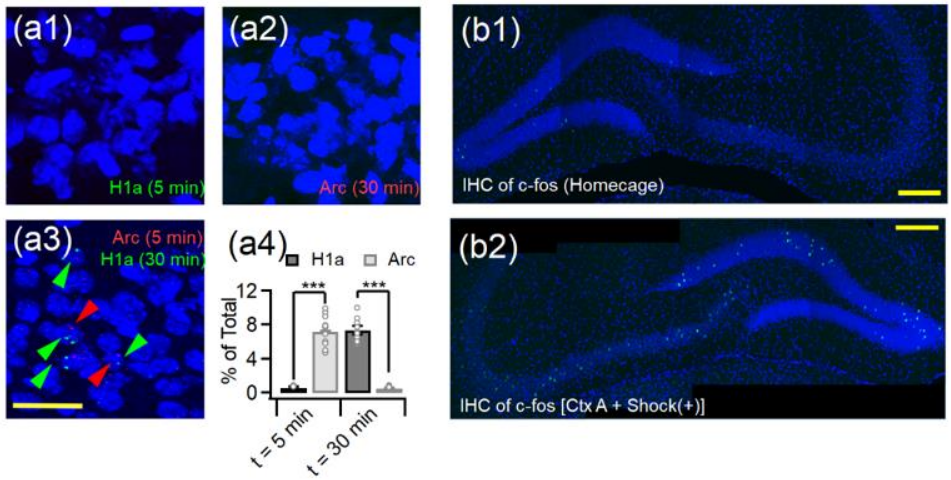

Figure 1. Validation of behavioral procedure and associated expression timing of *Arc* and *Homer 1a* mRNA in mice hippocampi. **(a1–a2)** To evaluate non-specific expression of *H1a* and *Arc* transcripts, *H1a* and *Arc* transcripts were stained at 5 min (*a1*) and 30 min (*a2*), respectively, after the mice being placed in a novel context. Scale bars, 30 μm. **(a3)** catFISH for *H1a* and *Arc* mRNA was performed at 30 min and at 5 min for comparison. Green and red arrowheads indicate *H1a* and *Arc* INF, respectively. **(a4)** Mean fractions of *H1a* and *Arc*-positive nuclei, when each was detected at 5 or 30 minutes after the mice were exposed to a novel context. Note that most nuclei were negative for *H1a* and *Arc* INF, when H1a and Arc mRNA were stained at 5 and 30 minutes after the mice visited a novel context (*H1a* INF: 7.34 ± 0.49% at 30 min, 0.54 ± 0.01% for 5 min, Mann-Whitney

U = 0.00, p = .004; *Arc* INF: 7.21 ± 0.37% at 5 min, 0.60 ± 0.02% for 30 min, Mann–Whitney U = 0.00, p = .004). **(b1–b2)** After handling for a week, the mice were killed immediately from their home cage (*b1*) or 30 minutes after being placed in a novel context (context A) with a footshock (*b2*), and then their dorsal hippocampi underwent immunostaining for c–Fos (*green*) with DAPI counterstaining of nuclei (blue). Antibody targeting c–Fos and DAPI were purchased from Cell Signaling (Cat# 2250, USA) and Sigma–Aldrich (St Louis, MO, USA), respectively. Proportions of c–Fos(+) nuclei in the CA3 area of mice from home cage (2 mice, two slices/mice; *b1*) and those from context A (5 slices, 2–3 slices/mice; *b2*) (Home cage, 0.23 ± 0.11%; Context A with footshock, 8.53 ± 0.75% for 5 min; Mann–Whitney U = 0.00, p = .014).

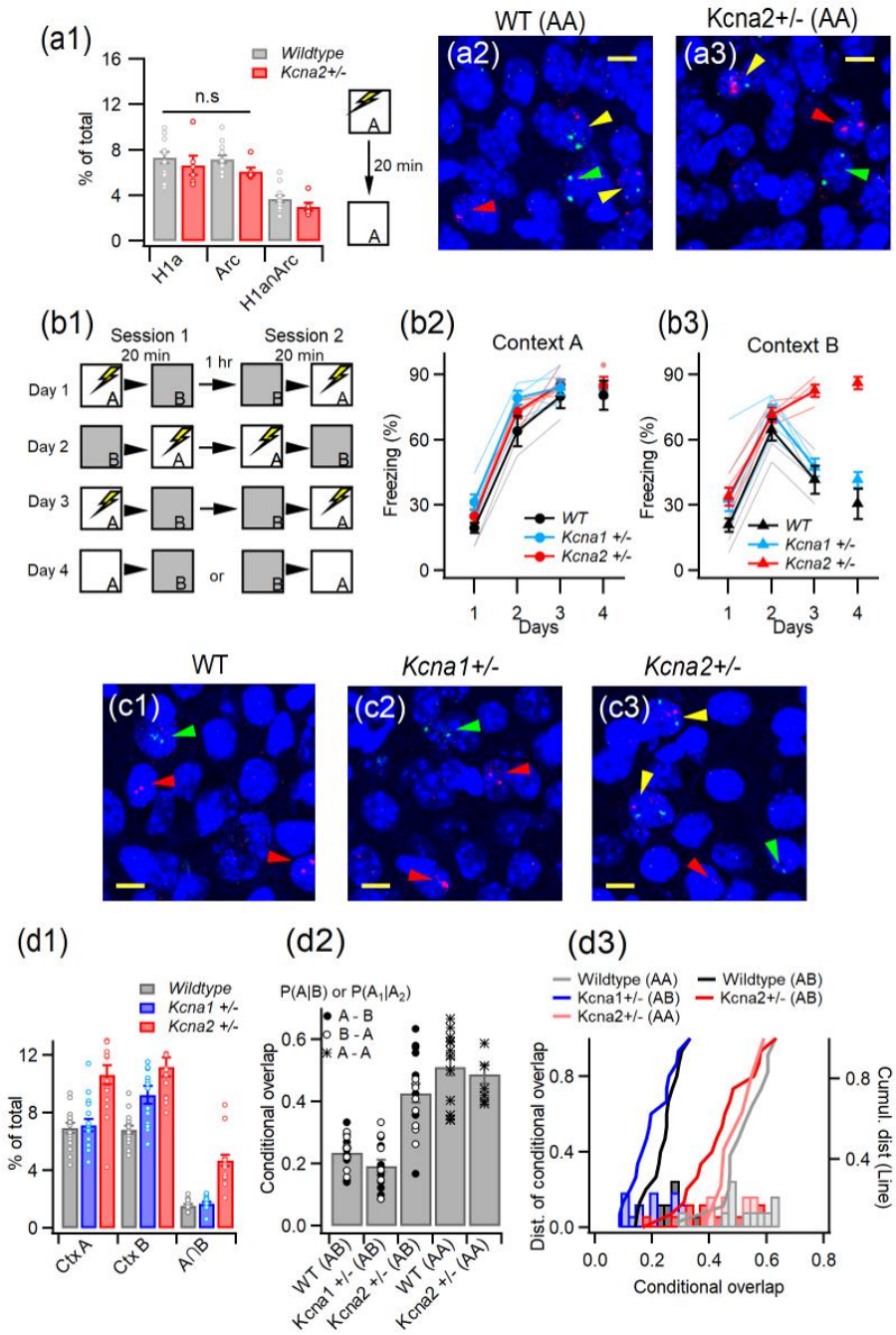
(a1)
Wildtype
Kcna2+/-
n.s
% of total
H1a
Arc
H1a∩Arc
20 min
WT (AA)
Kcna2+/- (AA)
(a2)
(a3)
(b1)
Session 1
20 min
1 hr
Session 2
20 min
Day 1
Day 2
Day 3
Day 4
or
(b2)
Context A
Freezing (%)
Days
WT
Kcna1 +/-
Kcna2 +/-
(b3)
Context B
WT
Kcna1+/-
Kcna2+/-
(c1)
(c2)
(c3)
(d1)
Wildtype
Kcna1 +/-
Kcna2 +/-
% of total
Ctx A
Ctx B
A∩B
(d2)
P(A|B) or P(A1|A2)
A - B
B - A
A - A
Conditional overlap
WT (AB)
Kcna1 +/- (AB)
Kcna2 +/- (AB)
WT (AA)
Kcna2 +/- (AA)
(d3)
Wildtype (AA)
Kcna1+/- (AB)
Kcna2+/- (AA)
Wildtype (AB)
Kcna2+/- (AB)
Dist. of conditional overlap
Cumul. dist (Line)
Conditional overlap

Figure 2. Insufficiency of Kv1.2, but not Kv1.1, causes impaired pattern separation in CA3. (a1) Proportion of H1a(+), Arc(+), and H1a/Arc(+) (overlap) cells in the CA3 from WT (*gray*) and *Kcna2+/−* (*red*) mice, which explored the same context A twice with an interval of 20 min. On the first visit, mice received a footshock. **(a2, a3)** An exemplar fluorescence image of H1a and Arc transcripts in CA3 cells in WT (c2) and *Kcna2+/−* (c3) mice. Scale bars, 10 μm. **(b1)** Protocol for modified contextual fear discrimination (CFD) test. For first 3 days, mice daily visited two similar contexts with 20 min interval with receiving a footshock always in context A. Mice were assessed for freezing for first 3 minutes after being placed in each context. On Day 4, mice were allowed to freely explore the context A or B for 4 min (epoch 1). After a 20 min rest period in the home cage, mice were exposed to other context for 4 min (epoch 2). In 5 minutes after epoch 2, mice were killed for cellular analysis of temporal activity by fluorescence in situ hybridization (catFISH). **(b2, b3)** Freezing ratio of mice in context A (b2) and B (b3) over 4 days, during which mice underwent the modified CFD test. WT and *Kcna1+/−* mice begun to discriminate two contexts in Day 3, but *Kcna2+/−* mice could not even on Day 4. Thin lines, freezing (%) of individual animals (the same color codes as averaged freezing [thick lines]). **(c)**

Representative confocal images of H1a and Arc transcripts in nuclei (blue, counterstained with 40,6−diamidino−2−phenylindole [DAPI]) of the CA3 pyramidal layer from WT (c1), *Kcna1+/−* (c2), and *Kcna2+/−* (c3) mice. Nuclei expressing H1a alone, Arc alone, and both are indicated by green, red, and yellow arrowheads, respectively. H1a (*green dots*) and Arc (*red*) intranuclear foci are activated during epoch 1 and 2, respectively. Scale bars, 10 μm. **(d1)** size of neuronal ensembles in CA3 activated in contexts A and B quantified as percentage of H1a(+) or Arc(+) cells among total cells in the CA3 pyramidal layer of each slice. The fraction of CA3 cells active in both of contexts A and B (ensemble overlap, denoted as A∩B) was not different between WT and *Kcna1+/−* mice, but higher in *Kcna2+/−* than other genotypes. The size of neuronal ensembles in *Kcna2+/−* was larger than that in WT and *Kcna1+/−*. **(d2)** The conditional probability for ensemble cells active in context A among those active in context B (denoted as conditional overlap; P(A|B)]. For comparison, conditional probability for re−activation of WT ensemble cells of the first visit of context A (A1) among ensemble cells of the second visit (A2) [P(A1|A2)] is shown as WT(AA) (four slices/mice, three mice) and *Kcna2+/−*(AA) (two slices/mice, three mice). **(d3)** Cumulative probability function (*line*) and probability density function (histogram) of the conditional

overlap for different genotypes. The conditional overlap between two ensembles in *Kcna2+/−* mice (four slices/mice, four mice) was significantly greater than that in *Kcna1+/−* (four slices/mice, four mice) or WT (four slices/mice, four mice) mice.

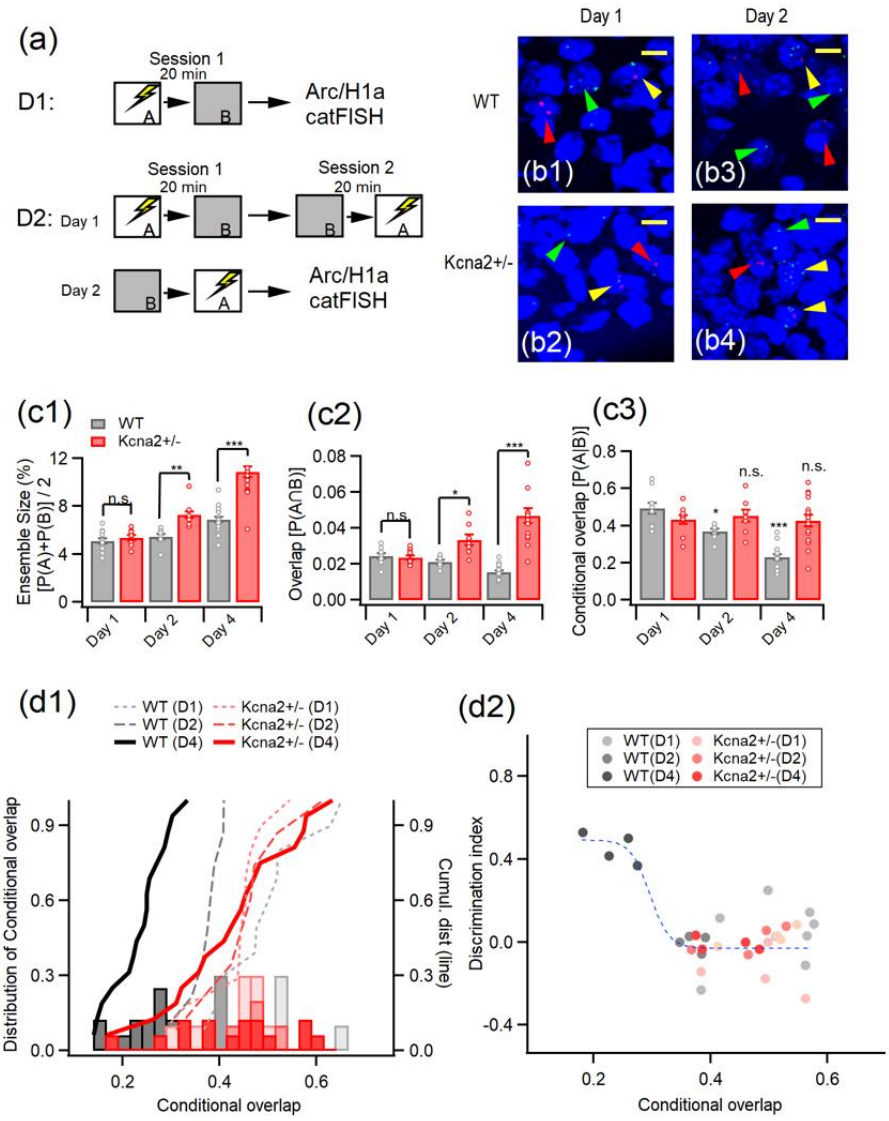
(a)
D1:
Session 1
20 min
A
B
Arc/H1a
catFISH
D2:
Day 1
Session 1
20 min
Session 2
20 min
Day 2
Day 1
Day 2
WT
Kcna2+/-
(b1)
(b2)
(b3)
(b4)
(c1)
WT
Kcna2+/-
Ensemble Size (%)
[P(A)+P(B)] / 2
n.s.
**
***
Day 1
Day 2
Day 4
(c2)
Overlap [P(A∩B)]
(c3)
Conditional overlap [P(A|B)]
(d1)
WT (D1)
WT (D2)
WT (D4)
Kcna2+/- (D1)
Kcna2+/- (D2)
Kcna2+/- (D4)
Distribution of Conditional overlap
Cumul. dist (line)
Conditional overlap
(d2)
WT(D1)
WT(D2)
WT(D4)
Kcna2+/-(D1)
Kcna2+/-(D2)
Kcna2+/-(D4)
Discrimination index
Conditional overlap

Figure 3. CA3 ensembles undergo decorrelation over training days. **(a)** Experimental procedures for catFISH of CA3 ensembles during training phase (Days 1 and 2), when mice do not discriminate the two contexts A and B. **(b)** Representative confocal images of H1a and Arc transcripts in nuclei (*blue*, counterstained with 40,6−diamidino−2−phenylindole [DAPI]) of the CA3 pyramidal layer from WT and *Kcna2+/−* mice in Day 1 (b1, WT; b2, *Kcna2+/−*), Day 2 (b3, WT; b4, *Kcna2+/−*). Nuclei expressing H1a alone, Arc alone, and both are indicated by green, red, and yellow arrowheads, respectively. **(c1)** Neuronal ensemble size activated by exposure of mice to contexts A and B on each day. Because there was no statistical difference in the fraction of H1a(+) and Arc(+) cells in the same slice for WT and *Kcna2+/−* mice, the ensemble size was quantified as the averaged value. Note that the CA3 ensemble size in *Kcna2+/−* mice (*red*) increased larger over training days compared to that in WT (*gray*). **(c2)** The fraction of CA3 cells activated in both contexts (ensemble overlap; P(A∩B)) over training days. The P(A∩B) in *Kcna2+/−* mice (red) increased over days, whereas that in WT (gray) decreased. Compared to Day 1, for WT, Day 2: $p = .457$, Day 4: $p = .017$. For *Kcna2+/−*, Day 2: $p = .025$, Day 4: $p < .001$ (two−way analysis of variance [ANOVA] and simple effect analysis). **(c3)** The conditional probability for

ensemble cells active in context A among those active in context B (conditional overlap, P(A|B)). The P(A|B) for WT mice decreased over days, but that for *Kcna2 +/−* mice did not. Compared to Day 1, for WT, Day 2: $p = .005$, Day 4: $p < .001$. For *Kcna2+/−*, Day 2: $p = .678$, Day 4, $p = .816$ (two−way ANOVA, simple effect analysis). The cellular analysis of temporal activity by fluorescence in situ hybridization (catFISH) data on D4 were adopted from Figure 4. **(d1)** Changes in the cumulative distribution curves (line) and probability density function (histogram; the same color codes as the lines) for P(A|B) in WT and *Kcna2+/−* mice over training days. Note that the cumulative distribution curves and probability mass functions shifted to the left over training days in WT mice, but not in *Kcna2+/−* mice. **(d2)** Discrimination index calculated from freezing in the two contexts as a function of ensemble conditional overlap measured in the same animals. In WT mice (gray solid symbols), the discrimination index increased in parallel with the decrease of conditional overlap. However, in *Kcna2+/−* mice (red solid symbols), the discrimination index and conditional overlap remained static over training days. This plot was fitted using a sigmoid function, $y = 0.52 - 0.3/(1+e^{-(x-(0.030)/0.0016)})$, and the coefficient of determination (R^2) was 0.89

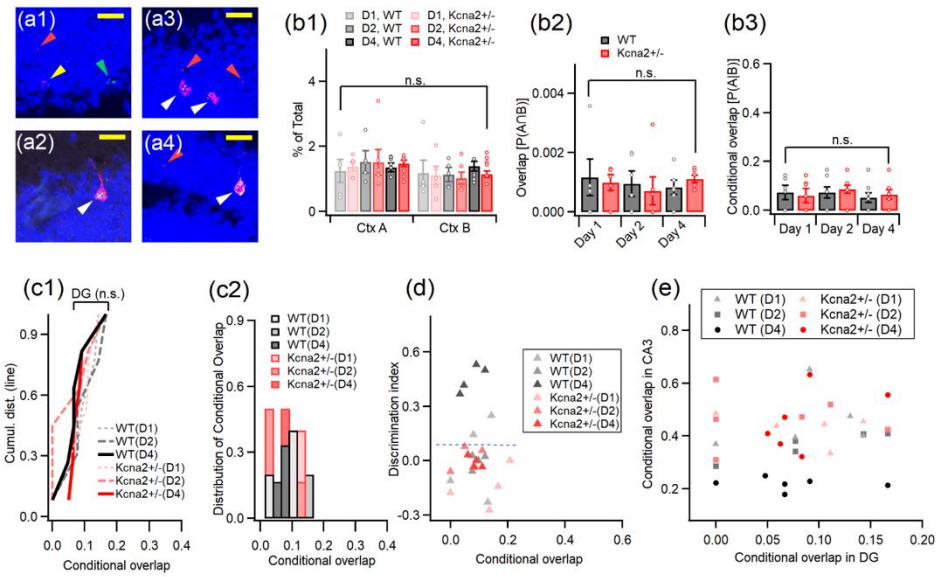

Figure 4. Dentate gyrus (DG) ensembles remained constant over training days, in contrast of CA3 ensembles. **(a)** Representative confocal images of H1a and Arc transcripts in nuclei (*blue*, counterstained with 40,6−diamidino−2−phenylindole [DAPI]) of the DG. **(a1)** Nuclei expressing H1a alone, intranuclear Arc alone, and both are indicated by green, red, and yellow arrowheads, respectively. **(a2)** Cells expressing cytosolic Arc are indicated by white arrowheads, regardless of the presence of intranuclear Arc. **(a3, a4)** Representative confocal images of H1a and Arc transcripts in DG, for WT (a3) and *Kcna2+/−* (a4) animals. Note that most cells expressing cytosolic Arc also express H1a, whereas overlapping of H1a and intranuclear Arc is very scarce. **(b1)** Neuronal ensemble size activated by exposure of mice to contexts

A and B on each day. In the size of DG ensemble, there was no statistical difference in Arc−INF cells and H1a(+) cells over the training days for WT and *Kcna2+/−* mice. Note that, unlike CA3, the DG ensemble sizes in *Kcna2+/−* mice (*red*) were stable over training days and not different from those of WT (*gray*). Days are indicated with gradation of colors. **(b2)** The fraction of DG granule cells activated in both contexts (denoted as P(A∩B)) over training days. **(b3)** The conditional probability for B ensemble cells to be activated in A [P(A|B)]. **(c1)** Cumulative distribution curves for P(A|B) of WT and *Kcna2+/−* mice over training days. Note that the curves of DG ensembles remained unchanged in both genotypes. **(c2)** For DG ensembles, the probability density function for P(A|B) (the same color codes as the cumulative plot). **(d)** Plot of discrimination index calculated from freezing (%) between two contexts as a function of conditional overlap [P(A|B)] measured in the same animals. **(e)** Conditional overlap of CA3 ensembles versus that of DG ensembles. Note that, whereas CA3 and DG ensembles were examined in the same mice in each data point, every data points were obtained from different mice

Discussion

While one trial learning is sufficient for an animal to discriminate two distinct contexts, it seems that repeated exposures with high valance are needed for an animal to discriminate two similar but slightly distinct contexts (McHugh, Jones et al. 2007). Gradual pattern separation of neuronal ensembles representing two similar contexts might underlie the contextual discrimination learning under the multi-trial fear conditioning. However, gradual pattern separation of neuronal ensembles over the training days has not previously been investigated in the hippocampus. The present study demonstrated the crucial role of Kv1.2 in pattern separation of the neuronal ensembles in CA3 activated by two similar contexts, which was well correlated with contextual discrimination behavior.

Gradual pattern separation in CA3 during multi-trial contextual discrimination training

Insufficiency of Kv1.2 subunits in CA3-PCs enhances E-S coupling of PP synaptic inputs to lower the PP-LTP threshold (Eom, Lee et al. 2022). I showed that Insufficiency of Kv1.2 closely correlates

not only with deficit in rapid contextual discrimination under multi-trial fear conditioning paradigm but also with impaired pattern separation of CA3 ensembles activated by retrieval of two slightly different contexts. The size and overlap of CA3 ensembles activated by the first visit to contexts A and B were not different between WT and *Kcna2*+/− mice, but the two ensemble parameters diverged over training days (Figure 3). The *Kcna2*+/− mice displayed rapid enlargement of the CA3 ensemble size with the overlap index static over training days, while WT mice displayed relatively stable ensemble size with decreasing overlap index. Because the ensemble properties of *Kcna2*+/− mice were initially similar to WT, the abnormal evolution of CA3 ensembles in *Kcna2*+/− mice cannot be explained by increased dendritic excitability alone, but implies that the CA3 networks of *Kcna2*+/− mice undergo plastic changes different from that of WT mice over subsequent training days. Moreover, contextual discrimination of *Kcna1*+/− mice, which displayed intrinsic excitability of CA3-PCs similar to *Kcna2*+/− mice (Eom et al., 2022), were not different from WT mice (Figure 2), arguing against the possibility that the baseline intrinsic excitability is responsible for the impaired pattern separation in the CA3 of *Kcna2*+/− mice. Although I did not examine the pattern separation of neuronal ensembles in the CA3 of

Kcna1+/− mice, I imagine that the pattern separation may not be different from that of WT considering that their contextual discrimination was normal (Figure 2) and that pattern separation in CA3 is closely correlated with contextual discrimination (Figure 3). Nevertheless, the present study cannot rule out the possibility that behavior of *Kcna1*+/− mice is similar to WT because multiple factors are impaired compensating for each other. Along this line, previous study mention that *Kcna2*+/− CA3−PCs lack MF−induced LTP−IE, different from WT and *Kcna1*+/− CA3−PCs (Eom, Lee et al. 2022). Because downregulation of Kv1.2 mediates LTP−IE, it is highly plausible that LTP−IE may lower the PP−LTP threshold. Lowering PP−LTP threshold by MF inputs may potentially increase the size and overlap of CA3 ensembles, and thus may have negative effects on pattern separation. The CA3 ensemble size in *Kcan2*+/− mice was 1.5 times larger on day 4 (Figure 2d1), even though *Kcna2*+/− CA3−PCs lack MF−induced LTP−IE, suggesting that non−specific lowering of PP−LTP threshold caused by *Kcna2*+/− seems to exert more adverse effects on pattern separation compared to MF−induced LTP−IE. Although the CA3 neuronal ensemble size would be larger in the presence of MF−induced LTP−IE than without it, the increment may be very limited, because induction of LTP−IE requires high frequency MF inputs (Eom,

Hyun et al. 2019).

LTP threshold and CA3 ensemble size

Eom et al. (2022) quantified the LTP threshold as the baseline EPSC, and showed that it is lowered at PP–CA3 synapses in *Kcna2*+/– mice. The concept of LTP threshold has been discussed in relation to metaplasticity, an activity and neuromodulator–dependent regulation of it (Abraham 2008). My results imply that lowered PP–LTP threshold may correlate with abnormal enlargement of the ensemble size during repeated exposure of the contexts. Given that only previously strengthened PP synaptic inputs can elicit postsynaptic firing and contribute to the ensemble size on retrieval, induction of LTP at small number of PP synapses (sparse encoding; (Treves and Rolls 1992) would be essential for keeping the ensemble size stable. MF inputs are expected to activate a small number of CA3–PCs because of low convergence of MFs to CA3–PC together with sparse firing of dentate GCs (Amaral, Ishizuka et al. 1990, Diamantaki, Frey et al. 2016). When PP–LTP depends on concurrent MF inputs, the sparse MF inputs to CA3 may ensure sparse encoding of memories at PP–CA3 synapses. In contrast to MFs, PP makes densely distributed

synapses on CA3-PCs (Amaral, Ishizuka et al. 1990), and thus nonspecific lowering of PP-LTP threshold caused by *Kcna2*+/- is expected to have profound effects on the CA3 ensemble size. Kv1.2 in CA3-PCs may reduce the probability for PP inputs alone to induce LTP without a help of MF inputs by keeping the LTP threshold high, and plays a crucial role in limiting the expansion of CA3 neuronal ensemble size during hippocampal learning. Therefore, my results imply that PP-LTP may be one of major players in gradual decorrelation of CA3 ensembles over multi-trial contextual fear discrimination task, and that Kv1.2-dependent regulation of PP-LTP threshold may be crucial for stabilizing the ensemble size and pattern separation.

Recent studies highlighted the role of MF-induced feedforward inhibition of CA3-PC in contextual discrimination (Ruediger, Vittori et al. 2011, Guo, Soden et al. 2018). These studies showed that hippocampal learning induces growth of filopodia from MF terminals, which increases feedforward inhibition triggered by MF inputs. The CA3 ensemble size was abnormally enlarged by contextual fear conditioning in the mutant mice in which the filopodial growth is abolished (Ruediger, Vittori et al. 2011). Conversely, genetic increase in the feedforward inhibition enhanced the memory precision, and thus prevented generalization of remote fear

memories (Guo, Soden et al. 2018). A series of studies showed that LTP at PP-CA3 synapses is regulated by MF input-dependent regulation of dendrtic excitability, which is mediated by Ca^{2+}-dependent endocytosis of dendritic Kv1.2 (Hyun et al, 2013, 2015). Moreover, Eom et al. (2022) recently showed that hetero-insufficiency of Kv1.2 lower the LTP threshold at PP-CA3 synapses. These studies together with my results suggest that balanced plastic changes at excitatory and inhibitory synapses are essential for the CA3 ensemble size to be maintained stable during hippocampal learning, and this may be the case for the wildtype mice. On the other hand, as *Kcna2*+/- mice are repeatedly exposed to the dangerous context, CA3 network may undergo too promiscuous plastic changes at PP synapses, which may not be counterbalanced by plastic changes at inhibitory synapses such as new filopodial growth from MF terminals. The increase in the ensemble size in *Kcna2*+/- after learning may be a sign of E/I imbalance resulting from promiscuous PP-LTP and increase in the PP-EPSCs.

Possible influence of pattern separation in EC on that in CA3

In the present study, I investigated overlap of neuronal ensembles activated by two similar contexts, and called a decrease in the conditional overlap over training days as ensemble decorrelation or pattern separation. More rigorous definition of pattern separation, however, is the separation of neuronal ensembles across input and output layers (O'Reilly and McClelland 1994, Madar, Ewell et al. 2019). Among two input layers to CA3, I examined only DG (Figure 4). It remains to be elucidated whether decorrelation of neuronal ensembles in the layer 2 (L2) of EC, another input layer to CA3, occurs over time in parallel with CA3. Previous studies support less pattern separation in EC compared to DG or CA3. Re-alignment of grid cells in MEC could be induced only by substantial change in the distal landmark such as different rooms, but not by changes in local cues (Fyhn, Hafting et al. 2007). Accordingly, it has been shown that stellate cells, but not pyramidal cells, of MEC layer II displayed context-specific responses, and the stellate cell ensembles were not different between similar contexts while they discriminated distinct contexts (Kitamura, Sun et al. 2015). Recently, (Lee and Lee 2020) showed that the firing rate of CA3 cells displayed categorical tuning curve across continuously changing ambiguous visual scenes, while they displayed gradual change after ablation of DG, implying that PP inputs to CA3 are linearly scaled with the

similarity of inputs, and that DG plays a crucial role in the CA3 ensemble decorrelation. Nevertheless, the extent of ‘similarity’ of two contexts in these previous studies cannot be directly compared to that of contexts A and B used in the present study. Moreover, contribution of LEC to the CA3 ensemble decorrelation remains to be elucidated, suggesting the possibility that not only DG but also direct EC input may contribute to the decorrelation of CA3 ensembles.

References

Abraham, W. C. (2008). "Metaplasticity: tuning synapses and networks for plasticity." Nat Rev Neurosci 9(5): 387.

Aiuchi, T., M. Matsunaga, K. Nakaya and Y. Nakamura (1985). "Effects of probes of membrane potential on metabolism in synaptosomes." Biochim Biophys Acta 843(1-2): 20-24.

Allegra, M., L. Posani, R. Gomez-Ocadiz and C. Schmidt-Hieber (2020). "Differential Relation between Neuronal and Behavioral Discrimination during Hippocampal Memory Encoding." Neuron 108(6): 1103-1112 e1106.

Almira, V., B. McNaughton, C. Barnes, P. Worley and J. Guzowski (2002). "Experience-dependent coincident expression of the effector immediate-early genes arc and Homer 1a in hippocampal and neocortical neuronal networks." Journal of Neuroscience 22(23): 5.

Amaral, D., N. Ishizuka and B. Claiborne (1990). "Neurons, numbers and the hippocampal network." Progress in Brain Research 83: 1-11.

Anastasiades, P. G. and A. G. Carter (2021). "Circuit organization of the rodent medial prefrontal cortex." Trends Neurosci 44(7): 550-563.

Bae, J. W., H. Jeong, Y. J. Yoon, C. M. Bae, H. Lee, S. B. Paik and M. W. Jung (2021). "Parallel processing of working memory and temporal information by distinct types of cortical projection neurons." Nat Commun 12(1): 4352.

Baeg, E. H., Y. B. Kim, J. Jang, H. T. Kim, I. Mook-Jung and M. W. Jung (2001). "Fast spiking and regular spiking neural correlates of fear conditioning in the medial prefrontal cortex of the rat." Cereb Cortex 11(5): 441-451.

Baker, A., B. Kalmbach, M. Morishima, J. Kim, A. Juavinett, N. Li and N. Dembrow (2018). "Specialized Subpopulations of Deep-Layer Pyramidal Neurons in the Neocortex: Bridging Cellular Properties to Functional Consequences." J Neurosci 38(24): 5441-5455.

Beierlein, M., D. Fioravante and W. G. Regehr (2007). "Differential expression of posttetanic potentiation and retrograde signaling mediate target-dependent short-term synaptic plasticity." Neuron 54(6): 949-959.

Bernier, B. E., A. F. Lacagnina, A. Ayoub, F. Shue, B. V. Zemelman, F. B. Krasne and M. R. Drew (2017). "Dentate Gyrus Contributes to Retrieval as well as Encoding: Evidence from Context Fear Conditioning, Recall, and Extinction." J Neurosci 37(26): 6359-6371.

Brew, H. M., J. X. Gittelman, R. S. Silverstein, T. D. Hanks, V. P. Demas, L. C. Robinson, C. A. Robbins, J. McKee-Johnson, S. Y. Chiu, A. Messing and B. L. Tempel (2007). "Seizures and reduced life span in mice lacking the potassium channel subunit Kv1.2, but hypoexcitability and enlarged Kv1 currents in auditory neurons." J Neurophysiol 98(3): 1501-1525.

Brito, G. N., G. J. Thomas, B. J. Davis and S. I. Gingold (1982). "Prelimbic cortex, mediodorsal thalamus, septum, and delayed alternation in rats." Exp Brain Res 46(1): 52-58.

Burgos-Robles, A., I. Vidal-Gonzalez and G. J. Quirk (2009). "Sustained conditioned responses in prelimbic prefrontal neurons are correlated with fear expression and extinction failure." J Neurosci 29(26): 8474-8482.

Chakroborty, S., E. S. Hill, D. T. Christian, R. Helfrich, S. Riley, C. Schneider, N. Kapecki, S. Mustaly-Kalimi, F. A. Seiler, D. A. Peterson, A. R. West, B. M. Vertel, W. N. Frost and G. E. Stutzmann (2019). "Reduced presynaptic vesicle stores mediate cellular and network plasticity defects in an early-stage mouse model of Alzheimer's disease." Mol Neurodegener 14(1): 7.

Chawla, M. K., J. F. Guzowski, V. Ramirez-Amaya, P. Lipa, K. L. Hoffman, L. K. Marriott, P. F. Worley, B. L. McNaughton and

C. A. Barnes (2005). "Sparse, environmentally selective expression of Arc RNA in the upper blade of the rodent fascia dentata by brief spatial experience " Hippocampus 15: 8.

Cohen, R. A., R. F. Kaplan, D. J. Moser, M. A. Jenkins and H. Wilkinson (1999). "Impairments of attention after cingulotomy." Neurology 53(4): 819-824.

Collins, D. P., P. G. Anastasiades, J. J. Marlin and A. G. Carter (2018). "Reciprocal Circuits Linking the Prefrontal Cortex with Dorsal and Ventral Thalamic Nuclei." Neuron 98(2): 366-379 e364.

Corcoran, K. A. and G. J. Quirk (2007). "Activity in prelimbic cortex is necessary for the expression of learned, but not innate, fears." J Neurosci 27(4): 840-844.

Csordas, G., P. Varnai, T. Golenar, S. Roy, G. Purkins, T. G. Schneider, T. Balla and G. Hajnoczky (2010). "Imaging interorganelle contacts and local calcium dynamics at the ER-mitochondrial interface." Mol Cell 39(1): 121-132.

Curzon, P., N. R. Rustay and K. E. Browman (2009). Cued and Contextual Fear Conditioning for Rodents. Methods of Behavior Analysis in Neuroscience. nd and J. J. Buccafusco. Boca Raton (FL).

Davis, K. D., W. D. Hutchison, A. M. Lozano, R. R. Tasker and J. O.

Dostrovsky (2000). "Human anterior cingulate cortex neurons modulated by attention-demanding tasks." J Neurophysiol 83(6): 3575-3577.

Dembrow, N. C., R. A. Chitwood and D. Johnston (2010). "Projection-specific neuromodulation of medial prefrontal cortex neurons." J Neurosci 30(50): 16922-16937.

DeNardo, L. A., D. S. Berns, K. DeLoach and L. Luo (2015). "Connectivity of mouse somatosensory and prefrontal cortex examined with trans-synaptic tracing." Nat Neurosci 18(11): 1687-1697.

Diamantaki, M., M. Frey, P. Berens, P. Preston-Ferrer and A. Burgalossi (2016). "Sparse activity of identified dentate granule cells during spatial exploration." Elife 5.

Eom, K., J. H. Hyun, D. G. Lee, S. Kim, H. J. Jeong, J. S. Kang, W. K. Ho and S. H. Lee (2019). "Intracellular Zn(2+) Signaling Facilitates Mossy Fiber Input-Induced Heterosynaptic Potentiation of Direct Cortical Inputs in Hippocampal CA3 Pyramidal Cells." J Neurosci 39(20): 3812-3831.

Eom, K., H. R. Lee, J. H. Hyun, H. An, Y. S. Lee, W. K. Ho and S. H. Lee (2022). "Gradual decorrelation of CA3 ensembles associated with contextual discrimination learning is impaired by Kv1.2 insufficiency." Hippocampus 32(3): 193-216.

Fujisawa, S., A. Amarasingham, M. T. Harrison and G. Buzsaki (2008). "Behavior-dependent short-term assembly dynamics in the medial prefrontal cortex." Nat Neurosci 11(7): 823-833.

Funahashi, S. and K. Takeda (2002). "Information processes in the primate prefrontal cortex in relation to working memory processes." Rev Neurosci 13(4): 313-345.

Fuster, J. M. and G. E. Alexander (1971). "Neuron activity related to short-term memory." Science 173(3997): 652-654.

Fyhn, M., T. Hafting, A. Treves, M. B. Moser and E. I. Moser (2007). "Hippocampal remapping and grid realignment in entorhinal cortex." Nature 446(7132): 190-194.

Gandhi, S., A. Wood-Kaczmar, Z. Yao, H. Plun-Favreau, E. Deas, K. Klupsch, J. Downward, D. S. Latchman, S. J. Tabrizi, N. W. Wood, M. R. Duchen and A. Y. Abramov (2009). "PINK1-associated Parkinson's disease is caused by neuronal vulnerability to calcium-induced cell death." Mol Cell 33(5): 627-638.

Genc, O., O. Kochubey, R. F. Toonen, M. Verhage and R. Schneggenburger (2014). "Munc18-1 is a dynamically regulated PKC target during short-term enhancement of transmitter release." Elife 3: e01715.

Gilmartin, M. R., N. L. Balderston and F. J. Helmstetter (2014). "Prefrontal cortical regulation of fear learning." Trends Neurosci 37(8): 455-464.

Gilmartin, M. R. and F. J. Helmstetter (2010). "Trace and contextual fear conditioning require neural activity and NMDA receptor-dependent transmission in the medial prefrontal cortex." Learn Mem 17(6): 289-296.

Gilmartin, M. R. and M. D. McEchron (2005). "Single neurons in the medial prefrontal cortex of the rat exhibit tonic and phasic coding during trace fear conditioning." Behav Neurosci 119(6): 1496-1510.

Gilmartin, M. R., H. Miyawaki, F. J. Helmstetter and K. Diba (2013). "Prefrontal activity links nonoverlapping events in memory." J Neurosci 33(26): 10910-10914.

Giorgi, C., S. Marchi and P. Pinton (2018). "The machineries, regulation and cellular functions of mitochondrial calcium." Nat Rev Mol Cell Biol 19(11): 713-730.

Goldman-Rakic, P. S. (1996). "Regional and cellular fractionation of working memory." Proc Natl Acad Sci U S A 93(24): 13473-13480.

GoodSmith, D., X. Chen, C. Wang, S. H. Kim, H. Song, A. Burgalossi, K. M. Christian and J. J. Knierim (2017). "Spatial

Representations of Granule Cells and Mossy Cells of the Dentate Gyrus." Neuron 93(3): 677-690 e675.

Guo, N., M. E. Soden, C. Herber, M. T. Kim, A. Besnard, P. Lin, X. Ma, C. L. Cepko, L. S. Zweifel and A. Sahay (2018). "Dentate granule cell recruitment of feedforward inhibition governs engram maintenance and remote memory generalization." Nat Med 24(4): 438-449.

Guzowski, J. F., B. L. McNaughton, C. A. Barnes and P. F. Worley (1999). "Environment-specific expression of the immediate-early gene Arc in hippocampal neuronal ensembles." Nat Neurosci. 2: 5.

Guzowski, J. F., J. A. Timlin, B. Roysam, B. L. McNaughton, P. F. Worley and C. A. Barnes (2005). "Mapping behaviorally relevant neural circuits with immediate-early gene expression." Curr Opin Neurobiol 15(5): 599-606.

Han, C. J., C. M. O'Tuathaigh, L. van Trigt, J. J. Quinn, M. S. Fanselow, R. Mongeau, C. Koch and D. J. Anderson (2003). "Trace but not delay fear conditioning requires attention and the anterior cingulate cortex." Proc Natl Acad Sci U S A 100(22): 13087-13092.

Harris, K. D. and G. M. Shepherd (2015). "The neocortical circuit: themes and variations." Nat Neurosci 18(2): 170-181.

Hempel, C. M., K. H. Hartman, X. J. Wang, G. G. Turrigiano and S. B. Nelson (2000). "Multiple forms of short-term plasticity at excitatory synapses in rat medial prefrontal cortex." J Neurophysiol 83(5): 3031-3041.

Herry, C. and R. Garcia (2002). "Prefrontal cortex long-term potentiation, but not long-term depression, is associated with the maintenance of extinction of learned fear in mice." J Neurosci 22(2): 577-583.

Hyun, J., K. Eom, K. Lee, J. Bae, Y. Bae, M. Kim, S. Kim, W. Ho and S. Lee (2015). "Kv1.2 mediates heterosynaptic modulation of direct cortical synaptic inputs in CA3 pyramidal cells." J Physiol 593(16): 3617-3643.

Hyun, J., K. Eom, K. Lee, W. Ho and S. Lee (2013). "Activity-dependent downregulation of D-type K+ channel subunit Kv1.2 in rat hippocampal CA3 pyramidal neurons." J Physiol 591(22): 5525-5540.

Jovicich, J., R. J. Peters, C. Koch, J. Braun, L. Chang and T. Ernst (2001). "Brain areas specific for attentional load in a motion-tracking task." J Cogn Neurosci 13(8): 1048-1058.

Kalmbach, B. E., R. A. Chitwood, N. C. Dembrow and D. Johnston (2013). "Dendritic generation of mGluR-mediated slow afterdepolarization in layer 5 neurons of prefrontal cortex." J

Neurosci 33(33): 13518-13532.

Karadjov, J. S., L. Kudzina and V. P. Zinchenko (1986). "TPP+ inhibits Na+-stimulated Ca2+ efflux from brain mitochondria." Cell Calcium 7(2): 115-119.

Kasper, E. M., A. U. Larkman, J. Lubke and C. Blakemore (1994). "Pyramidal neurons in layer 5 of the rat visual cortex. I. Correlation among cell morphology, intrinsic electrophysiological properties, and axon targets." J Comp Neurol 339(4): 459-474.

Kim, E., B. A. Bari and J. Y. Cohen (2021). "Subthreshold basis for reward-predictive persistent activity in mouse prefrontal cortex." Cell Rep 35(5): 109082.

Kim, K. R., S. Yeon Lee, S. Ho Yoon, Y. Kim, H. J. Jeong, S. Lee, Y. Ho Suh, J. S. Kang, H. Cho, S. H. Lee, M. H. Kim and W. K. Ho (2020). "Kv4.1, a key ion channel for low frequency firing of dentate granule cells, is crucial for pattern separation." J Neurosci.

Kirry, A. J., R. C. Twining and M. R. Gilmartin (2020). "Prelimbic input to basolateral amygdala facilitates the acquisition of trace cued fear memory under weak training conditions." Neurobiol Learn Mem 172: 107249.

Kitamura, T., C. Sun, J. Martin, L. J. Kitch, M. J. Schnitzer and S.

Tonegawa (2015). "Entorhinal Cortical Ocean Cells Encode Specific Contexts and Drive Context-Specific Fear Memory." Neuron 87: 32.

Korogod, N., X. Lou and R. Schneggenburger (2007). "Posttetanic potentiation critically depends on an enhanced Ca(2+) sensitivity of vesicle fusion mediated by presynaptic PKC." Proc Natl Acad Sci U S A 104(40): 15923-15928.

Kostic, M., M. H. Ludtmann, H. Bading, M. Hershfinkel, E. Steer, C. T. Chu, A. Y. Abramov and I. Sekler (2015). "PKA Phosphorylation of NCLX Reverses Mitochondrial Calcium Overload and Depolarization, Promoting Survival of PINK1-Deficient Dopaminergic Neurons." Cell Rep 13(2): 376-386.

Krishnamoorthy, K. and J. Thomson (2004). "A more powerful test for comparing two Poisson means." Journal of Statistical Planning and Inference 119(1): 23-35.

Kwapis, J. L., T. J. Jarome, J. L. Lee, M. R. Gilmartin and F. J. Helmstetter (2014). "Extinguishing trace fear engages the retrosplenial cortex rather than the amygdala." Neurobiol Learn Mem 113: 41-54.

Kwapis, J. L., T. J. Jarome, J. L. Lee and F. J. Helmstetter (2015). "The retrosplenial cortex is involved in the formation of memory for context and trace fear conditioning." Neurobiol

Learn Mem 123: 110-116.

Larkman, A. and A. Mason (1990). "Correlations between morphology and electrophysiology of pyramidal neurons in slices of rat visual cortex. I. Establishment of cell classes." J Neurosci 10(5): 1407-1414.

Lee, C. H. and I. Lee (2020). "Impairment of Pattern Separation of Ambiguous Scenes by Single Units in the CA3 in the Absence of the Dentate Gyrus." J Neurosci 40(18): 3576-3590.

Lee, D., K. H. Lee, W. K. Ho and S. H. Lee (2007). "Target cell-specific involvement of presynaptic mitochondria in post-tetanic potentiation at hippocampal mossy fiber synapses." J Neurosci 27(50): 13603-13613.

Lee, I. and R. Kesner (2004). "Encoding versus retrieval of spatial memory: double dissociation between the dentate gyrus and the perforant path inputs into CA3 in the dorsal hippocampus." Hippocampus 14(66-76).

Lee, J., J. H. Choi and J. C. Rah (2020). "Frequency-dependent gating of feedforward inhibition in thalamofrontal synapses." Mol Brain 13(1): 68.

Lee, J. S., M. H. Kim, W. K. Ho and S. H. Lee (2008). "Presynaptic release probability and readily releasable pool size are regulated by two independent mechanisms during posttetanic

potentiation at the calyx of Held synapse." J Neurosci 28(32): 7945-7953.

Lee, S., T. Ahmed, S. Lee, H. Kim, S. Choi, D. S. Kim, S. J. Kim, J. Cho and H. S. Shin (2011). "Bidirectional modulation of fear extinction by mediodorsal thalamic firing in mice." Nat Neurosci 15(2): 308-314.

Lee, S. H., K. R. Kim, S. Y. Ryu, S. Son, H. S. Hong, I. Mook-Jung, S. H. Lee and W. K. Ho (2012). "Impaired short-term plasticity in mossy fiber synapses caused by mitochondrial dysfunction of dentate granule cells is the earliest synaptic deficit in a mouse model of Alzheimer's disease." J Neurosci 32(17): 5953-5963.

Leutgeb, J. K., S. Leutgeb, M. B. Moser and E. I. Moser (2007). "Pattern separation in the dentate gyrus and CA3 of the hippocampus." Science 315(5814): 961-966.

Leutgeb, S., J. K. Leutgeb, A. Treves, M. B. Moser and E. I. Moser (2004). "Distinct ensemble codes in hippocampal areas CA3 and CA1." Science 305(5688): 1295-1298.

Madar, A. D., L. A. Ewell and M. V. Jones (2019). "Pattern separation of spiketrains in hippocampal neurons." Sci Rep 9(1): 5282.

Marrone, D. F., A. A. Adams and E. Satvat (2011). "Increased

pattern separation in the aged fascia dentata." Neurobiol Aging 32(12): 2317 e2323-2332.

Mason, A. and A. Larkman (1990). "Correlations between morphology and electrophysiology of pyramidal neurons in slices of rat visual cortex. II. Electrophysiology." J Neurosci 10(5): 1415-1428.

McClelland, J. and N. Goddard (1996). "Considerations arising from a complementary learning systems perspective on hippocampus and neocortex." Hippocampus 6: 12.

McHugh, T. J., M. W. Jones, J. J. Quinn, N. Balthasar, R. Coppari, J. K. Elmquist, B. B. Lowell, M. S. Fanselow, M. A. Wilson and S. Tonegawa (2007). "Dentate gyrus NMDA receptors mediate rapid pattern separation in the hippocampal network." Science 317(5834): 94-99.

McMahon, D. and G. Barrionuevo (2002). "Short- and long-term plasticity of the perforant path synapse in hippocampal area CA3." J Neurophysiol 88: 528-533.

Mishra, R. K., S. Kim, S. J. Guzman and P. Jonas (2016). "Symmetric spike timing-dependent plasticity at CA3-CA3 synapses optimizes storage and recall in autoassociative networks." Nat Commun 7: 11552.

Molnar, Z. and A. F. Cheung (2006). "Towards the classification of

subpopulations of layer V pyramidal projection neurons." Neurosci Res 55(2): 105-115.

Mongillo, G., O. Barak and M. Tsodyks (2008). "Synaptic theory of working memory." Science 319(5869): 1543-1546.

Mukherjee, A. and P. Caroni (2018). "Infralimbic cortex is required for learning alternatives to prelimbic promoted associations through reciprocal connectivity." Nat Commun 9(1): 2727.

Nakayama, H., I. Ibanez-Tallon and N. Heintz (2018). "Cell-Type-Specific Contributions of Medial Prefrontal Neurons to Flexible Behaviors." J Neurosci 38(19): 4490-4504.

Norman, K. A. (2010). "How hippocampus and cortex contribute to recognition memory: revisiting the complementary learning systems model." Hippocampus 20(11): 1217-1227.

O'Reilly, R. C. and J. L. McClelland (1994). "Hippocampal conjunctive encoding, storage, and recall: avoiding a trade-off." Hippocampus 4: 661-682.

Ozdemir, A. T., M. Lagler, S. Lagoun, H. Malagon-Vina, B. Lasztoczi and T. Klausberger (2020). "Unexpected Rule-Changes in a Working Memory Task Shape the Firing of Histologically Identified Delay-Tuned Neurons in the Prefrontal Cortex." Cell Rep 30(5): 1613-1626 e1614.

Parent, M. A., L. Wang, J. Su, T. Netoff and L. L. Yuan (2010).

"Identification of the hippocampal input to medial prefrontal cortex in vitro." Cereb Cortex 20(2): 393-403.

Pennington, Z. T., Z. Dong, Y. Feng, L. M. Vetere, L. Page-Harley, T. Shuman and D. J. Cai (2019). "ezTrack: An open-source video analysis pipeline for the investigation of animal behavior." Sci Rep 9(1): 19979.

Pnevmatikakis, E. A. and A. Giovannucci (2017). "NoRMCorre: An online algorithm for piecewise rigid motion correction of calcium imaging data." J Neurosci Methods 291: 83-94.

Ramirez-Amaya, V., A. Angulo-Perkins, M. K. Chawla, C. A. Barnes and S. Rosi (2013). "Sustained transcription of the immediate early gene Arc in the dentate gyrus after spatial exploration." J Neurosci 33(4): 1631-1639.

Rolls, E. T. and R. P. Kesner (2006). "A computational theory of hippocampal function, and empirical tests of the theory." Prog Neurobiol 79(1): 1-48.

Ruediger, S., C. Vittori, E. Bednarek, C. Genoud, P. Strata, B. Sacchetti and P. Caroni (2011). "Learning-related feedforward inhibitory connectivity growth required for memory precision." Nature 473(7348): 514-518.

Runyan, J. D., A. N. Moore and P. K. Dash (2004). "A role for prefrontal cortex in memory storage for trace fear

conditioning." J Neurosci 24(6): 1288-1295.

Sierra-Mercado, D., Jr., K. A. Corcoran, K. Lebron-Milad and G. J. Quirk (2006). "Inactivation of the ventromedial prefrontal cortex reduces expression of conditioned fear and impairs subsequent recall of extinction." Eur J Neurosci 24(6): 1751-1758.

Sierra-Mercado, D., N. Padilla-Coreano and G. J. Quirk (2011). "Dissociable roles of prelimbic and infralimbic cortices, ventral hippocampus, and basolateral amygdala in the expression and extinction of conditioned fear." Neuropsychopharmacology 36(2): 529-538.

Sotres-Bayon, F., D. Sierra-Mercado, E. Pardilla-Delgado and G. J. Quirk (2012). "Gating of fear in prelimbic cortex by hippocampal and amygdala inputs." Neuron 76(4): 804-812.

Spellman, T., M. Svei, J. Kaminsky, G. Manzano-Nieves and C. Liston (2021). "Prefrontal deep projection neurons enable cognitive flexibility via persistent feedback monitoring." Cell 184(10): 2750-2766 e2717.

Storm, J. (1988). "Temporal integration by a slowly inactivating K+ current in hippocampal neurons." Nature 336(6197): 379.

Tang, Y. and R. S. Zucker (1997). "Mitochondrial involvement in post-tetanic potentiation of synaptic transmission." Neuron

18(3): 483-491.

Treves, A. and E. Rolls (1992). "Computational constraints suggest the need for two distinct input systems to the hippocampal CA3 network. ." Hippocampus 2: 189-199.

Twining, R. C., K. Lepak, A. J. Kirry and M. R. Gilmartin (2020). "Ventral Hippocampal Input to the Prelimbic Cortex Dissociates the Context from the Cue Association in Trace Fear Memory." J Neurosci 40(16): 3217-3230.

Ueda, N., R. Nakano, Z. Ghahramani and G. E. Hinton (2000). "SMEM algorithm for mixture models." Neural Comput 12(9): 2109-2128.

Vandael, D., C. Borges-Merjane, X. Zhang and P. Jonas (2020). "Short-Term Plasticity at Hippocampal Mossy Fiber Synapses Is Induced by Natural Activity Patterns and Associated with Vesicle Pool Engram Formation." Neuron 107(3): 509-521 e507.

Vazdarjanova, A. and J. F. Guzowski (2004). "Differences in hippocampal neuronal population responses to modifications of an environmental context: evidence for distinct, yet complementary, functions of CA3 and CA1 ensembles." J Neurosci 24(29): 6489-6496.

Voigts, J., J. P. Newman, M. A. Wilson and M. T. Harnett (2020).

"An easy-to-assemble, robust, and lightweight drive implant for chronic tetrode recordings in freely moving animals." J Neural Eng 17(2): 026044.

Wang, C. C., C. Weyrer, M. Paturu, D. Fioravante and W. G. Regehr (2016). "Calcium-Dependent Protein Kinase C Is Not Required for Post-Tetanic Potentiation at the Hippocampal CA3 to CA1 Synapse." J Neurosci 36(24): 6393-6402.

Wang, M., B. P. Ramos, C. D. Paspalas, Y. Shu, A. Simen, A. Duque, S. Vijayraghavan, A. Brennan, A. Dudley, E. Nou, J. A. Mazer, D. A. McCormick and A. F. Arnsten (2007). "Alpha2A-adrenoceptors strengthen working memory networks by inhibiting cAMP-HCN channel signaling in prefrontal cortex." Cell 129(2): 397-410.

Wierda, K. D., R. F. Toonen, H. de Wit, A. B. Brussaard and M. Verhage (2007). "Interdependence of PKC-dependent and PKC-independent pathways for presynaptic plasticity." Neuron 54(2): 275-290.

Wood-Kaczmar, A., E. Deas, N. W. Wood and A. Y. Abramov (2013). "The role of the mitochondrial NCX in the mechanism of neurodegeneration in Parkinson's disease." Adv Exp Med Biol 961: 241-249.

Woods, N. I., F. Stefanini, D. L. Apodaca-Montano, I. M. C. Tan, J. S.

Biane and M. A. Kheirbek (2020). "The Dentate Gyrus Classifies Cortical Representations of Learned Stimuli." Neuron 107(1): 173-184 e176.

Xiao, D., B. Zikopoulos and H. Barbas (2009). "Laminar and modular organization of prefrontal projections to multiple thalamic nuclei." Neuroscience 161(4): 1067-1081.

Yang, S. T., Y. Shi, Q. Wang, J. Y. Peng and B. M. Li (2014). "Neuronal representation of working memory in the medial prefrontal cortex of rats." Mol Brain 7: 61.

Yassa, M. A. and C. E. L. Stark (2011). "Pattern separation in the hippocampus." Trends in Neurosciences 34(10): 515-525.

Yoon, J. Y., H. R. Lee, W. K. Ho and S. H. Lee (2020). "Disparities in Short-Term Depression Among Prefrontal Cortex Synapses Sustain Persistent Activity in a Balanced Network." Cereb Cortex 30(1): 113-134.

Zlokolica, V., A. Pizurica and W. Philips (2006). "Noise estimation for video processing based on spatio-temporal gradients." Ieee Signal Processing Letters 13(6): 337-340.

Zucker, R. S. and W. G. Regehr (2002). "Short-term synaptic plasticity." Annu Rev Physiol 64: 355-405.

국문초록

환경적 자극과 혐오스러운 사건의 상관관계를 학습하는 것은 생존에 필수적인 요소다. 공포 조건화 (fear conditioning)는 상관 학습의 기초적인 형태로 행동 심리학에서 많이 이용되는 패러다임 중 하나이다. 공포 조건화는 문맥 공포 조건화 (contextual fear conditioning; CFC)와 단서 공포 조건화로 나뉜다. 또한 단서 공포 조건화는 조건 자극 (conditioned stimulus; CS)과 무조건 자극 (unconditioned stimulus; US) 사이의 짧은 시간 간격의 유무를 바탕으로 각각 지연 공포 조건화 (delayed fear conditioning; DFC)과 흔적 공포 조건화 (trace fear conditioning; TFC)로 세분화된다. 편도체는 모든 종류의 공포 조건화에서 상관 기억의 형성과 공포 반응의 발현에 핵심적인 역할을 한다. DFC에서는 공포 기억의 학습 및 발현이 편도체만으로 충분한데 반해, TFC와 CFC에서는 해마, 전전두엽 그리고 팽대후피질 (retrosplenial cortex)과 같은 다른 피질 영역의 기여가 필요하다. 따라서 CFC와 TFC는 피질 영역의 기능을 연구하는데 큰 도움을 준다. 지금까지 대부분의 연구는 공포 조건화와 신경망 활성의 상관관계에 초점이 맞춰져 있었기에 시냅스 특이적 가소성의 기능장애가 행동에 미치는 영향은 연구는 미진하다. 나는 내측 전전두엽 (medial prefrontal cortex; PFC) 변연계전 (prelimbic; PL) 부위의 레이어 2/3 (L2/3)와 레이어 5 (L5)의 피라미드 세포 (pyramidal neuron; PN) 사이의 시냅스와 천공경로 (perforant pathway; PP)와 해마 CA3의 시냅스에서의 가소성 장애와

행동 양상의 관계에 대해 연구하였다.

TFC의 흔적 기간 (trace interval) 동안 PFC 신경세포의 지속적으로 증가된 활성은 흔적 공포 기억의 습득에 필요하다. 그러나 PFC에서 나타나는 지속적으로 증가된 활성의 신경생리학적인 메커니즘의 이해도는 낮다. 단기가소성의 종류 중 하나 강축후 강화 (post-tetanic potentiation; PTP)는 작업 기억 동안 지속적으로 증가하는 활성을 중개할 것으로 예상된다. 따라서 나는 PL에서 발생하는 PTP의 신경생물학적 메커니즘과 PTP가 TFC와 지속적으로 증가된 활성에 영향을 미치는지에 대해서 연구했다. 광유전학을 통해 나는 L5 PN의 들신경섬유 (afferent fiber)를 세포 타입 그리고 층 특이적으로 자극했다. 그 결과 L2/3 PN과 L5의 맞교차 (commissural; COM) PN이 L5 피질뇌교투사 (corticopontine; CPn) PN과 연결되는 시냅스에서 PTP가 유도되고 L5 COM과 연결되는 시냅스에서는 유도되지 않는 것을 발견했다. 두개의 시냅스에서 유도되는 PTP는 protein kinase C (PKC) 억제제로 모두 억제되었지만, 미토콘드리아 Na/Ca exchanger (mNCX) 차단제인 tetraphenylphosphonium (TPP)는 L2/3-CPn 시냅스에서 유도되는 PTP만을 억제했다. TPP를 PL 부위에 주입한 후 TFC를 수행한 결과, 흔적 공포 소거 실험에서 TPP는 흔적 공포 형성에는 영향을 미치지 않았지만 공포 기억을 짧게 유지시키는 것을 밝혔다. 또한, 생체 내 기록 실험에서 TFC동안 CS 이후에 지속적으로 증가한 활성을 가지는 PL-PNs이 약 20% 인 것을 밝혔다. TPP의 주입은 공포 조건화 실험과 공포 기억 소거 실험에서 CS 이후에 나타나는 지속적인 활성 증가를 억제

했다. COM과 CPn 세포 특이적 생체내 칼슘 이미징 실험에서 두 세포는 다른 비율의 활성 양상을 나타냈다. COM과 다르게 CPn은 CS의 시작점에서 예상되는 US 시간까지 지속적으로 증가한 활성을 보이는 Delay 세포 타입의 비율이 훨씬 많았다. 이러한 결과들은 L2/3-CPn 시냅스에서 발생하는 PTP가 TFC에서 CS 이후에 지속적으로 증가한 활성에 필요하며, 흔적 공포 기억 유지에 중요하다는 것을 시사한다.

해마는 맥락 공포의 형성, 강화 그리고 검색에 중요하다. 두 개의 유사한 맥락을 나타내는 앙상블 형성의 기초가 되는 네트워크 프로세스를 패턴 분리 (pattern separation)라고 하며 해마의 중요한 기능 중 하나이다. 그러나 CA3에서 신경 앙상블의 패턴 분리의 기본이 되는 네트워크 메커니즘은 거의 알려져 있지 않다. CA3 피라미드 세포 (CA3-PN)에서 Kv1.2 발현은 말단 정점 수상돌기 (distal apical dendrite)로 집중되어 있고, 그것의 하향 조절 (downregulation)은 PP 시냅스 입력에 대한 수지상 (dendritic) 반응을 향상시킨다. CA3-PN에서 Kv1.2의 반수체 부족 개체 (*Kcna2+/-*)는 PP-CA3 시냅스에서 장기 강화 (Long-term potentiation; LTP)의 임계값 (threshold)을 낮춘다. *Kcna2+/-* 개체는 확실히 구별되는 상황을 식별하는 행동은 정상이지만 약간의 차이가 있는 유사한 상황을 식별하는 행동에는 장애를 보이는 것을 이전 연구에서 밝혔다. 나는 초기 발현 유전자 (*Homer1a, Arc*)와 절편상 하이브리드 형성법을 사용하여 두 가지 유사한 컨텍스트에서 나타나는 CA3 및 치아이랑 (Dentate gyrus; DG)의 신경 앙상블의 패턴 분리를 조사했다. 비슷한 문맥에 처음 노출되었을 때 활성화되는 CA3

앙상블의 크기와 교집합은 야생형 (wildtype; WT)과 *Kcna2+/−* 마우스 간에 차이가 없었다. 그러나 두 그룹간의 앙상블 크기와 교집합은 실험이 진행될수록 점차 차이를 보였다. 이는 Kcna2+/− 마우스의 PP−CA3 시냅스에서 비정상적인 가소성 변화가 나타나며 결과적으로 WT과 다르게 비정상적인 패턴 분리를 야기한다는 것을 제안한다. 이와 다르게 DG의 앙상블은 두 그룹간의 차이가 없었다. DG 앙상블은 실험 첫날부터 이미 분리되어 있었으며, 앙상블의 교집합은 실험이 진행되어도 변화하지 않았다. 결과적으로 *Kcna2+/−* 마우스는 WT과 *Kcna1+/−* 마우스에 비해서, CA3 앙상블의 크기와 두개의 문맥에 대한 앙상블의 교집합이 크다. 이러한 결과는 이끼 섬유 (mossy fiber)의 입력에 의해 지도되는 PP−CA3 시냅스의 희소한 LTP가 CA3의 점진적 패턴 분리에 필수적임을 시사한다.

주요어

흔적 공포 조건화, 전전두엽, 지속적인 활성 증가, 강축후 강화, 해마, CA3, Perforant pathway, 패턴 분리, Kv1.2.

Student number: 2015−23245